1-1-1979

The design of a direct side force control system for the NASA HiMAT remotely piloted research vehicle.

Russell Lund Schuetz

THE DESIGN OF A DIRECT SIDE FORCE CONTROL SYSTEM FOR THE NASA HiMAT REMOTELY PILOTED RESEARCH VEHICLE

by

Russell Lund Schuetz

A Thesis
Presented to the Graduate Committee
of Lehigh University
in Candidacy for the Degree of
Master of Science
in
Mechanical Engineering

Lehigh University
1979

This thesis is accepted and approved in partial fulfillment of the requirements for the degree of Master of Science.

2 MAY 1979
(date)

Stanley H. Johnson
Professor in Charge

Douglas E. Abbott
Professor and Chairman

ACKNOWLEDGMENTS

I would like to express my sincere thanks to two people who made the completion of this project possible. The first is Professor Stan Johnson who has not only been responsible for much of my enthusiasm throughout this Masters program, but who has also been a very understanding friend through times of frustration and procrastination.

Secondly, I would like to express my gratitude to Dwain Deets who has given much of his valuable time and advice to help me with this study.

Thank you both.

This work was supported by the National Aeronautics and Space Administration Research Grant #NSG 4010 at the Dryden Flight Research Center, Edwards, California.

CONTENTS

CONTENTS (continued)

CONTENTS (continued)

LIST OF FIGURES

LIST OF FIGURES (continued)

LIST OF FIGURES (continued)

LIST OF FIGURES (continued)

LIST OF SYMBOLS

		Typical Units
A_y	lateral acceleration	m/s^2
A_z	normal acceleration	m/s^2
b	wing span	meters
$\bar{c}$	mean chord	meters
C_{ℓ_p}	dimensionless coefficient of rolling moment due to roll rate	
C_{ℓ_r}	dimensionless coefficient of rolling moment due to yaw rate	
C_{ℓ_β}	dimensionless coefficient of rolling moment due to sideslip angle	
C_{ℓ_δ}	dimensionless coefficient of rolling moment due to control surface deflection	
C_{n_p}	dimensionless coefficient of yawing moment due to roll rate	
C_{n_r}	dimensionless coefficient of yawing moment due to yaw rate	
C_{n_β}	dimensionless coefficient of yawing moment due to sideslip angle	
C_{n_δ}	dimensionless coefficient of yawing moment due to control surface deflection	
C_{y_p}	dimensionless coefficient of side force due to roll rate	
C_{y_r}	dimensionless coefficient of side force due to yaw rate	

LIST OF SYMBOLS (continued)

		Typical Units
C_{y_β}	dimensionless coefficient of side force due to sideslip angle	
C_{y_δ}	dimensionless coefficient of side force due to control surface deflection	
g	gravitational acceleration	9.81 m/sec^2
G	control system filter	
hp	altitude	meters
$\underline{I}$	identity matrix	
I_{xx}	moment of inertia about x-axis	$kg\text{-}m^2$
I_{zz}	moment of inertia about z-axis	$kg\text{-}m^2$
I_{xz}	product of inertia	$kg\text{-}m^2$
I*	$1 - (I_{xz})^2/(I_{xx}I_{zz})$	
k	ratio of 'command roll performance' to 'applicable roll performance requirement'	
K	constant or control system gain	
ℓ_{xx}	longitudinal distance between accelerometer and C. G.	meters
L_p	rolling moment due to roll rate	
L_r	rolling rate due to yaw rate	
L_β	rolling moment due to sideslip angle	
L_δ	rolling moment due to control surface deflection	
Mn	Mach number	

LIST OF SYMBOLS (continued)

		Typical Units
N_p	yawing moment due to roll rate	N - m
N_r	yawing moment due to yaw rate	
N_β	yawing moment due to sideslip angle	
N_δ	yawing moment due to control surface deflection	
p	roll rate	rad/sec^2
$\bar{q}$	dynamic pressure	N/m^2
r	yaw rate	rad/sec^2
s	Laplace operator	
S	sensitivity function	
S_{REF}	wing surface area	$meters^2$
t	time	
U	x-component of velocity	m/sec^2
$\underline{V}$	velocity vector	
W_o	mid-mission weight	slugs
X	command input	meters
Y_p	lateral force due to roll rate	Newtons
Y_r	lateral force due to yaw rate	
Y_β	lateral force due to sideslip angle	
Y_δ	lateral force due to control surface deflection	

LIST OF SYMBOLS (continued)

		Typical Units
α	angle of attack	degrees or radians
α_T	trim angle of attack	degrees or radians
β	sideslip angle	
Δ	incremental variation of a given quantity	
δ	control surface deflection (symmetrical	degrees or radians
δ'	differential control surface deflection (asymmetrical)	degrees or radians
δ_y	damping ratio	
λ	eigenvalue	
ϕ	bank angle	radians
ψ	heading angle	radians
ω	natural frequency	rad/sec

Superscripts

$(\cdot)$	first derivative with respect to time
$(\ddot{\cdot})$	second derivative with respect to time

Subscripts

A	ailerons
V	elevons
C	canards

ABBREVIATIONS

AFFDL	Air Force Flight Dynamics Lab
CCV	Control Configured Vehicle
cg	Center of Gravity
DSF	Direct Side Force
FP	Fuselage Pointing
HiMAT	Highly Maneuverable Aircraft Technology
kg	Kilograms
LT	Lateral Translation
LTV	Ling Tempco Vought
m	Meters
McAIR	McDonnell Aircraft Company
N	Newtons
RI	Rockwell International
RPV	Remotely Piloted (Research) Vehicle
sec	Seconds
WLT	Wings Level Turn

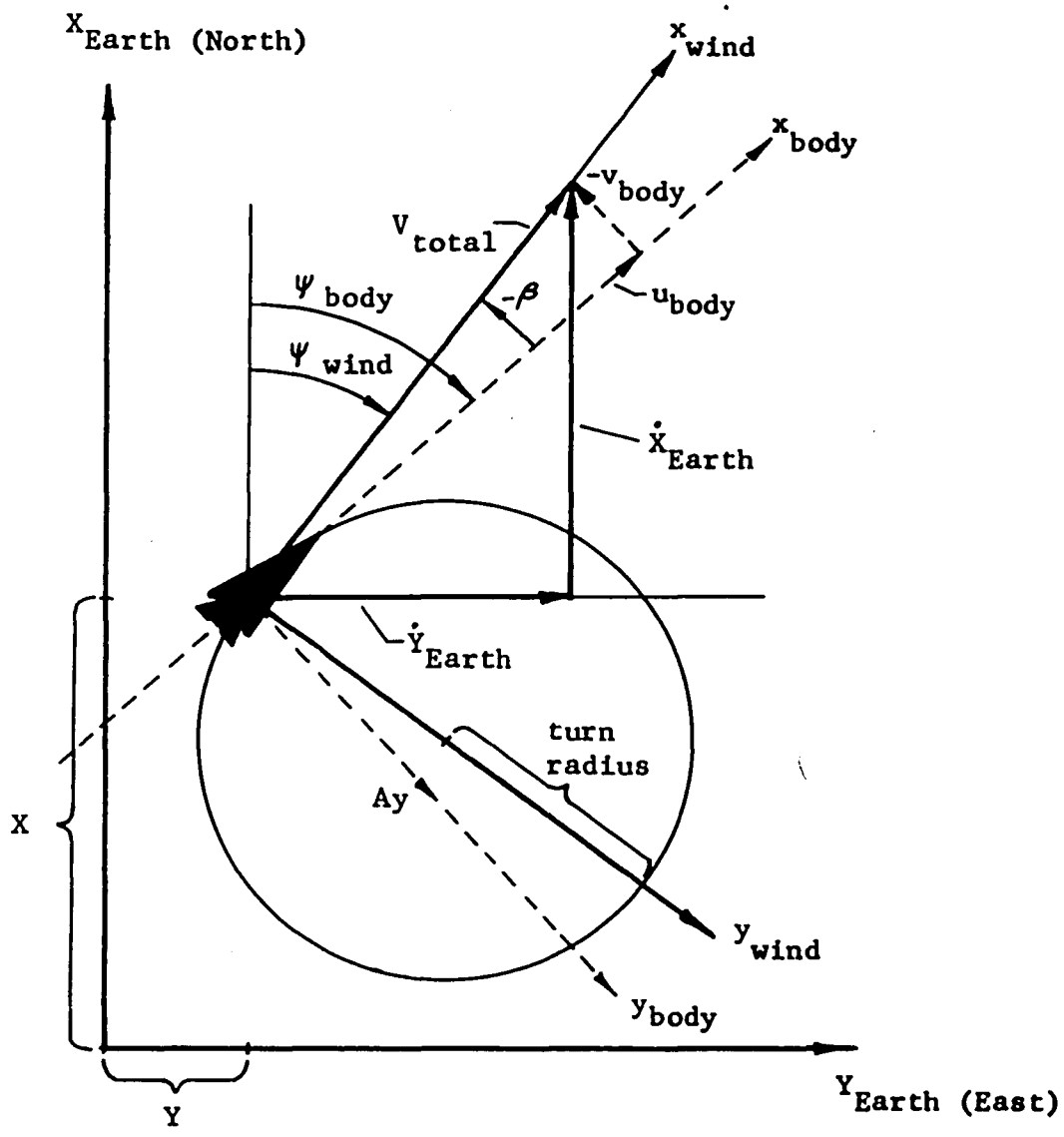

Coordinate System Convention

ABSTRACT

The summary of a literature survey of Direct Side Force control systems is presented and a system is designed for the NASA/Rockwell HiMAT Remotely Piloted Research Vehicle.

The emphasis of the survey is on defining a set of general design criteria. Once this is complete, the results are discussed and recommendations are made concerning a Direct Side Force system for the HiMAT aircraft. Three modes of operation are defined. The'Wings Level Turn' (WLT) mode allows direct lateral acceleration control of the vehicle without generating any sideslip angle. Ideally, this yields a flat turn with no rolling moment and with wings horizontal. The 'Lateral Translation" (LT) mode changes the flight path of the vehicle without changing the heading. In this mode, lateral velocity becomes the controlled motion. The last mode, called 'Fuselage Pointing' (FP), is similar to Lateral Translation, except that the heading of the vehicle is controlled without altering the flight path. Again, as with the other modes, this is accomplished without inducing any rolling moment and with wings horizontal. Sideslip angle is commanded.

Only the WLT and FP modes are recommended for the HiMAT vehicle, and the rudder pedals are the suggested form of cockpit control. Specified design criteria include that the system ideally be decoupled from the longitudinal axis and that the original handling qualities of the craft, while under the Primary Flight Control System (PFCS) not be degraded. Military dutch roll specifications are also considered.

The side force system designed for HiMAT is an addition to the PFCS with no added feedback paths. It consists of open loop interconnect paths to the elevons, rudders, and canards which include compensating filters and gains. These are scheduled as needed on flight conditions and vary in complexity. An analysis is included to show the sensitivity of the interconnect gains to errors in the aerodynamic coefficients. The final system is pleasingly uncomplicated and yields satisfactory vehicle responses as generated by a linear simulation on a digital computer. No actual flight test has been made. The results predict maximum commanded responses of approximately 2.0 G's lateral acceleration in the WLT mode and approximately 6.0 degrees sideslip angle in the FP mode.

INTRODUCTION

Recent interest has developed in new control modes for high performance aircraft. Three of these modes are related to a vehicle's lateral-directional capabilities and are referred to as direct side force control.

The HiMAT RPRV (Highly Maneuverable Aircraft Technology Remotely Piloted Research Vehicle), which is being built by Rockwell International Corporation for NASA, is control - configured and has direct side force capabilities due to its unique design which includes closely coupled forward canards. No specific design criteria have been defined, however, since little research has been done in this area to date.

The first part of this paper presents a brief survey of the research results available. The emphasis is placed on defining a set of design criteria for a direct side force control system and how it would apply to the HiMAT Program.

The concluding sections use the results of the survey in developing a system design for the HiMAT vehicle.

1. DSF MODES

1.1 Definition

There are three distinct DSF modes which have been recognized and studied, and which will be considered here. Specifically, they are the wings level turn mode (WLT), the lateral translation mode (LT), and the fuselage pointing mode (FP), defined as follows:

WLT - Direct control of lateral acceleration with a minimum change in sideslip and roll angles

LT - Direct control of lateral flight path and sideslip angle with a minimum change in yaw and roll angles

FP - Direct control of yaw and sideslip angles with a minimum change in lateral flight path and roll angle

Figure 1 [10]* presents these schematically.

1.2 Mechanization

The various DSF modes are mechanized through a simultaneous combination of inputs to one or more vehicle control surfaces, asymmetrical drag devices, or vectored thrust exhaust nozzles which impart the required aerodynamic forces. The most popular mechanization scheme has been the scheduling of rudder and canard surfaces to provide lateral motion, with aileron input to cancel any rolling tendency. This has been used

*Numbers in square brackets refer to references.

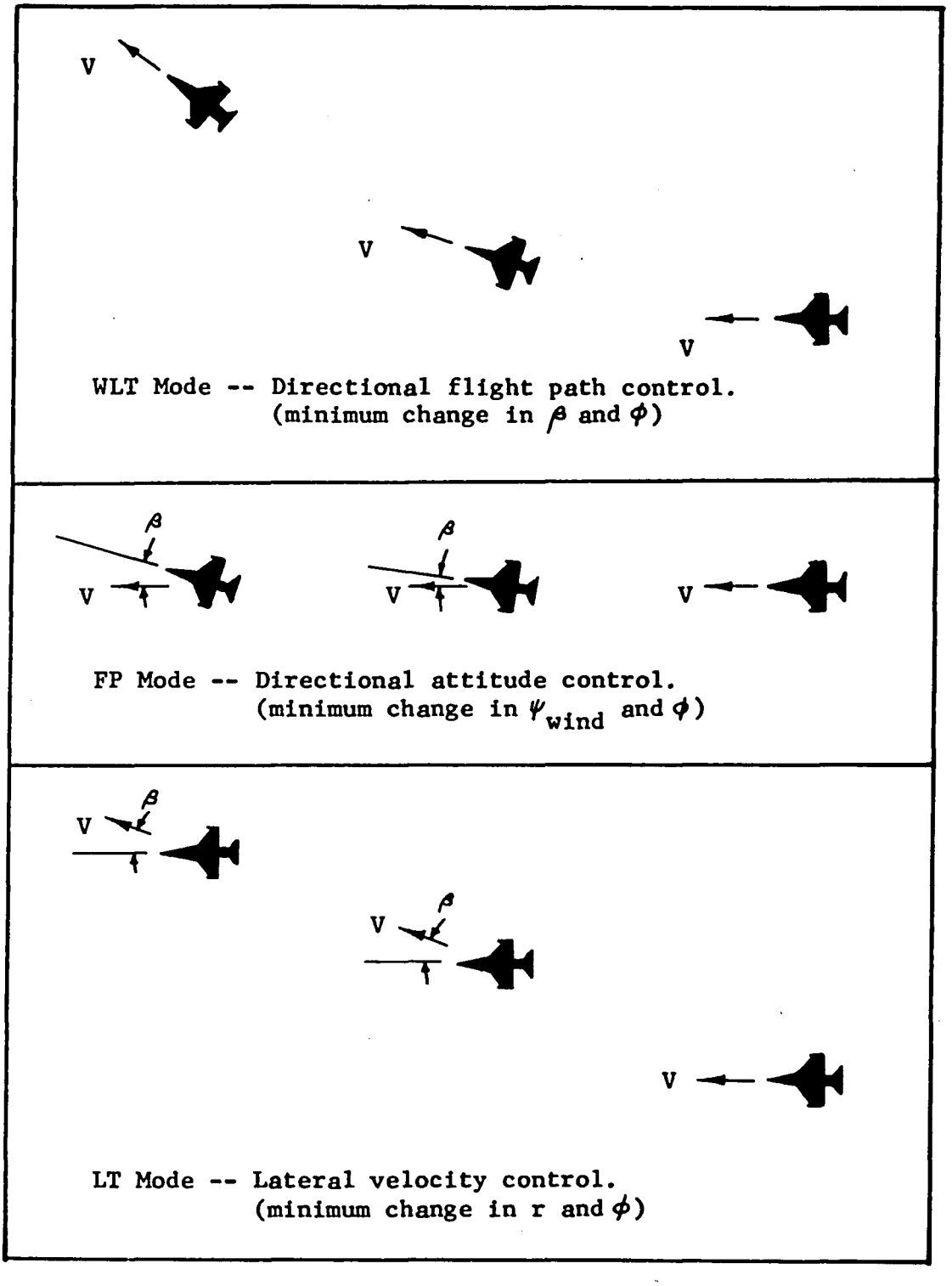

Figure 1. Direct Side Force Mode Definition

successfully on the General Dynamics YF-16 CCV vehicle [9,10], and successfully simulated for an LTV F-8 [1]. The use of asymmetrical drag devices has been used on an Air Force variable stability T-33 airplane during one of the first flight test studies of DSF. The drag force was provided by clam-shell type speed brakes located on modified wing-tip tanks [4].

1.3 Uses of DSF

Many potential uses have been suggested and/or verified for the DSF control functions, all inherently related since they are aimed at improving the accuracy or ease of negotiating some precise flying task. The McDonnell Aircraft Company has determined that the use of both the WLT and LT modes greatly increase dive bombing accuracy [12]. Other tasks which may benefit from DSF include tracking, station keeping, and cross-wind landing. Also, by integrating any or all of the DSF functions with the primary flight control system, the overall handling qualities of a vehicle may be enhanced.

2. PREVIOUSLY ESTABLISHED CRITERIA AND TEST RESULTS

2.1 Handling Qualities, Sensitivity, and Authority

General Dynamics, in contract with the Air Force Flight Dynamics Lab, has specified the three basic DSF modes for their YF-16 CCV flight test program [9,10]. The modes are designated Ay, β_1, and β_2 which correspond to WLT, FP, and LT. Since

one of the objectives of the program is DSF research, only basic guidelines have been specified. The most general guideline, and considered the most important, is that the additional functions will not degrade the reliability of the basic YF-16 flight control system, and that the augmented vehicle satisfy the requirements specified in the MIL-F-8785B document [14]. Other, more specific guidelines include a set of function definitions similar to those presented earlier, and an 'ideal' set of time responses, shown in Figures 2-4. These curves represent the best system obtainable from the YF-16 flight control system as per references 9 & 10. Other quantities which have been considered in the system development are given in Figure 5.

A joint Boeing/Navy investigation of DSF [1], utilizing both a moving and a fixed-base LTV F-8 simulation, yielded general criteria similar to that of the YF-16 CCV program. The simulation results were gathered for several different piloting tasks including 1) crosswind landings, 2)inflight refueling, 3) ground attack, and 4) weapons delivery. In all cases, a decoupled DSF system was utilized. An important result was that most pilots felt that a lateral acceleration range of .6 to 1.G's would be adequate for dive bombing and that this force would not adversely affect them.

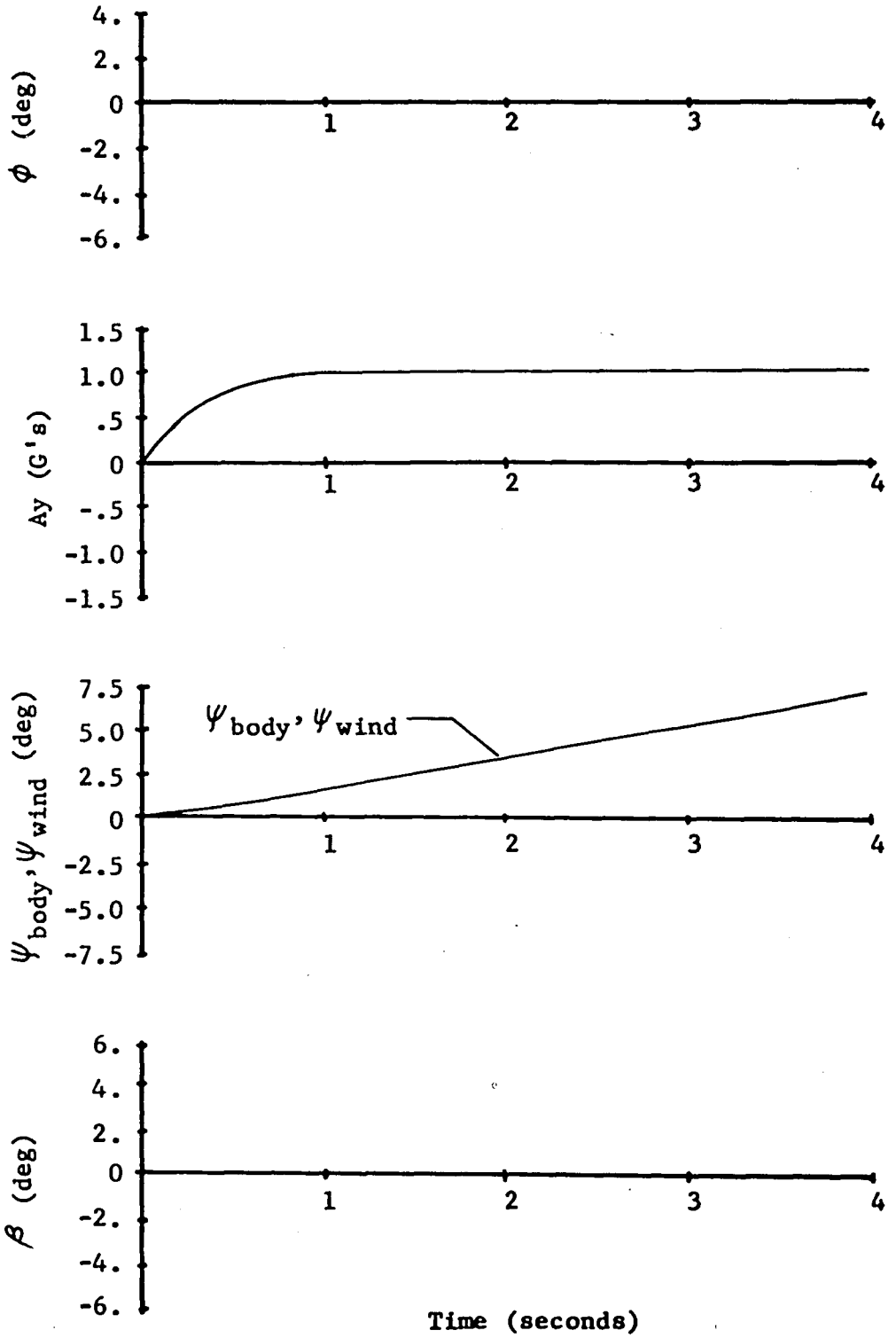

Figure 2. WLT Mode: Ideal System Response

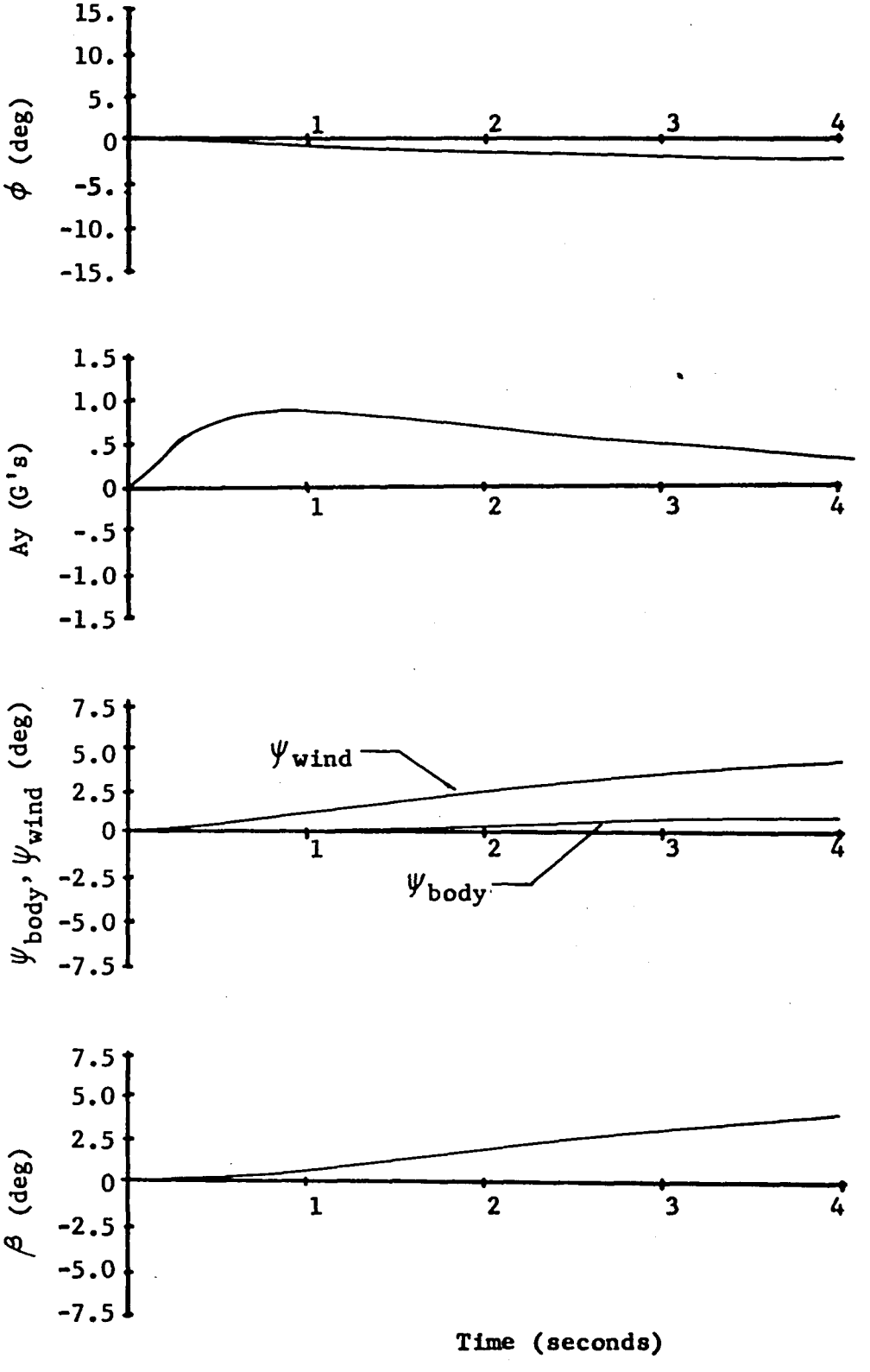

Figure 3. LT Mode: Ideal System Response

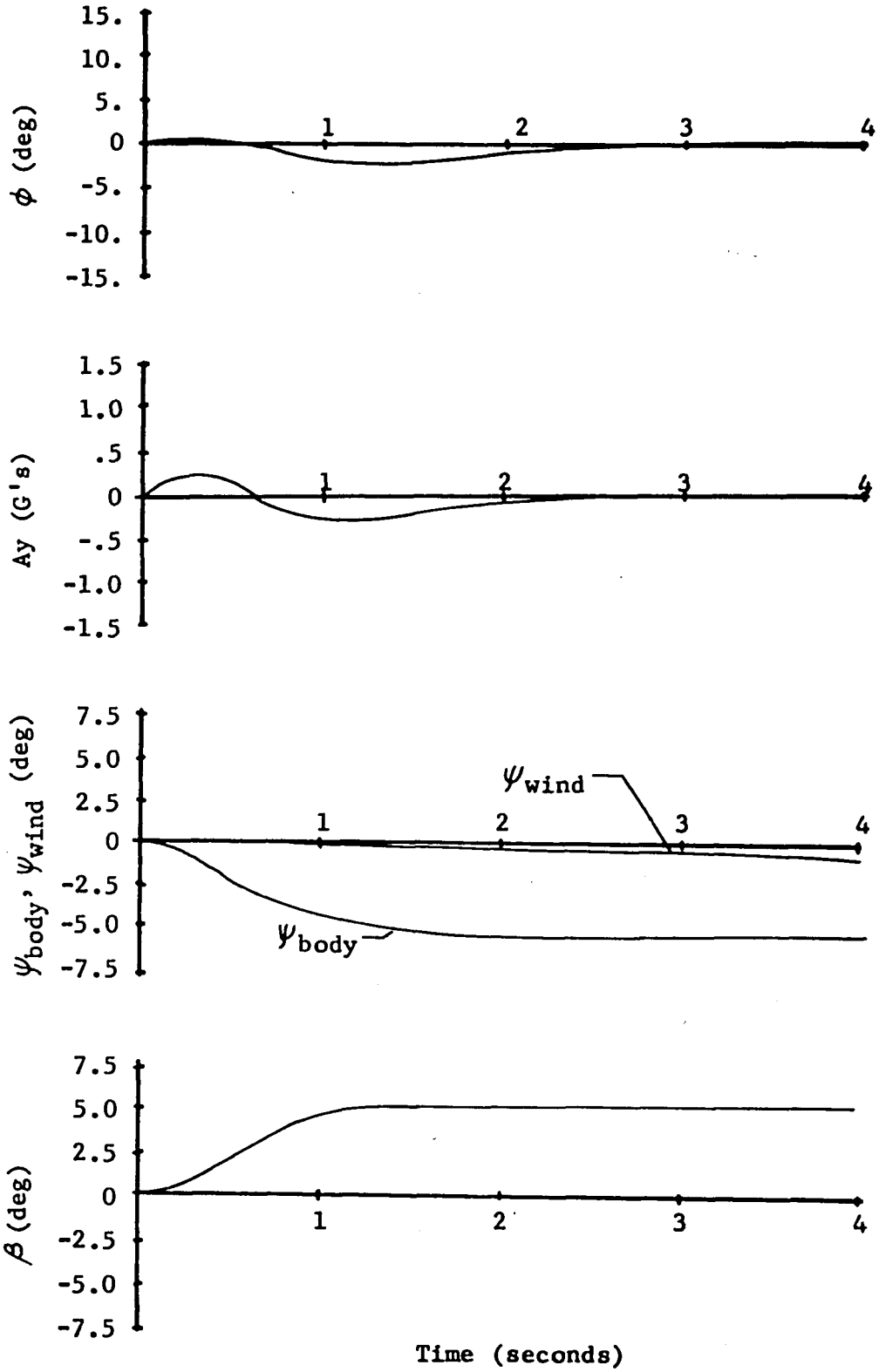

Figure 4. FP Mode: Ideal System Response

Pertinent CCV Criteria	Quantitative Data	Modes of Operation to be Analyzed *
A. Directional Response Characteristics Following Programmed (Step, Pulse) Inputs from the Rudder Pedals, Ay Mode and β Mode Controller	Damping, Period, Overshoots, and Rise Time of Significant Lateral-Directional Parameters (Ay, β , ψ_{wind}, ψ_{body}, ϕ)	1, 2, 3, 4
B. Time Required and Accuracy in Establishing and Holding a Prescribed Lateral Acceleration with Wings Level	Time to Settle within a Nominal Bandwidth of Desired Response, Steady State Accuracy, Workload Indicator (RMS Level of Controller Inputs)	1, 2
C. Time Required and Accuracy in Accomplishing a Prescribed Coordinated Flight Path Change with Wings Level	" " "	1, 2, 4
D. Time Required and Accuracy in Accomplishing a Prescribed Coordinated Flight Path Change by Use of Roll Control	" " "	1
E. Time Required and Accuracy in Establishing and Holding a Prescribed Yaw and Sideslip Angle Change with Zero Steady State Ay and Near Constant Ground Track	" " "	3

Figure 5. General Dynamics YF-16 CCV Design Criteria

Pertinent CCV Criteria	Quantitative Data	Modes of Operation to be Analyzed
F. Time Required and Accuracy in Establishing and Holding a Prescribed Sideslip Angle Change with Zero Steady State Ay and Near Constant Fuselage Pointing Direction (Ψ Body)	Time to Settle within a Nominal Bandwidth of Desired Response, Steady State Accuracy, Workload Indicator (RMS Level of Controller Inputs)	4
G. Precision Flying Tasks Evaluation - Air-to-Air Tracking; Air-to-Ground Weapon Delivery; Formation Flying; Tanker Refuel; Programmed Maneuver Flying	Statistical Tracking Accuracy, Weapons Delivery Accuracy (Aim Error in Air-to-Ground Delivery, Calculated Miss Distances, Circular Error Probable), Workload Indicators (RMS Level of Controller Inputs)	1, 2, 3, 4

* Modes of Operation

1. Conventional Operation - Normal YF-16 Configuration
2. Ay Mode (Direct Sideforce)
3. β 1 Mode (Fuselage Pointing)
4. β 2 Mode (Direct Flight Path Control)

Figure 5. General Dynamics YF-16 CCV Design Criteria (con't)

One of the first flight test studies of DSF was done by the Cornell Aeronautical Laboratory for the Air Force, utilizing a modified variable stability T-33 airplane [4]. The program objectives included the study of two DSF functions designated steady sideslip and steady yaw rate, corresponding to LT and WLT. As stated earlier, the mode mechanization was through rudder and asymmetrical drag device scheduling. The basic design criteria was qualitative, defining desired aircraft motion with the steady state specifications that $\phi = p = \dot{\beta} = r = \dot{r} = 0$ for the sideslip mode and $\phi = p = \beta = \dot{\beta} = \dot{r} = 0$ for the steady yaw rate mode. Figure 6 shows these schematically.

The major conclusions from the program were in the form of pilot comments and included the following:

- o In general, the system authority was too low. (The maximum lateral acceleration was .17 G, the maximum yaw rate was .5°/sec, and maximum steady state sideslip angle was 3.5°.)
- o The steady sideslip mode was not practical for controlling a lateral aim point during weapons delivery, but might be useful for station keeping, aerial refueling, or crosswind landing.
- o The DSF modes were found unsatisfactory when there was light dutch-roll damping, about $\delta_o = .1$; a damping ratio of $\delta_o = .7$ yielded very smooth operation.

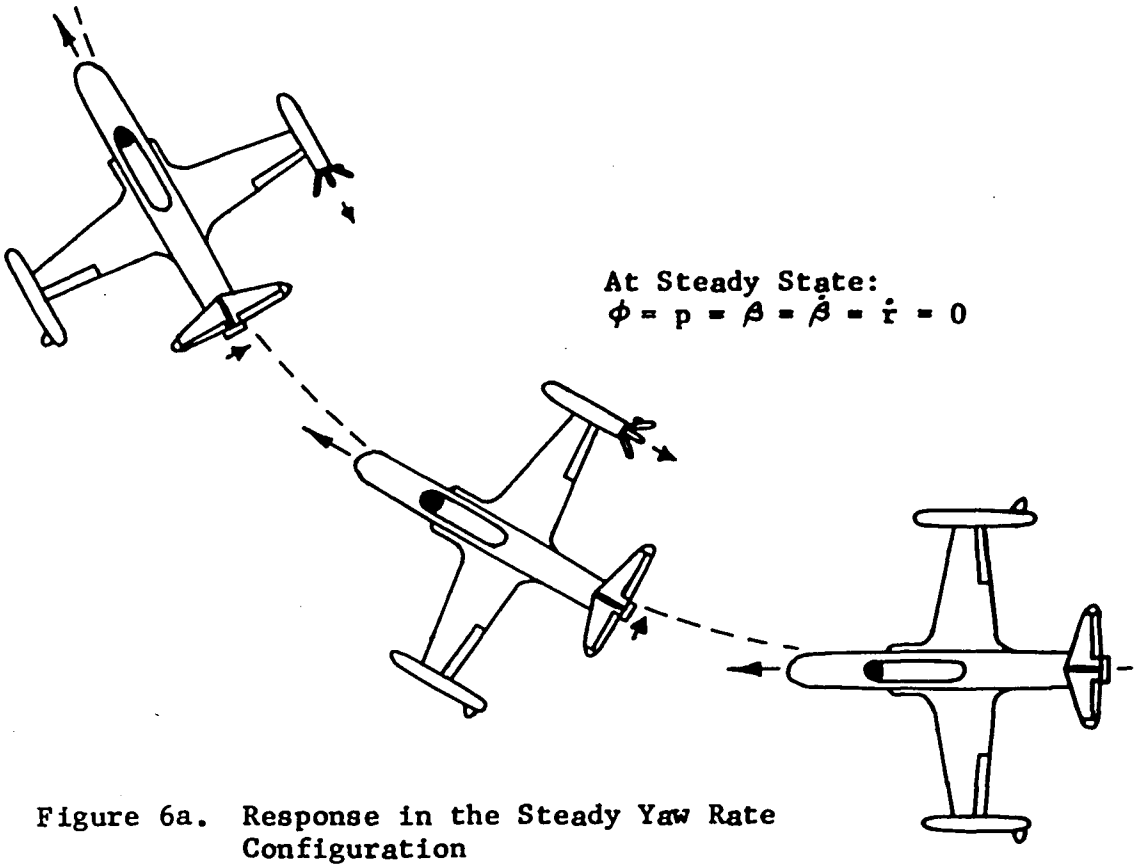

Figure 6a. Response in the Steady Yaw Rate Configuration

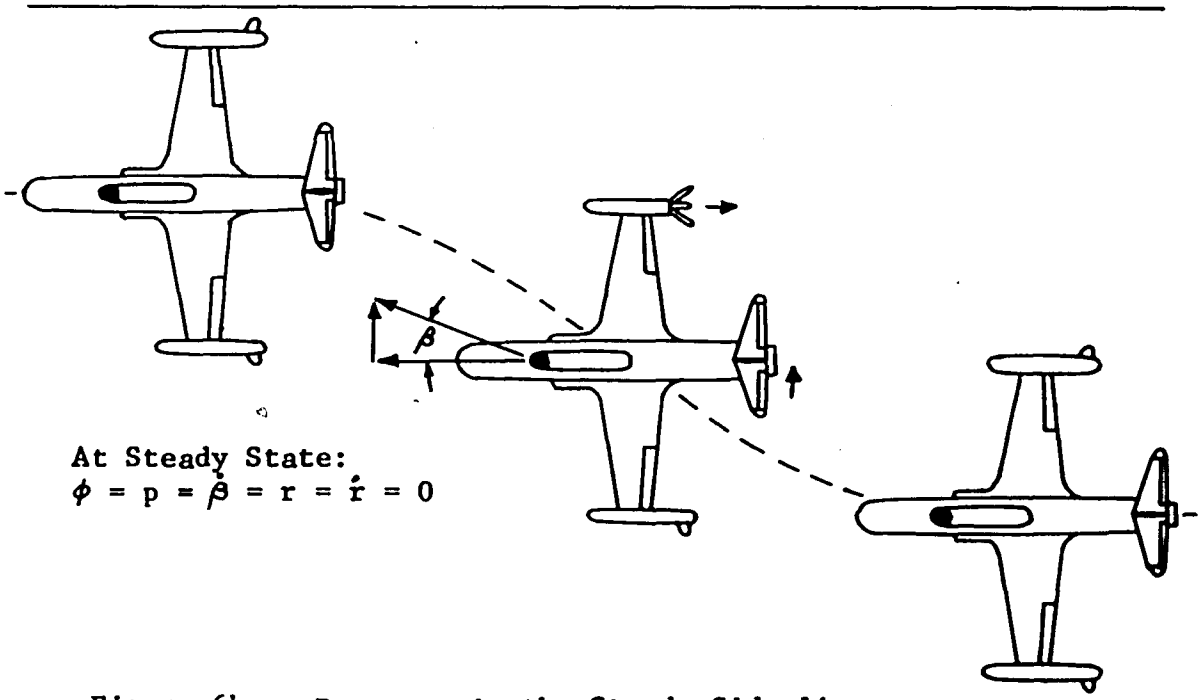

Figure 6b. Response in the Steady Sideslip Configuration

The most in-depth quantitative study that is available has been prepared by the McDonnell Aircraft Company (MCAIR) for the Air Force Flight Dynamics Lab [12]. The program involves using a fixed-base simulation to study the effectiveness of three DSF modes applied to a dive bombing task. The functions evaluated were the WLT mode and two LT modes: one which commanded a sideslip angle, designated LT-P, and one which commanded a sideslip rate, designated LT-I. The following major results were obtained from pilot comments:

- o The WLT mode was considered the most effective for increasing bombing accuracy.
- o The LT-P and LT-I modes were considered better than a conventional mode, but were not as effective as WLT for dive bombing, and the majority of pilots preferred LT-P over LT-I.
- o Both of the LT modes were considered impractical for dive bombing when used with a fixed bomb sight.

In addition, a set of design criteria goals were suggested not only for use during a dive bombing task, but for use in an overall design. It was determined that the high-order lateral acceleration transfer functions could be very closely modelled with a low-order system of the following form:

$$\frac{A_y}{\delta} = K \frac{s + a}{s^2 + 2\delta_y\omega_y s + \omega_y^2}$$

Frequency response matching was chosen over the time domain because of the greater generality. The design goal recommended for all three modes was

$a = 1.8$

$\delta_y = 1.6$

$\omega_y = 2.0$

with the level I flying quality limits of $a \leq 4.0$ and $\delta_y > .3$. An example of this frequency matching is shown in Figure 7.

Sensitivity and authority design goals were also suggested:

- For WLT and LT-I modes, a design goal of
  - 169 N/lat G rudder gradient
  - 1.0 G's lateral accel. authority
- with the level I flying quality limits of
  - 489.3 N/G maximum rudder gradient
  - 89 N/G minimum rudder gradient
  - 0.5 G's minimum lateral accel. authority

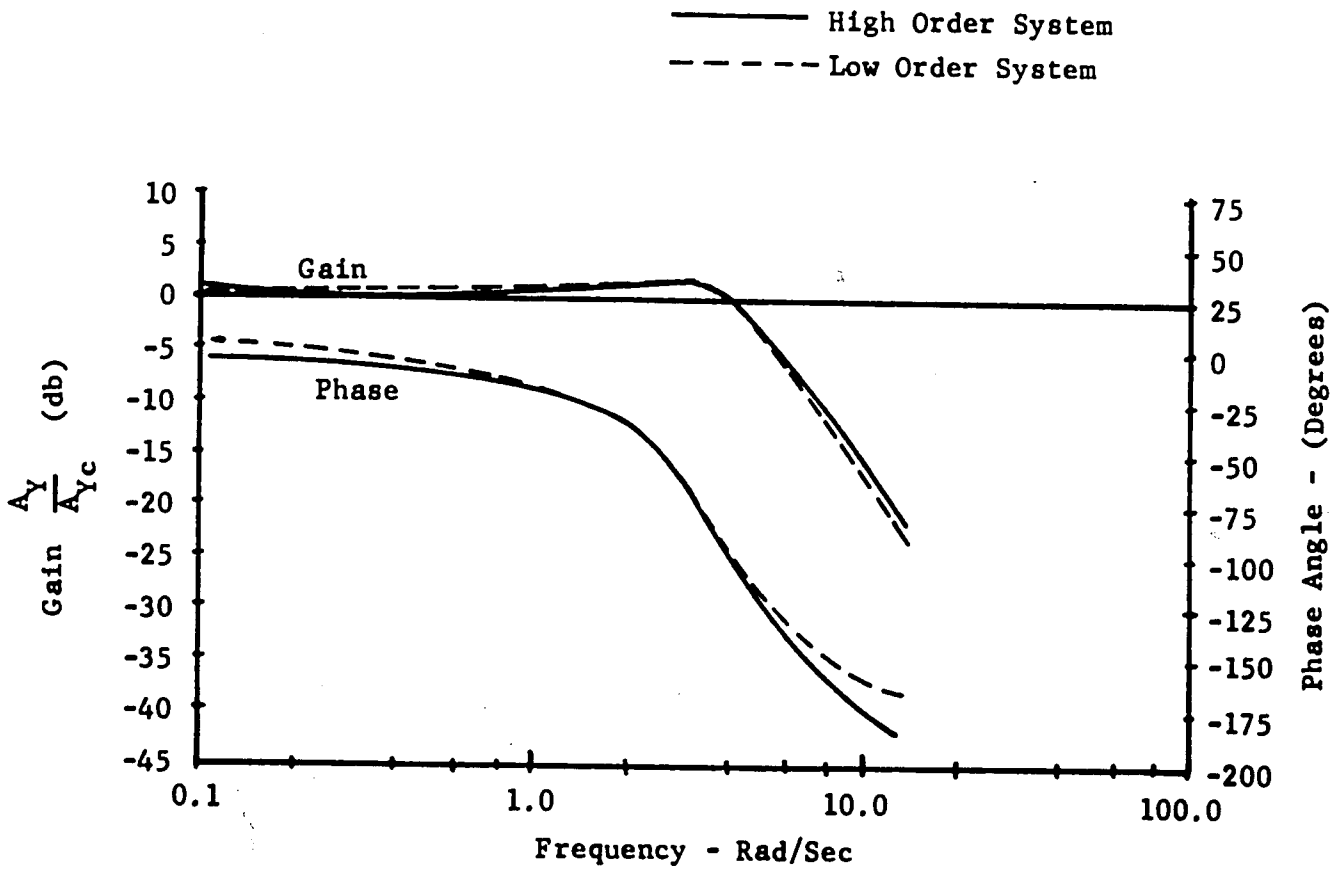

Note: A_{Yc} is the Commanded Steady State Lateral Acceleration

Figure 7. Example of McDonnell Aircraft Co. Ay/δ Frequency Matching

- o For the LT-P mode, a design goal of

  44.5 N/deg rudder gradient for $\delta_y \leq 1.2$

  31.1 N/deg rudder gradient for $\delta_y > 1.2$

  4.5 deg turn angle authority

  1.0 lateral acceleration authority (G's)

  - with the level I flying quality limits of

  75.6 N/deg maximum rudder gradient

  26.7 N/deg minimum rudder gradient for $\delta_y < 1.2$

  3 deg minimum turn angle authority

  0.5 G's minimum lateral acceleration authority

It was also determined that an uncoupled system yielded the best characteristics, with the following level I flying qualities limits:

- o WLT sideslip coupling limits

  $\beta/A_y \geq -2$ deg/G

  no positive limit set

- o Longitudinal coupling limits

  $\Delta A_z/A_y = 0.3$ steady state for WLT

  $\Delta A_z/A_y = 0.2$ transient for WLT

  $\Delta A_z/\beta = .025$ G's/deg, transient and steady state for LT-P

- o Roll coupling limits

  no negative coupling

  p/r = 8, maximum

2.2 Cockpit Controllers

The various types of cockpit controllers that have been considered for DSF control are:

1. Lateral control stick
2. Rudder pedals
3. Stick mounted force button
4. Brake pedals
5. Stick mounted rotational thumb wheel
6. Twist grip
7. Throttle mounted button

The twist grip, brake pedals, and rotational thumb wheel have been investigated only by the General Dynamics YF-16 Program. The twist grip was quickly discarded as an option due to the relatively large amount of roll-axis cross-talk during inputs. The brake pedals were also considered unsatisfactory because of inadvertent rudder pedal input and awkward foot position. The rotational thumb wheel was considered easy to coordinate, but has not been flight tested because of its unnatural location on the grip.

General Dynamics has also considered a stick mounted force button and conventional rudder pedals for DSF control. Both were deemed feasible and have been flight tested. The test pilots found the rudder pedals to be a natural input for all

three modes, but that 50% or less of full pedal movement should be used for maximum DSF input to prevent fatigue. The force button was found to have the disadvantage of a slight amount of roll-axis cross-talk, but was dual-axis, allowing DSF and longitudinal direct lift control simultaneously.

The Boeing study employed a conventional lateral control stick, conventional rudder pedals, and a throttle-mounted button for DSF control, but each method was used for a different mode, with no apparent comparisons made to determine a best mechanization. Pilot comments were favorable for all three modes.

The research program utilizing the variable stability T-33 [4] made comparisons between the conventional lateral stick, conventional rudder pedals and a non-centering stick-mounted button for DSF input. The lateral stick control was found to be very natural and easy to coordinate, but was disregarded since roll control was disabled while in a DSF mode. The thumb controller concept appeared feasible, but the type employed was awkward and confusing to the pilots since the button was not self-centering and did not have any noticeable artificial feel system. The rudder pedal control was the most natural and promising, but as in the General Dynamics study, it was recommended that full rudder pedal deflection not be used for full DSF input.

The study by the McDonnell Aircraft Company included both the rudder pedals and a stick-mounted force button for DSF control [12]. While performing only side force inputs, the pilots thought both controllers acceptable. The rudder pedals were chosen as most desirable, however, since operating the thumb button and bomb button simultaneously was extremely difficult during a dive bombing task.

A summary of the candidate cockpit controllers is given in Figure 8, including brief conclusions about each.

3. HiMAT VEHICLE [16,17]

3.1 -19 Configuration

The final design configuration for the HiMAT RPV has been designated the -19 and is shown in Figures 9 and 10. Its proposed operating envelope is shown in Figure 11.

The DSF mechanization is to be by scheduled asymmetrical inputs to the elevons, rudders, and canard surfaces. The elevons are the control surfaces on the trailing edge of the wing, next to and outboard of the rudder booms. The HiMAT vehicle also has ailerons which are not considered to be necessary for DSF control. As will be verified later, the amount of deflection of either the elevons or ailerons will be small so that the use of both is not warranted. Maximum specified deflections for the involved surfaces are as follows:

CONTROLLER \ STUDY	General Dynamics	Boeing	Cornell Aeronautical	McDonnell Aircraft
Lateral Stick	--	* Satisfactory	No Roll Control in DSF Mode	--
Rudder Pedals	* Should use only 50% Pedal Authority	* Satisfactory	* Natural, but Pedal Pressure Too High	* Natural Input
Stick-Mounted Force Button	* Some Roll Axis Cross-Talk	--	--	Awkward While Using Bomb Button
Stick-Mounted Thumb Button	--	--	Awkward and Confusing	--
Brake Pedals	Inadvertant Rudder Input; Awkward	--	--	--
Rotational Thumbwheel	Unnatural Location	--	--	--
Twist Grip	Too Much Roll Axis Cross-Talk	--	--	--
Throttle-Mounted Button	--	* Satisfactory	--	--

NOTE: An asterisk (*) denotes a preferred controller.

Figure 8. COCKPIT CONTROLLER SUMMARY

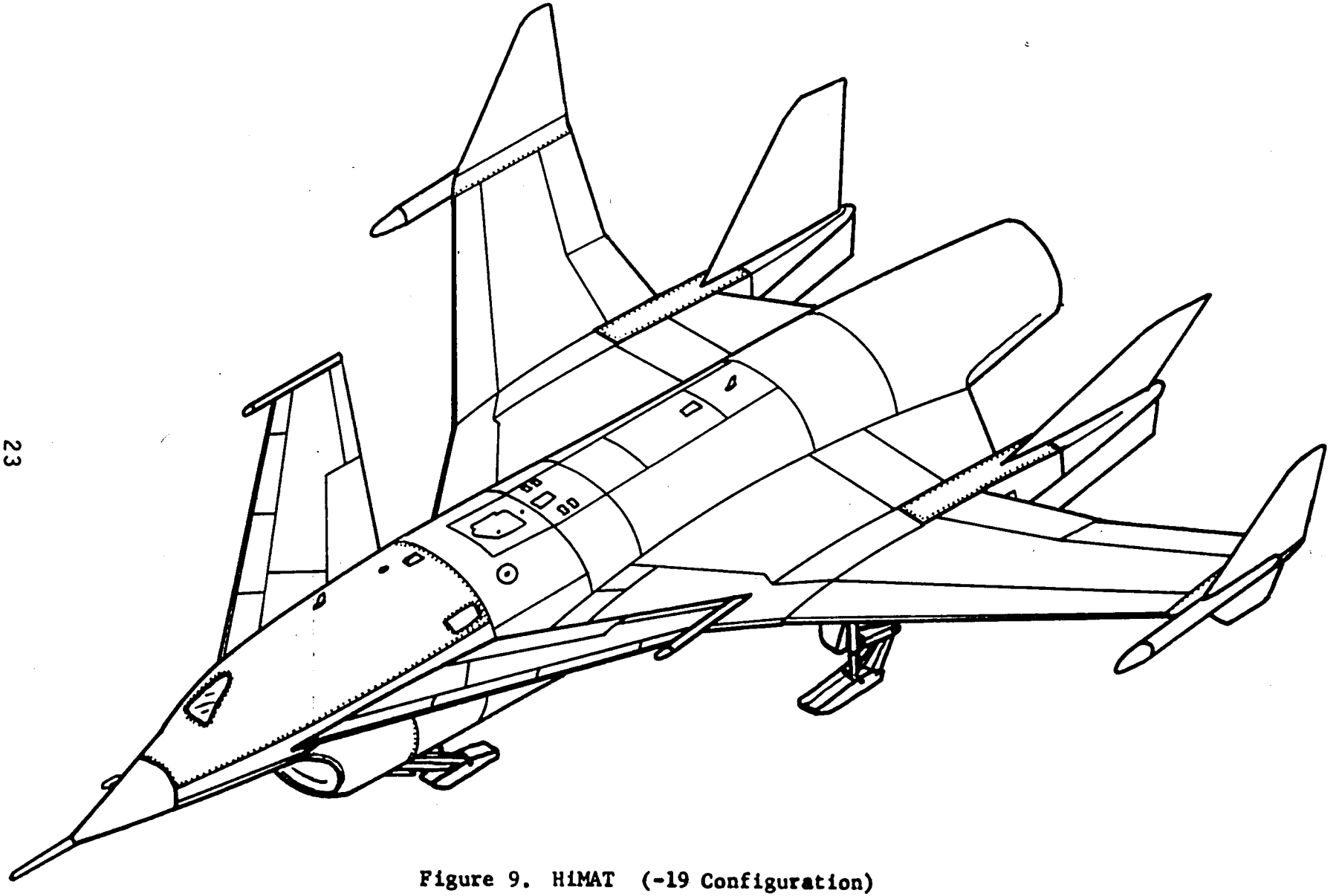

Figure 9. HiMAT (-19 Configuration)

Takeoff Gross Wt.*	1528.6 kg
Thrust/Wt. (Launch)	1.36
G-Limit (Struct)	12.0
Wing Area (launch)	5.40 m^2
Fuel Capacity *	285.76 kg
Center of Gravity	3.485 m
% Mean Aero. Chord	5.8

* Target Value

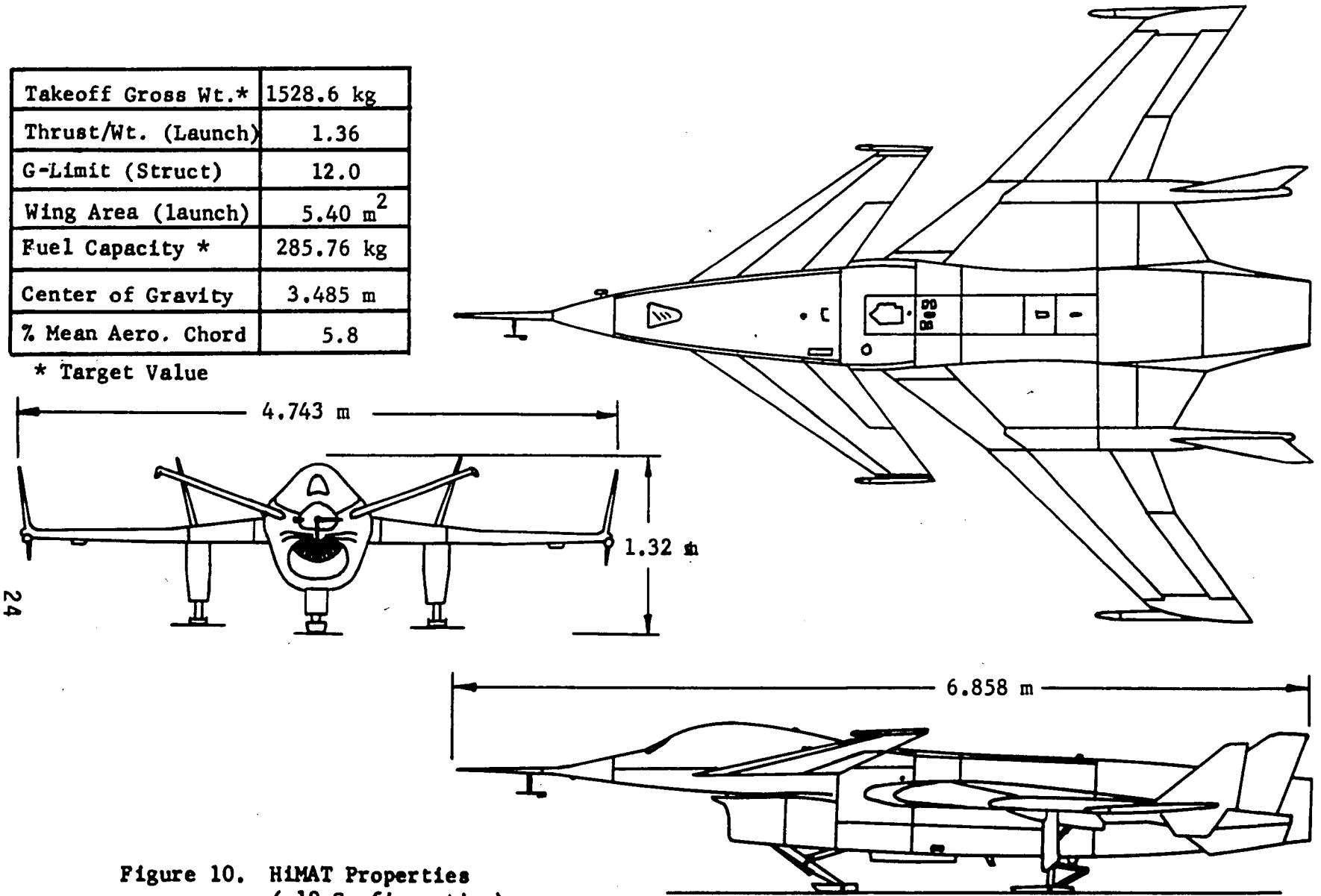

Figure 10. HiMAT Properties
(-19 Configuration)

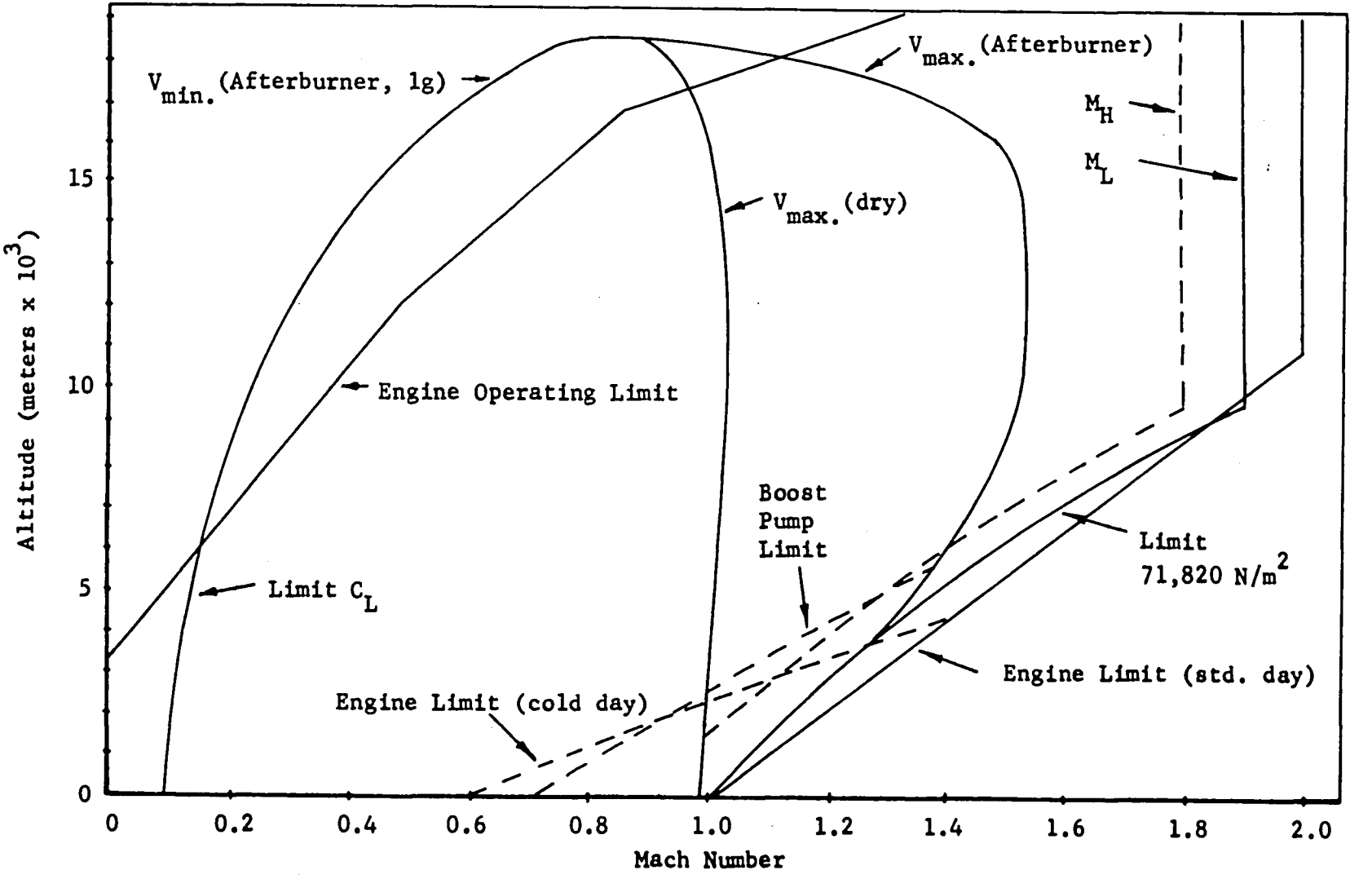

Figure 11. HiMAT Operating Envelope

Elevons +30°, -20°

Rudders ± 10°

Canards ± 20°

3.2. Primary Flight Control System

The basic flight control system as specified by Rockwell International at the time of this report is shown schematically in Figure 12. The gains are scheduled as per reference [17] and are subject to change.

4. DESIGN CRITERIA COMPARISON AND RECOMMENDATION

4.1 General

Throughout the design of a DSF system for the HiMAT vehicle, some conceptually basic constraints should be kept in mind. The vehicle will have a side force capability because of its design, but this was not a high priority objective during the early stages of the program. With this understood, it becomes apparent that the system under consideration will be an add-on to the basic flight control network. More explicitly, the DSF system should not change the general structure, or in any way degrade the overall quality of the primary system.

4.2. Vehicle Dynamics

4.2.1 Mode Definition

In order to obtain the most information from a DSF program, the HiMAT vehicle should be capable of all three modes -- wings level turn, fuselage pointing, and lateral translation. Consistent with previous programs, the WLT function should

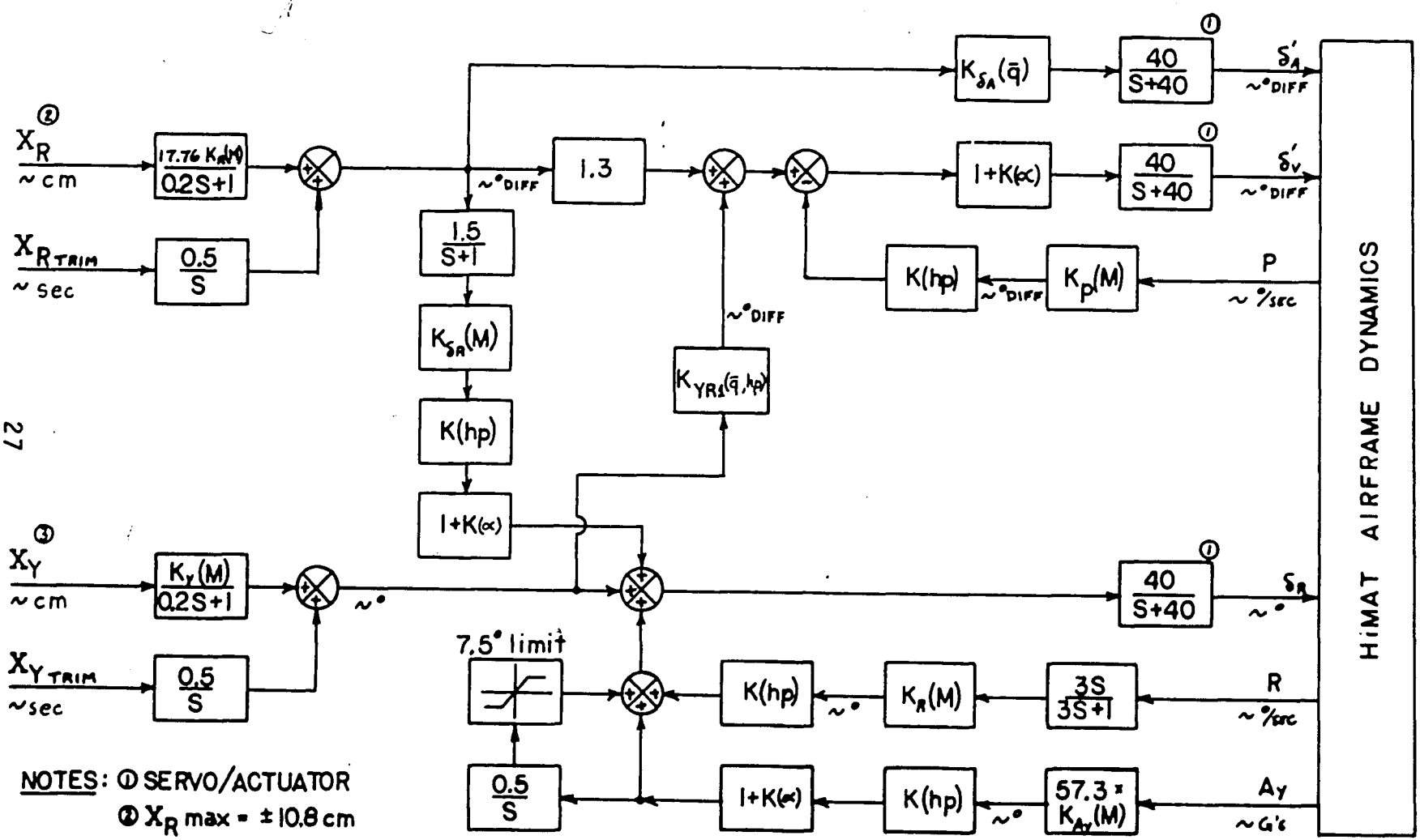

NOTES: ① SERVO/ACTUATOR
② X_R max = ±10.8 cm
③ X_Y max = ±8.89 cm
(left pedal fwd is pos)

Figure 12. HiMAT, Lateral-Directional Control System

command a proportional lateral acceleration with a minimum change in both sideslip and roll angles; the FP function should proportionally control yaw attitude and sideslip angle, with a minimum change in the lateral flight path and roll angles; and the LT mode should command a proportional change in flight path and sideslip angle, with a minimum change in yaw attitude and roll angle. The proportional LT mode has been chosen instead of the integral mode to allow for more rapid lateral changes without a requirement for 'integrating back' to stop lateral movement. It should be noted that FP and LT modes require equal, but opposite, steady state control surface input, the only major difference arising during the transient period.

A normalized set of step input time histories can also be used to define the DSF mode characteristics. These are presented in Figures 13-15 and are similar to those used by General Dynamics [9, 10], with minor changes to the A_y responses since lateral acceleration of the HiMAT vehicle will be measured at the C.G. rather than at the pilot station. These curves are to be used as guidelines rather than as precise definitions.

4.2.2 Quantitative Criteria

Initial considerations should be given to the dutch roll requirements of MIL-F-8785B (military specifications) for class IV aircraft operating in a category A, level I flight environment. Figure 16 summarizes these limits in graphical form.

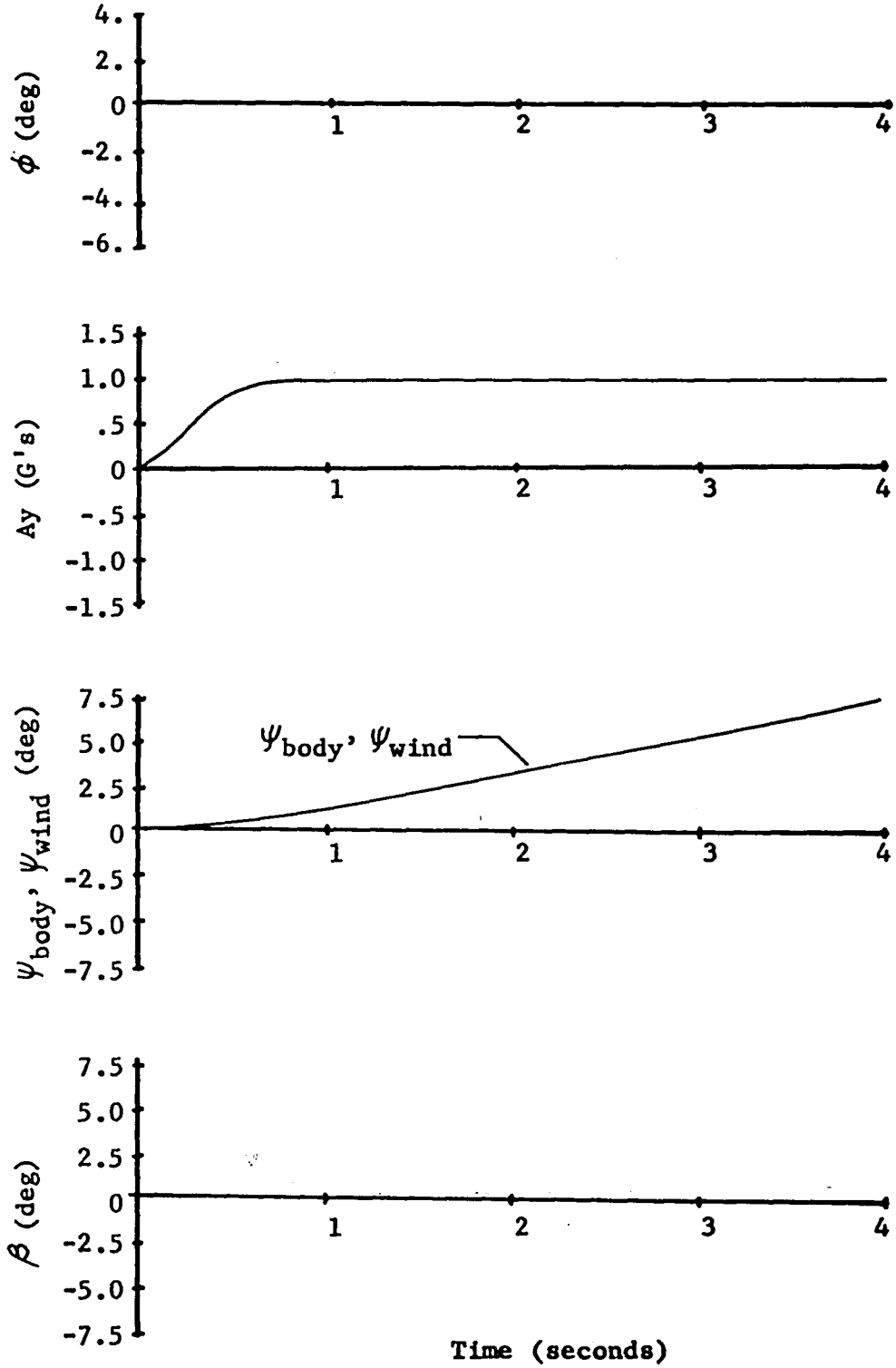

Figure 13. WLT Mode: Normalized Ideal System Response Recommended for HiMAT

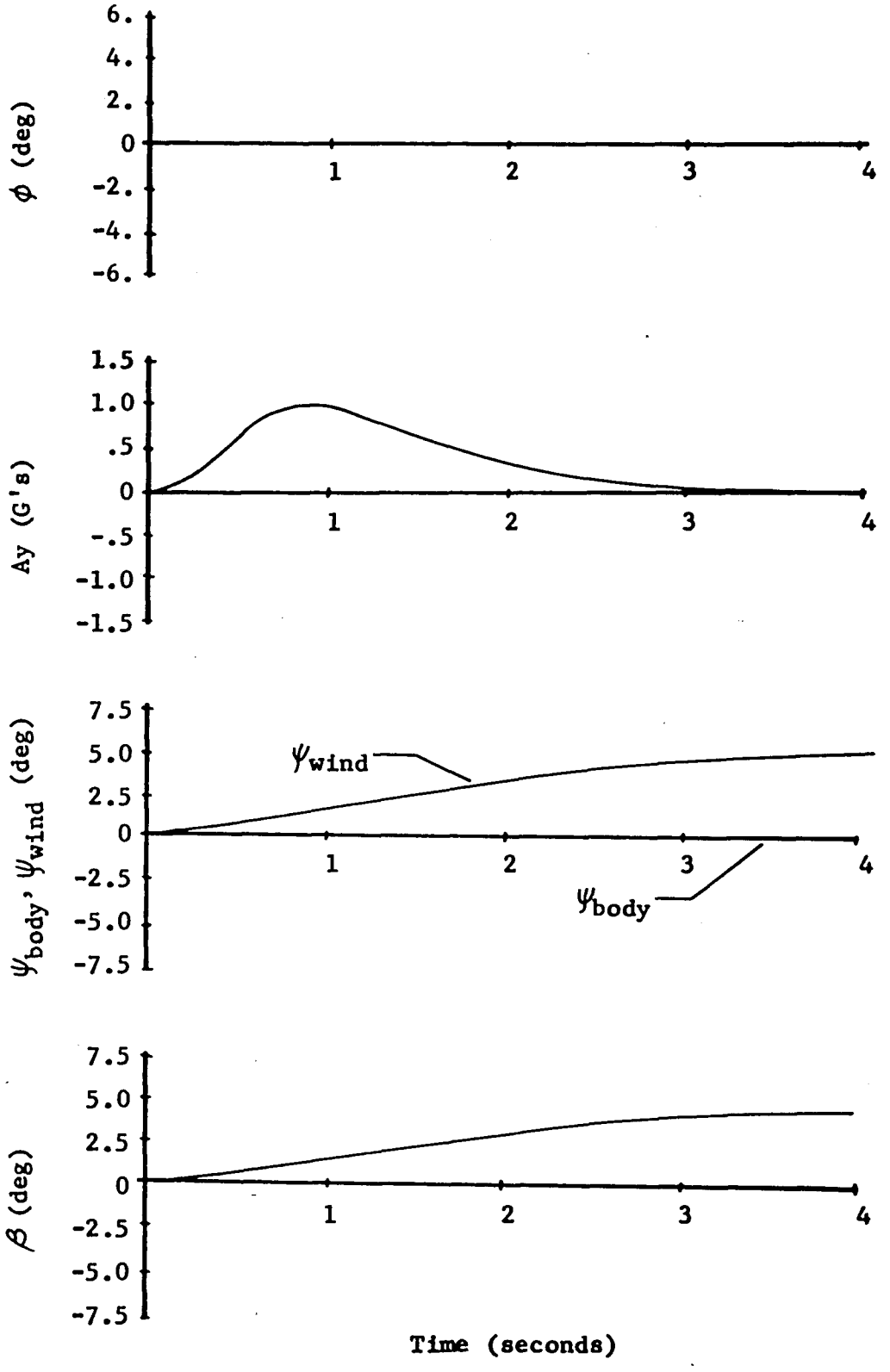

Figure 14. LT Mode: Normalized Ideal System Response Recommended for HiMAT

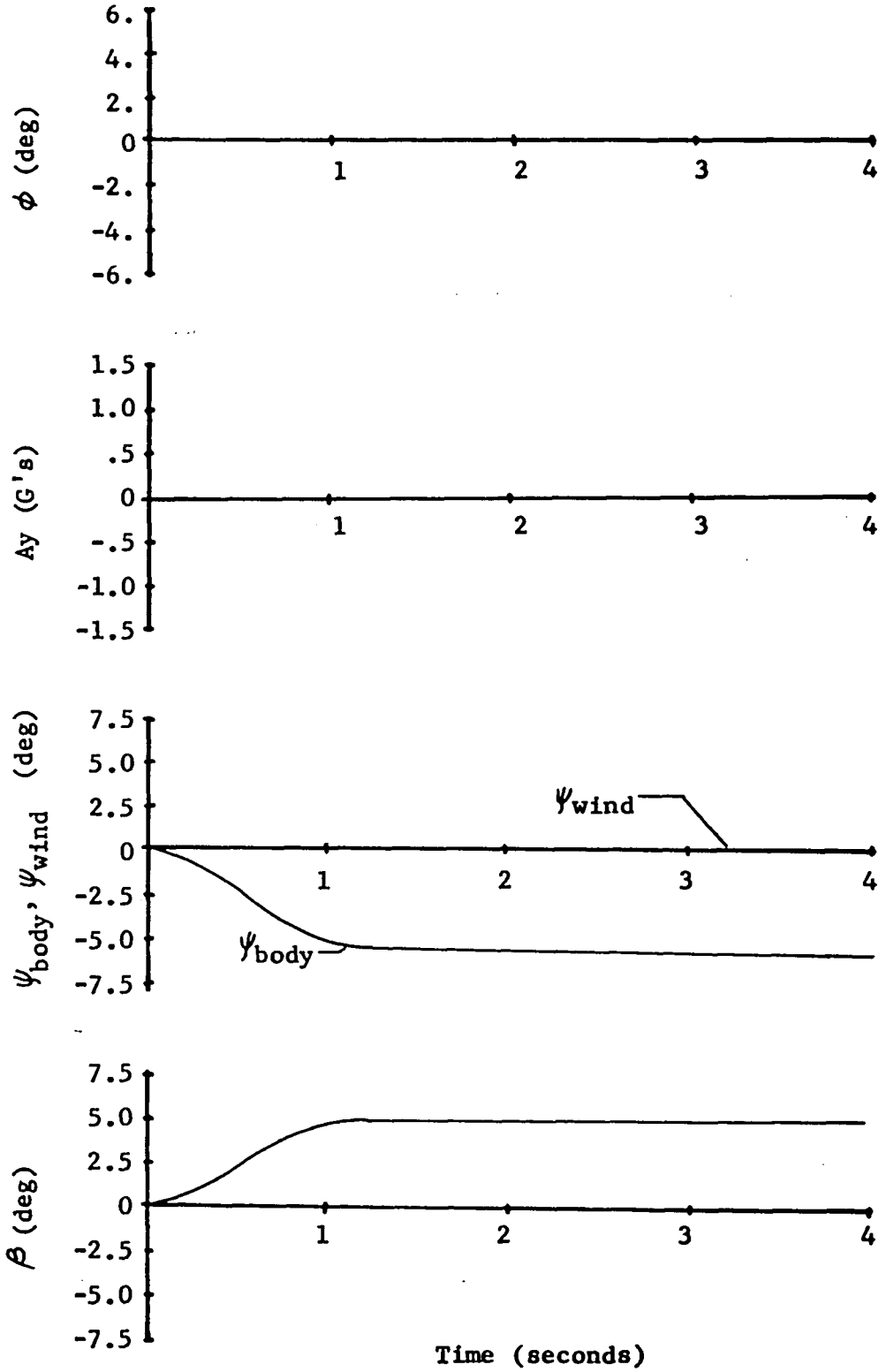

Figure 15. FP Mode: Normalized Ideal System Response Reccomended for HiMAT

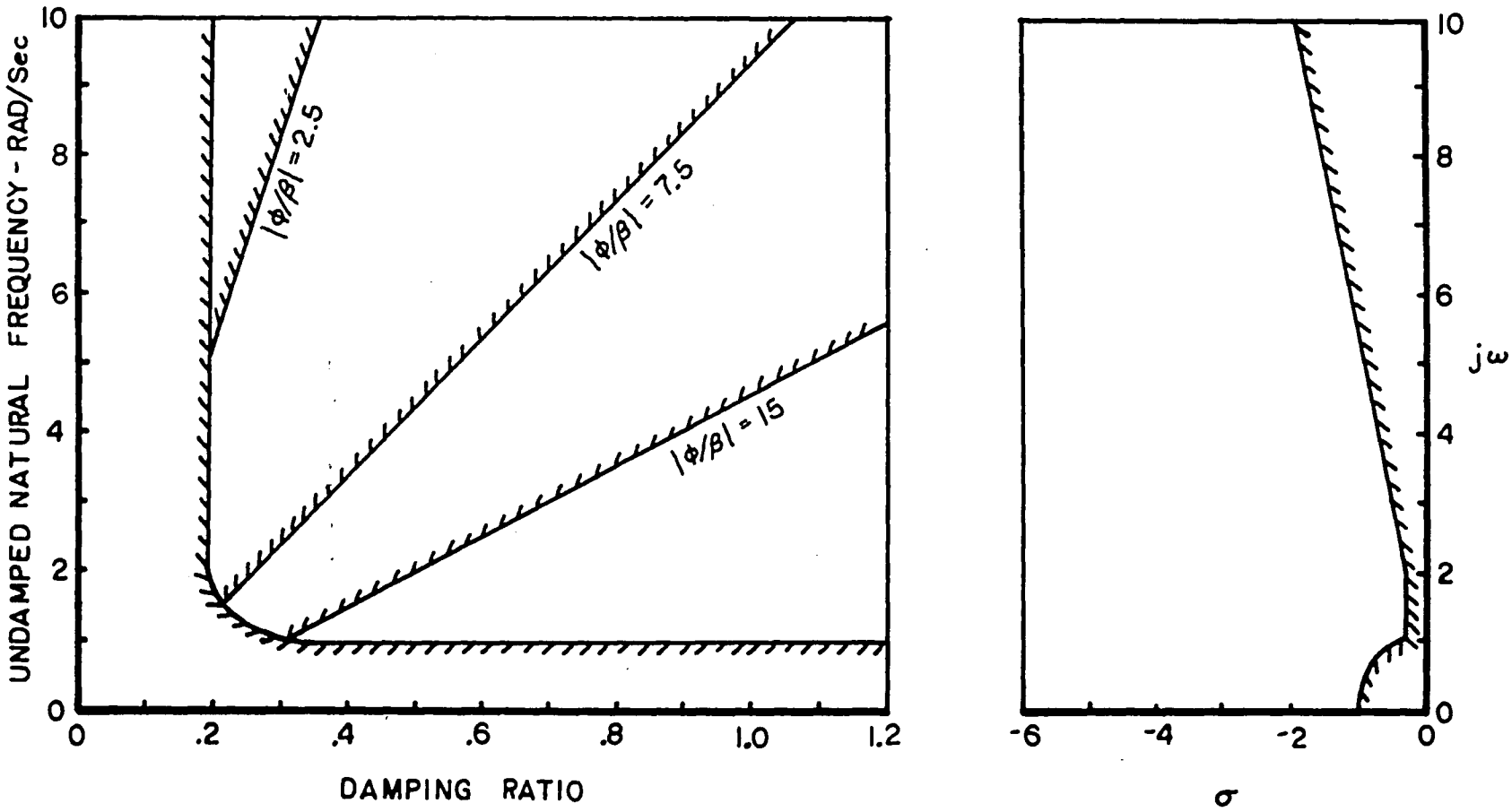

Figure 16. Military Specifications for Dutch Roll

Secondly, the reports cited earlier have concluded that a completely uncoupled DSF system yields the best overall handling qualities, and level I flying quality limits have been recommended by the McDonnell Aircraft Company [12] for non-ideal systems. These limits are:

- o WLT sideslip coupling limits

  $\Delta A_y \geq -2$ deg/G

  no positive limit set

- o Longitudinal coupling limits

  $\Delta A_z/A_y = 0.3$ steady state for WLT

  $\Delta A_z/A_y = 0.2$ transient for WLT

  $\Delta A_z/\beta = .025$ G's/deg, transient and steady state for LT-P

- o Roll coupling limits

  $0 \leq p/r \leq 8.$

Finally, again on recommendation from the McDonnell Aircraft Company report [12], a low-order frequency response model would be specified, to be a design goal for the higher-order responses. For the WLT mode, the model applies to the lateral acceleration response and has the form

$$\frac{A_y}{\delta} = K \frac{s + a}{s^2 + 2\delta_y w_y s + w_y^2}$$

where

$a = 1.8$

$\delta_y = 1.6$

$w_y = 2.0$

with the design limits that $a < 4.0$ and $\delta_y < 0.3$.

For the FP and LT modes, the model applies to the sideslip response rather than lateral acceleration, but still retains the same form, design values, and design limits. The sideslip angle response is used for these modes since that is what is commanded, rather than lateral acceleration which has a zero steady state value. Figure 17 shows this frequency response model.

4.3. Cockpit Controllers

Based on the literature survey, the method of cockpit control for all three DSF functions should be the rudder pedals. The main arguments for this choice are as follows:

- Except during slow flight maneuvers such as takeoff and landing, piloting of class IV aircraft can be accomplished without rudder control, leaving the pedals free.
- Most test pilots have found pedal control very natural and easy to coordinate.

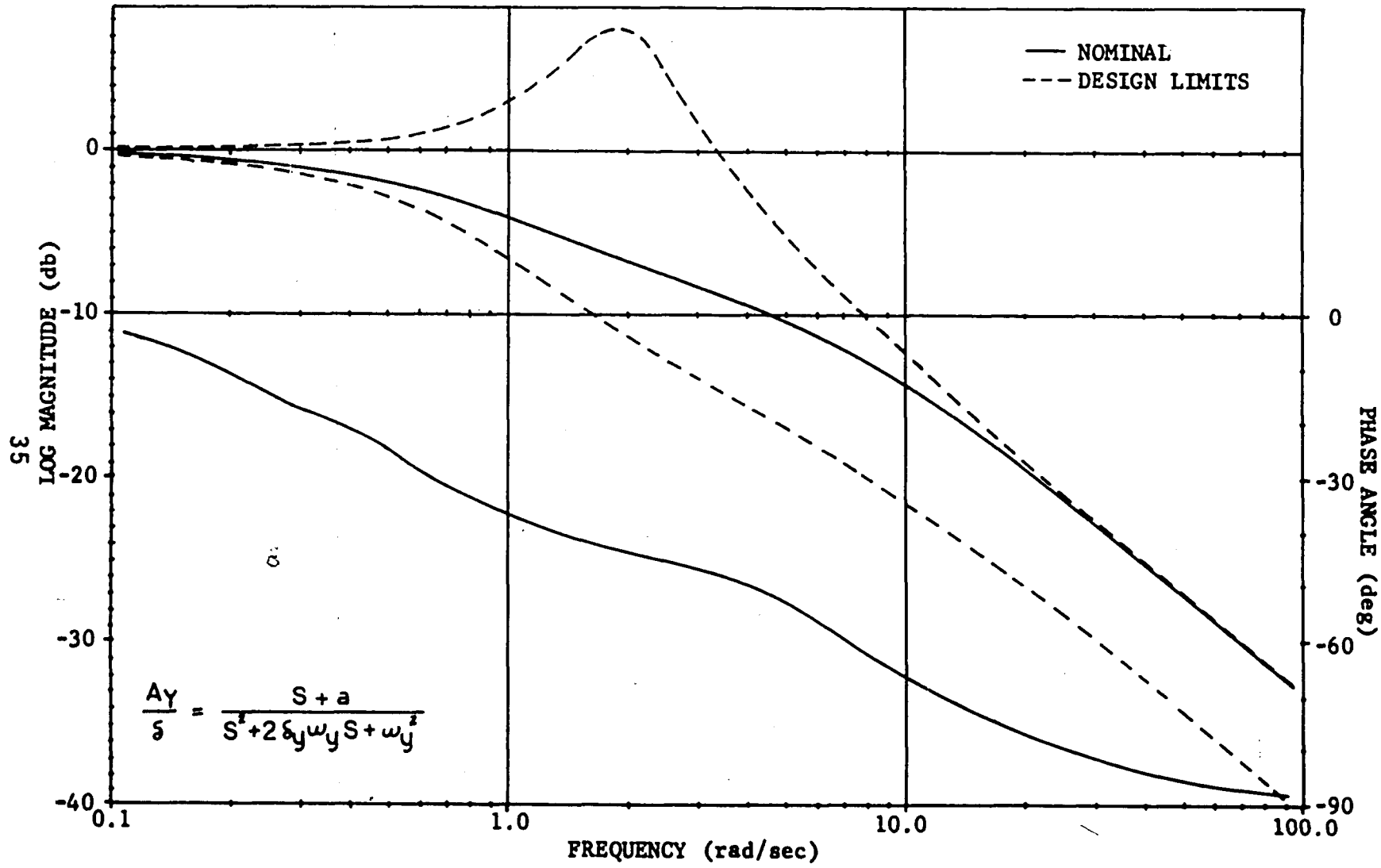

Figure 17. Frequency Response Model for Lateral Acceleration

- o Rudder pedal control seems to be insensitive to external forces, resulting in a less demanding piloting task.

The stick-mounted force button, which was the other candidate for a controller, was not selected due to the added work load on the pilot's right hand. Also, the force button would replace the trim button which would have to be relocated, adding to pilot confusion.

Finally, a three position switch should be included in the cockpit to allow DSF mode selection.

4.4 Sensitivity and Authority

The sensitivity and authority of the DSF control system should be as follows:

- o For WLT mode, a design goal of
  - 155.7 N/lateral G rudder gradient
  - 1.0 G's lateral acceleration authority
  - with the level I flying quality limits of
  - 89. $\leq X_R \leq$ 444.8 N/G rudder gradient
  - 0.25 G's minimum lateral acceleration authority
- o For LT mode, a design goal of
  - 35.6 N/deg rudder gradient
  - 4.5 deg turn angle authority
  - 1.0 lateral acceleration authority

- with the level I flying quality limits of

  $22.24 \leq X_R \leq 66.72$ N/deg rudder gradient

  3 deg minimum turn angle authority

  0.25 G's minimum lateral acceleration authority

o For FP mode, a design goal of

  35.6 N/deg rudder gradient

  4.5 deg sideslip angle authority

- with the level I flying quality limits of

  $22.24 \leq X_R \leq 66.72$ N/deg rudder gradient

  3 deg minimum sideslip angle authority

The maximum lateral acceleration authority may be increased for HiMAT within physical limitations (such as load factors) since pilot comfort will not be a factor.

4.5. Special Note on LT Mode

The lateral translation mode will not be considered in the following Direct Side Force system design for the HiMAT vehicle. The reasons for this are two-fold. All of the studies previously mentioned concentrated mainly on the mechanization, system response, and/or pilot reactions to direct side force. They did not consider to any great deal the practical uses of the specific modes.

This author feels that of the three possible choices, the lateral translation mode will be the least useful. This stems from the realization that while in LT there is no possibility for a commanded change of heading. This would be a great disadvantage if the vehicle were to encounter a wind shear which would generate a yawing moment while in a landing or refueling maneuver.

Secondly, initial calculations showed that a more complicated control system is necessary for the LT mode than for either WLT or FP. It must be pointed out that the LT and FP modes are very similar to each other, differing only in the transient portion of the maneuver. In lateral translation, the beginning transient yields a net non-zero lateral acceleration to the vehicle, imparting a velocity in the Y direction. The fuselage pointing transient ideally creates no acceleration in the lateral direction so that the flight path is not altered. The steady state portions of the two modes are identical with only a change in direction of the sideslip angle.

Under the initial study, two methods had been considered for generating lateral velocities with no heading change. The first was to utilize the WLT mode while simultaneously employing a heading hold autopilot function. There would be a possibility, however, that these combined systems might negate one

another creating very little motion at all. The other method was to alter the fuselage pointing system so that a finite lateral acceleration would indeed be given to the vehicle. This promised to create more complicated filtering and/or feedback systems than the usefulness of the mode warranted.

Since the following Direct Side Force system design will consider only the WLT and FP modes, it will need only a two position switch in the cockpit.

5. DIRECT SIDE FORCE SYSTEM DYNAMICS

For reasons which are readily apparent, the study of the system dynamics is divided into two sections: 1) steady state, and 2) transient response. The steady state work is relatively straightforward, compared to the transients, so this will be considered first.

5.1 Steady State

5.1.1 Interconnect Gain Calculation

Given the fixed physical configuration and the accompanying aerodynamic data of the HiMAT vehicle, there can only be certain relative combinations of control surface deflections which yield the desired steady state flight characteristics for a given DSF mode. These control surface deflections are expressed as interconnect gains and their approximation may be calculated by imposing the correct assumptions for the desired

steady state conditions on the small-perturbation aircraft equations of motion. As previously stated, the DSF mechanization will be through asymmetric canards, rudder, and elevon usage.

The general, linearized, small-perturbation, 3 DOF lateral-directional equations are:

$$\begin{bmatrix} 1 & -\frac{I_{xz}}{I_{xx}} & 0 & 0 \\ -\frac{I_{xz}}{I_{zz}} & 1 & 0 & 0 \\ 0 & 0 & 1 & 0 \\ 0 & 0 & 0 & 1 \end{bmatrix} \begin{bmatrix} \dot{p} \\ \dot{r} \\ \dot{\phi} \\ \dot{\psi} \end{bmatrix} = \begin{bmatrix} \ell_p & \ell_r & 0 & \ell_\beta \\ N_p & N_r & 0 & N_\beta \\ 1 & 0 & 0 & 0 \\ \alpha_T+Y_p & Y_r-1 & \frac{g}{V} & Y_\beta \end{bmatrix} \begin{bmatrix} p \\ r \\ \phi \\ \beta \end{bmatrix}$$

$$+ \begin{bmatrix} \ell_{\delta_V'} & \ell_{\delta_C'} & \ell_{\delta_R} \\ N_{\delta_V'} & N_{\delta_C'} & N_{\delta_R} \\ 0 & 0 & 0 \\ Y_{\delta_V'} & Y_{\delta_C'} & Y_{\delta_R} \end{bmatrix} \begin{bmatrix} \delta_V' \\ \delta_C' \\ \delta_R \end{bmatrix} .$$

For any wings-level, steady-state, DSF mode, we can impose the following assumptions:

$$V = \text{constant}$$

$$\dot{\phi} = 0$$

$$\ddot{\phi} = 0$$

$$\dot{\alpha} = 0$$

$$\ddot{\psi} = 0$$

$$\phi = 0$$

$$\dot{\beta} = 0$$

The equations thus reduce to:

$$\begin{bmatrix} | \\ 0 \\ | \end{bmatrix} = \begin{bmatrix} \ell_r & \ell_\beta \\ N_r & N_\beta \\ Y_r - 1 & Y_\beta \end{bmatrix} \begin{bmatrix} r \\ \beta \end{bmatrix} + \begin{bmatrix} \ell_{\delta'_V} & \ell_{\delta'_C} & \ell_{\delta_R} \\ N_{\delta'_V} & N_{\delta'_C} & N_{\delta_R} \\ Y_{\delta'_V} & Y_{\delta'_C} & Y_{\delta_R} \end{bmatrix} \begin{bmatrix} \delta'_V \\ \delta'_C \\ \delta_R \end{bmatrix}$$

It should be noted that there are now only three equations rather than the original four, since the $\dot{\phi}$ equation became trivial and was dropped.

5.1.1.1 Wings Level Turn Mode

During steady state in the WLT mode, there are also the conditions that

$$\beta = 0$$

and

$$\dot{\psi} = g \frac{A_y}{V} = \text{constant}.$$

When these are applied, the equations are further simplified to yield finally:

$$\begin{bmatrix} 0 \\ 0 \\ 0 \end{bmatrix} = \begin{bmatrix} \ell_r \\ N_r \\ Y_r - 1 \end{bmatrix} g \frac{A_y}{V} + \begin{bmatrix} \ell_{\delta_v'} & \ell_{\delta_c'} & \ell_{\delta_R} \\ N_{\delta_v'} & N_{\delta_c'} & N_{\delta_R} \\ Y_{\delta_c'} & Y_{\delta_c'} & Y_{\delta_R} \end{bmatrix} \begin{bmatrix} \delta_v' \\ \delta_c' \\ \delta_R \end{bmatrix} .$$

This may now be solved for the interconnect ratios δ_v'/δ_c' and δ_R/δ_c', and also for the control authority ratio A_y/δ_c'. The solution becomes

$$\frac{\delta_R}{\delta_c'} = \frac{F/D - C/A}{B/A - E/D}$$

$$\frac{\delta_v'}{\delta_c'} = \frac{1}{A}\left(B \frac{\delta_R}{\delta_c'} + C\right)$$

$$\frac{A_y}{\delta_c'} = \frac{V}{g\ell_r}\left(\ell_{\delta_v'} \frac{\delta_v'}{\delta_c'} + \ell_{\delta_R} \frac{\delta_R}{\delta_c'} + \ell_{\delta_c'}\right) ,$$

where

$$A = \left(\frac{\ell_{\delta_v'}}{\ell_r} - \frac{N_{\delta_v'}}{N_r}\right)$$

$$B = \left(\frac{\ell_{\delta_R}}{\ell_r} - \frac{N_{\delta_R}}{N_r}\right)$$

$$C = \left(\frac{\ell_{\delta_c'}}{\ell_r} - \frac{N_{\delta_c'}}{N_r}\right)$$

$$D = \left(\frac{\ell_{\delta_v'}}{\ell_r} - \frac{Y_{\delta_v'}}{Y_r - 1}\right)$$

$$E = \left(\frac{\ell_{\delta_R}}{\ell_r} - \frac{Y_{\delta_R}}{Y_r - 1}\right)$$

$$F = \left(\frac{\ell_{\delta_c'}}{\ell_r} - \frac{Y_{\delta_c'}}{Y_r - 1}\right).$$

This solution was programmed on a CDC Cyber 70 Digital Computer and solved to obtain values at points throughout the entire HiMAT flight envelope. The input data was read from a magnetic tape supplied to NASA, Dryden FRC by R. I. per reference [17].

Some of the results that were deemed most useful have been plotted versus Mach number, angle of attack, and altitude in Figures 18, 19, 20, and 21. Notice the extreme nonlinearity around the Mach 1 flight regime. The values for both the δ_V'/δ_C' and δ_R/δ_C' ratios vary very little with altitude. Thus, the values for an altitude of 9,144 m. (30,000 ft.) have been chosen as a mean for control system calculations throughout the flight envelope.

It can be seen from the graphs that the canard surfaces will attain the greatest deflections, while the rudder and elevons will be used mostly for trimming the vehicle to the desired steady state attitude. Because of this, the A_y/δ_C' ratio yields the maximum system authority given the maximum allowable canard surface deflection. For example, at mach .8 and 9,144 m. altitude and at an angle of attack of 0°, given a maximum differential canard deflection of 40°, the HiMAT vehicle will be capable of $\simeq$ 0.3 G's lateral acceleration.

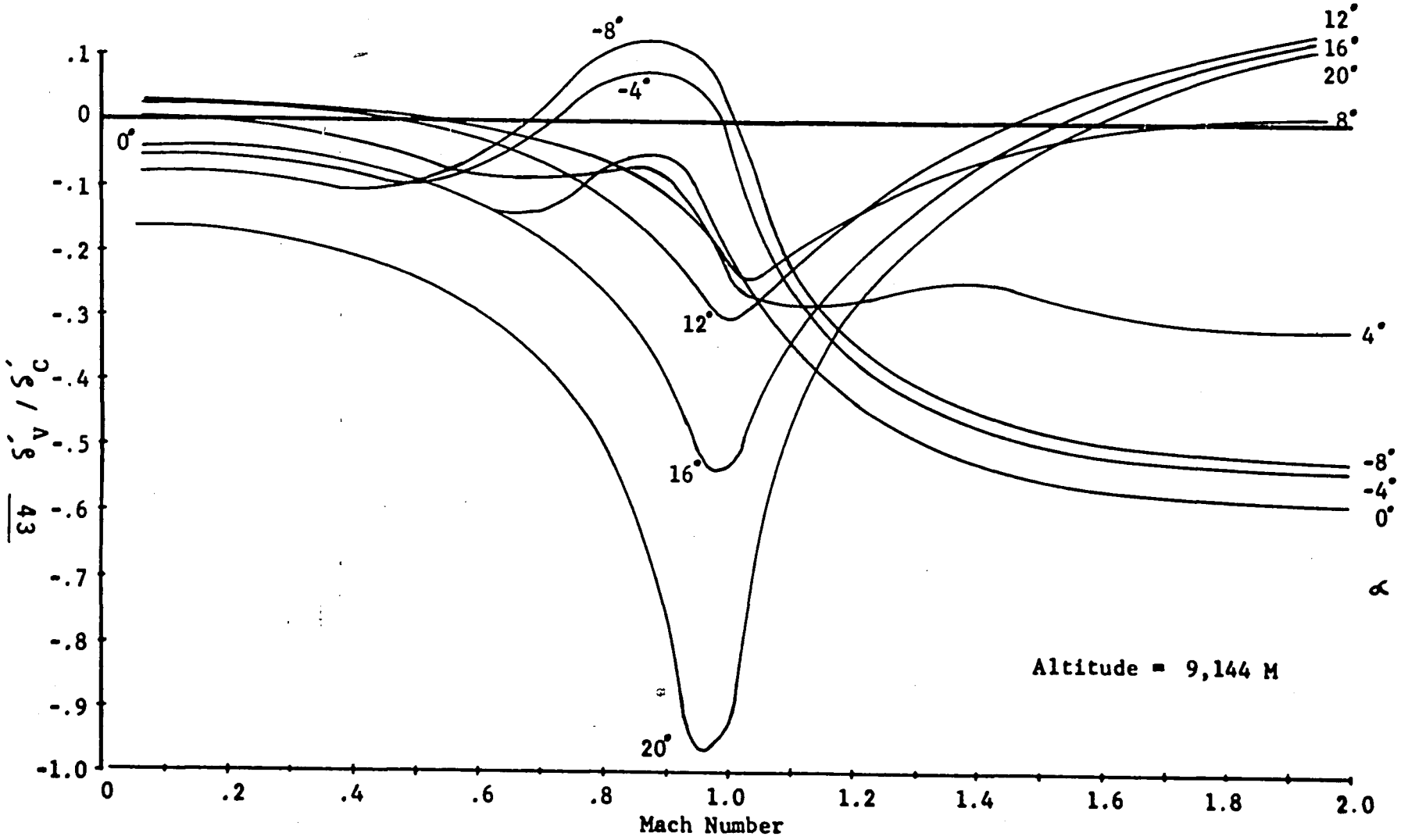

Figure 18. WLT Mode: Elevon to Canard Ratio

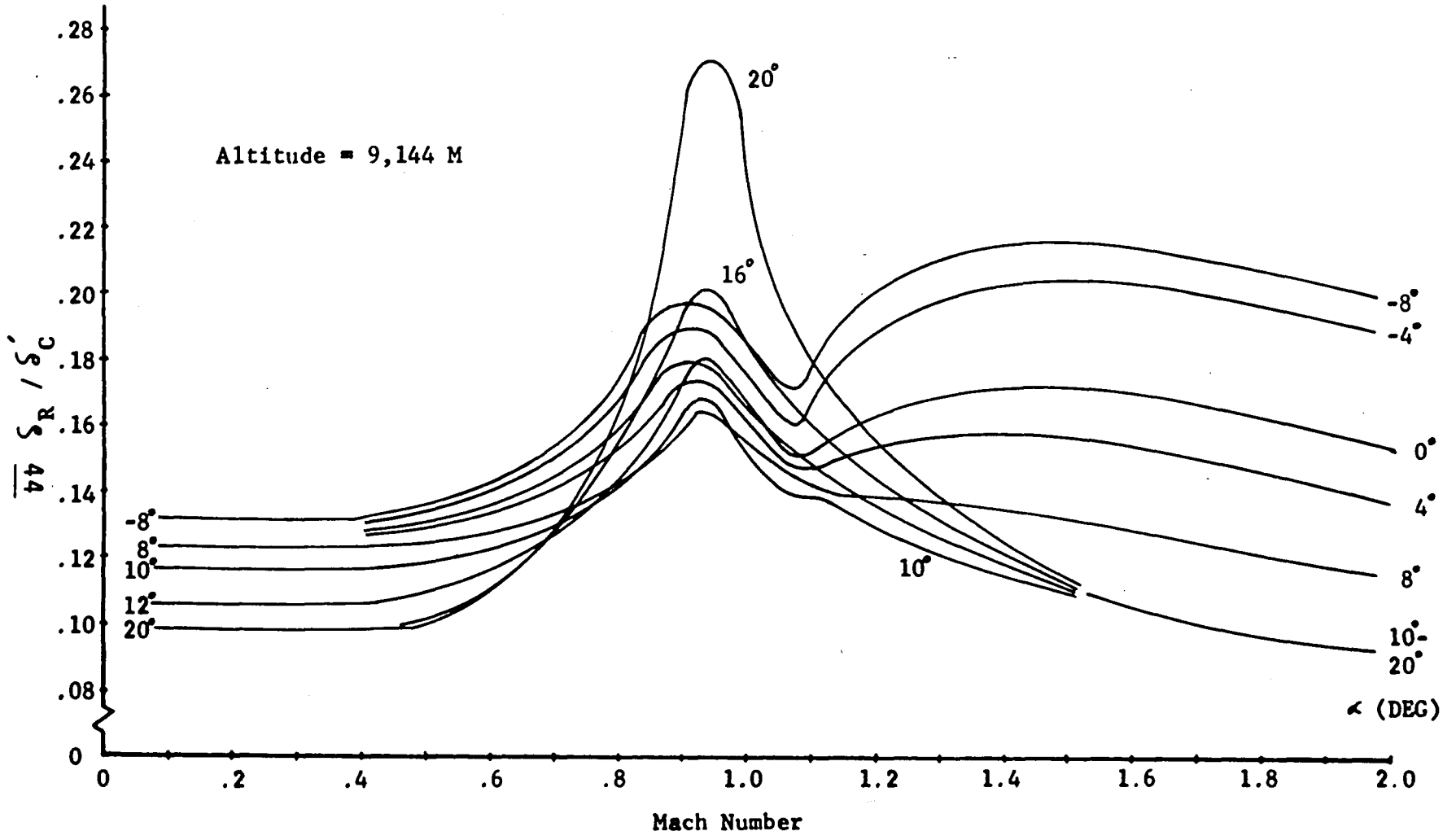

Figure 19. WLT Mode: Rudder to Canard Ratio

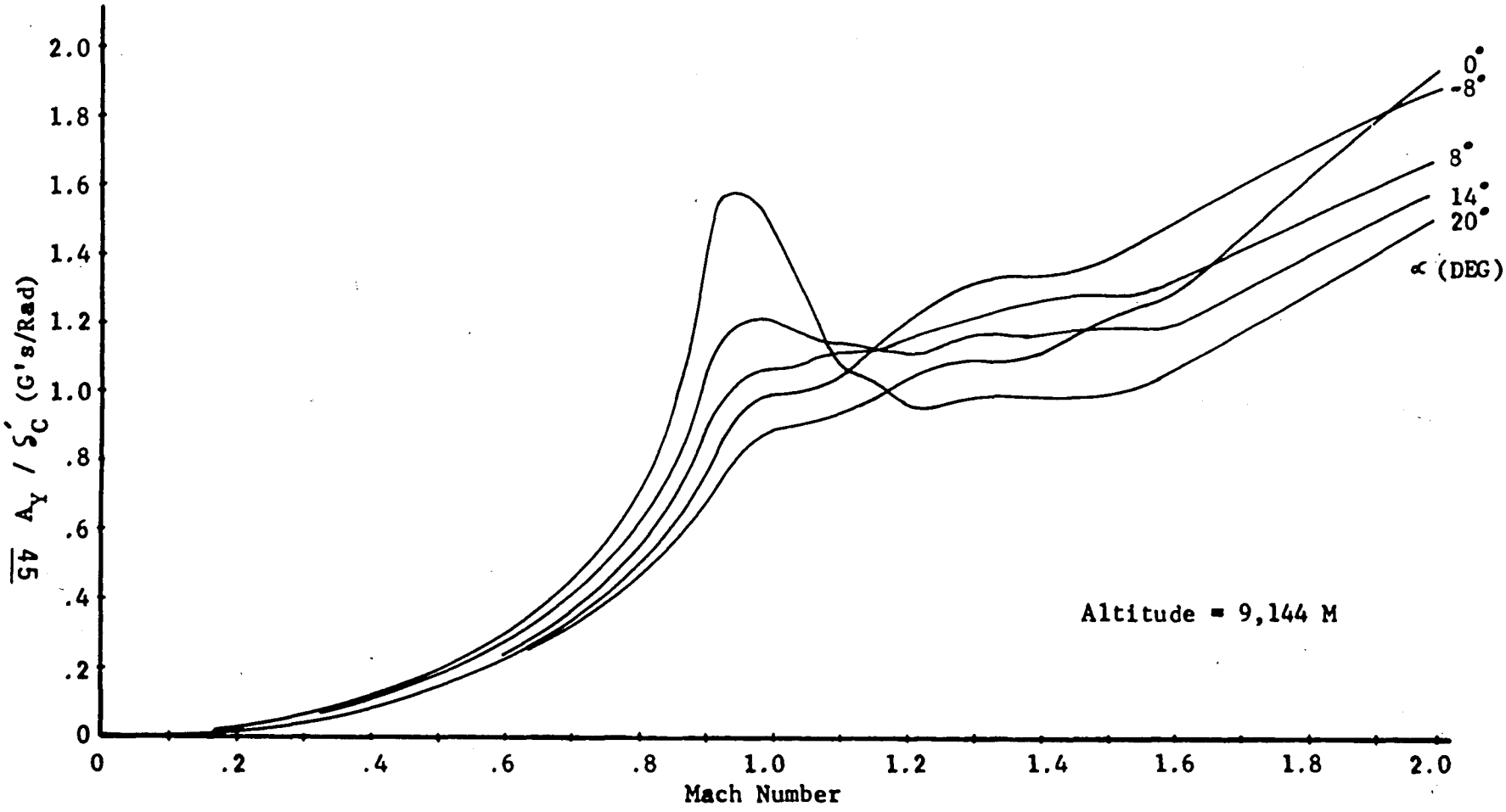

Figure 20. WLT Mode: Lateral Acceleration to Canard Ratio

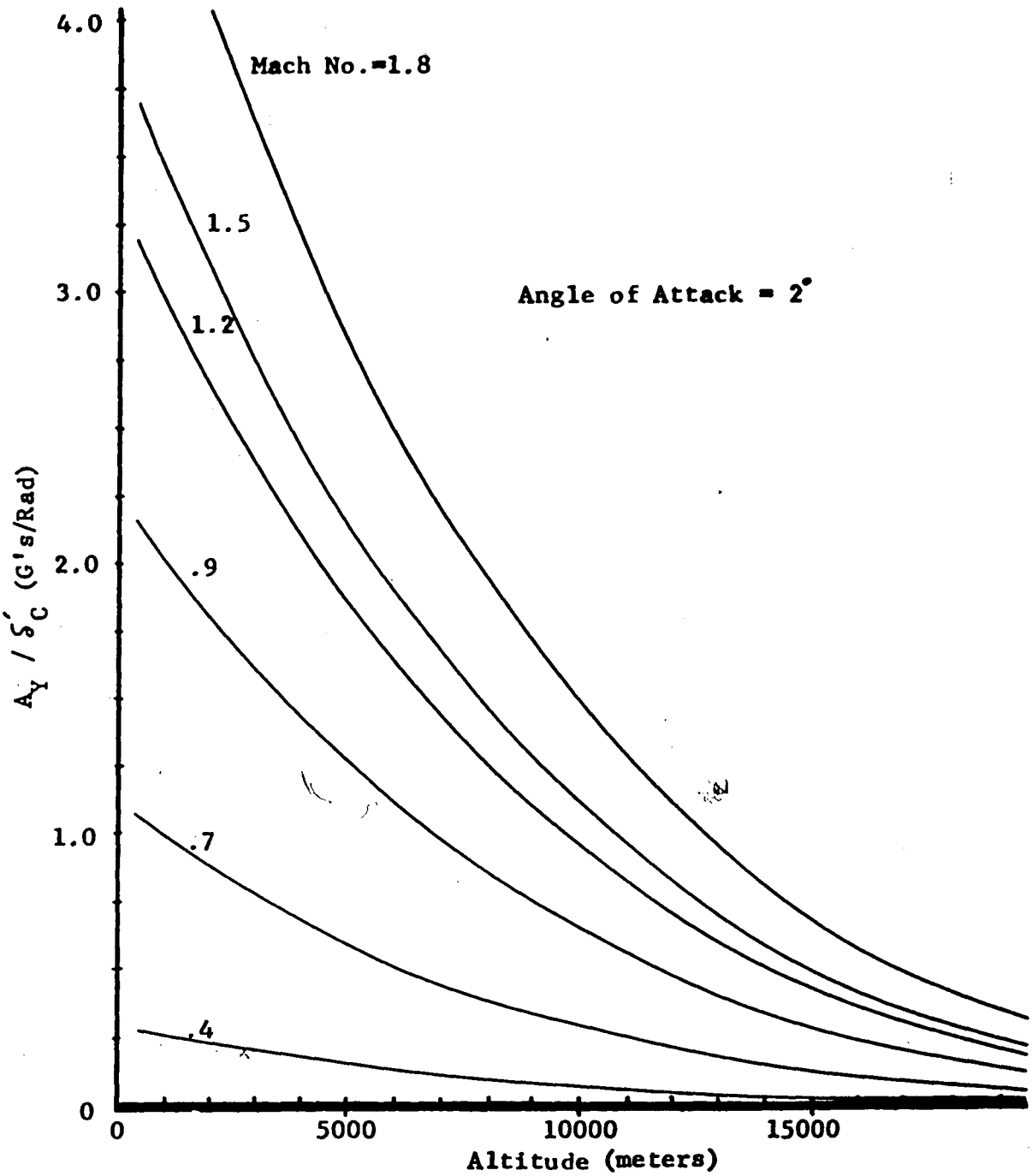

Figure 21. WLT Mode: Lateral Acceleration to Canard Ratio vs. Altitude

5.1.1.2 *Fuselage Pointing Mode*

During the FP mode, in addition to the conditions stated in Section 5.1.1, we also have the steady state conditions that

$$A_y = 0$$

and

$$\dot{\psi} = 0 ,$$

reducing the equations of motion to

$$\begin{bmatrix} 0 \\ 0 \\ 0 \end{bmatrix} = \begin{bmatrix} \ell_\beta \\ N_\beta \\ Y_\beta \end{bmatrix} \beta + \begin{bmatrix} \ell_{\delta_V'} & \ell_{\delta_C'} & \ell_{\delta_R} \\ N_{\delta_V'} & N_{\delta_C'} & N_{\delta_R} \\ Y_{\delta_V'} & Y_{\delta_C'} & Y_{\delta_R} \end{bmatrix} \begin{bmatrix} \delta_V' \\ \delta_C' \\ \delta_R \end{bmatrix} .$$

These are now solved for the interconnect ratios δ_V'/δ_C' and δ_R/δ_C' and also for the system authority ratio β/δ_C' yielding

$$\frac{\delta_R}{\delta_C'} = \frac{E/D - C/A}{B/A - E/D}$$

$$\frac{\delta_V'}{\delta_C'} = -\frac{1}{A}\left(B\,\frac{\delta_R}{\delta_C'} + C\right)$$

$$\frac{\beta}{\delta_C'} = -\frac{1}{\ell_\beta}\left(\ell_{\delta_V'}\,\frac{\delta_V'}{\delta_C'} + \ell_{\delta_R} + \ell_{\delta_C'}\right) ,$$

where

$$A = \frac{\ell_{\delta_V'}}{\ell_\beta} - \frac{N_{\delta_V'}}{N_\beta}$$

$$B = \frac{\ell_{\beta_R}}{\ell_\beta} - \frac{N_{\delta_R}}{N_\beta}$$

$$C = \frac{\ell_{\delta_C'}}{\ell_\beta} - \frac{N_{\delta_C'}}{N_\beta}$$

$$D = \frac{\ell_{\delta_V'}}{\ell_\beta} - \frac{Y_{\delta_V'}}{Y_\beta}$$

$$E = \frac{\ell_{\delta_R}}{\ell_\beta} - \frac{Y_{\delta_R}}{Y_\beta}$$

$$F = \frac{\ell_{\delta_C'}}{\ell_\beta} - \frac{Y_{\delta_C'}}{Y_\beta} \quad .$$

As with the WLT mode, these solutions were programmed on a digital computer and solved for values representing the entire HiMAT flight envelope.

The most meaningful results have been plotted versus Mach number, altitude, and angle of attack, and are shown in Figures 22-25. Extreme nonlinearity is again seen around Mach 1, as was the case for the WLT mode. The canard surfaces attain the largest deflections, thus being the limiting factor in FP authority. Given a maximum differential canard surface deflection, at Mach .8, 9,144 meters altitude, and 0° angle of attack, the HiMAT vehicle will be capable of approximately 3.7° steady state sideslip angle (see Figure 24). A simplified sketch of the fuselage pointing response is shown in Figure 26.

5.1.2 *Sensitivity Analysis*

Given a function T(k), the sensitivity function $S_K^{T(k)}$ is defined as the change in T(h) due to a change in k.

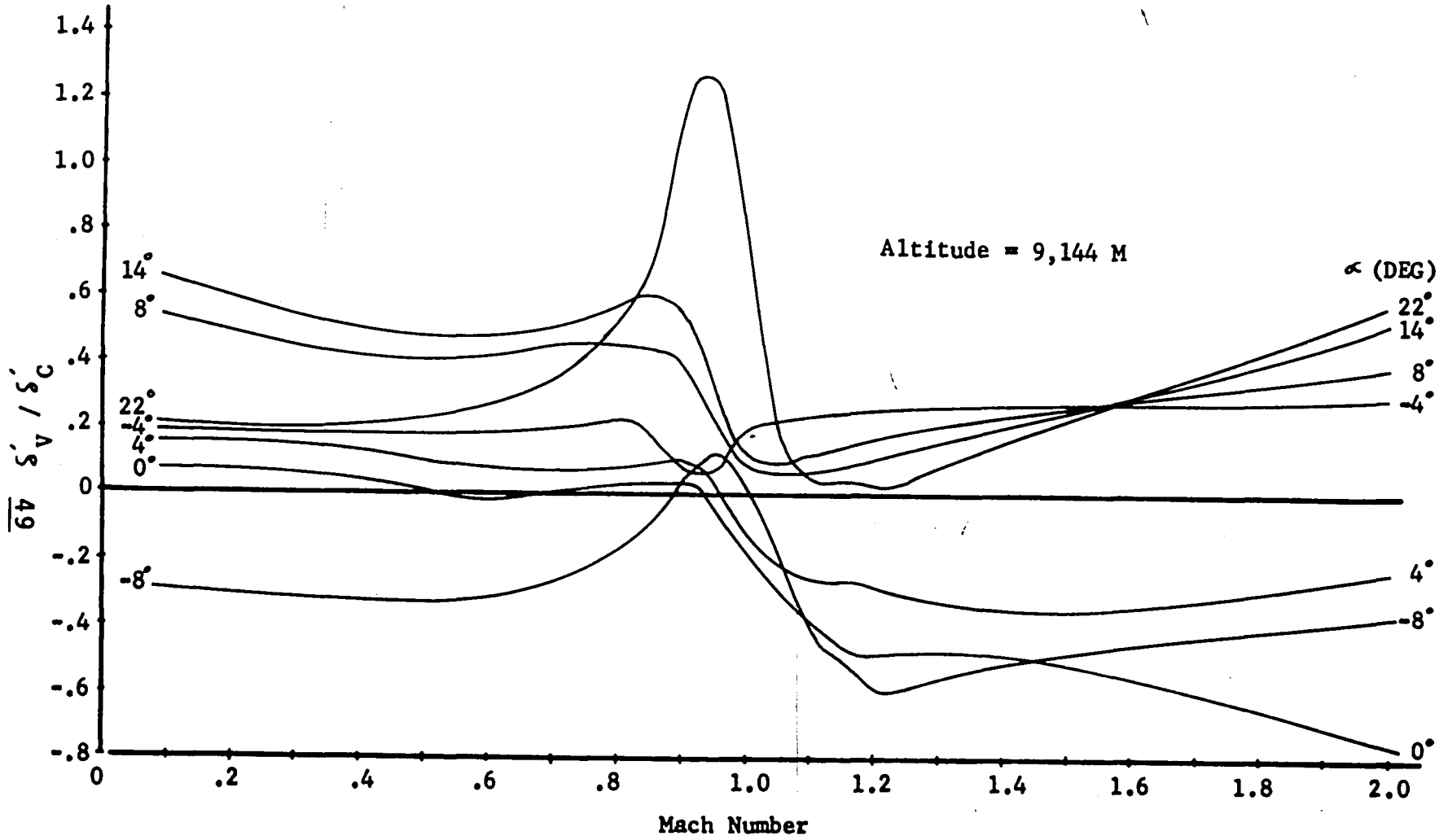

Figure 22. FP Mode: Elevon to Canard Ratio

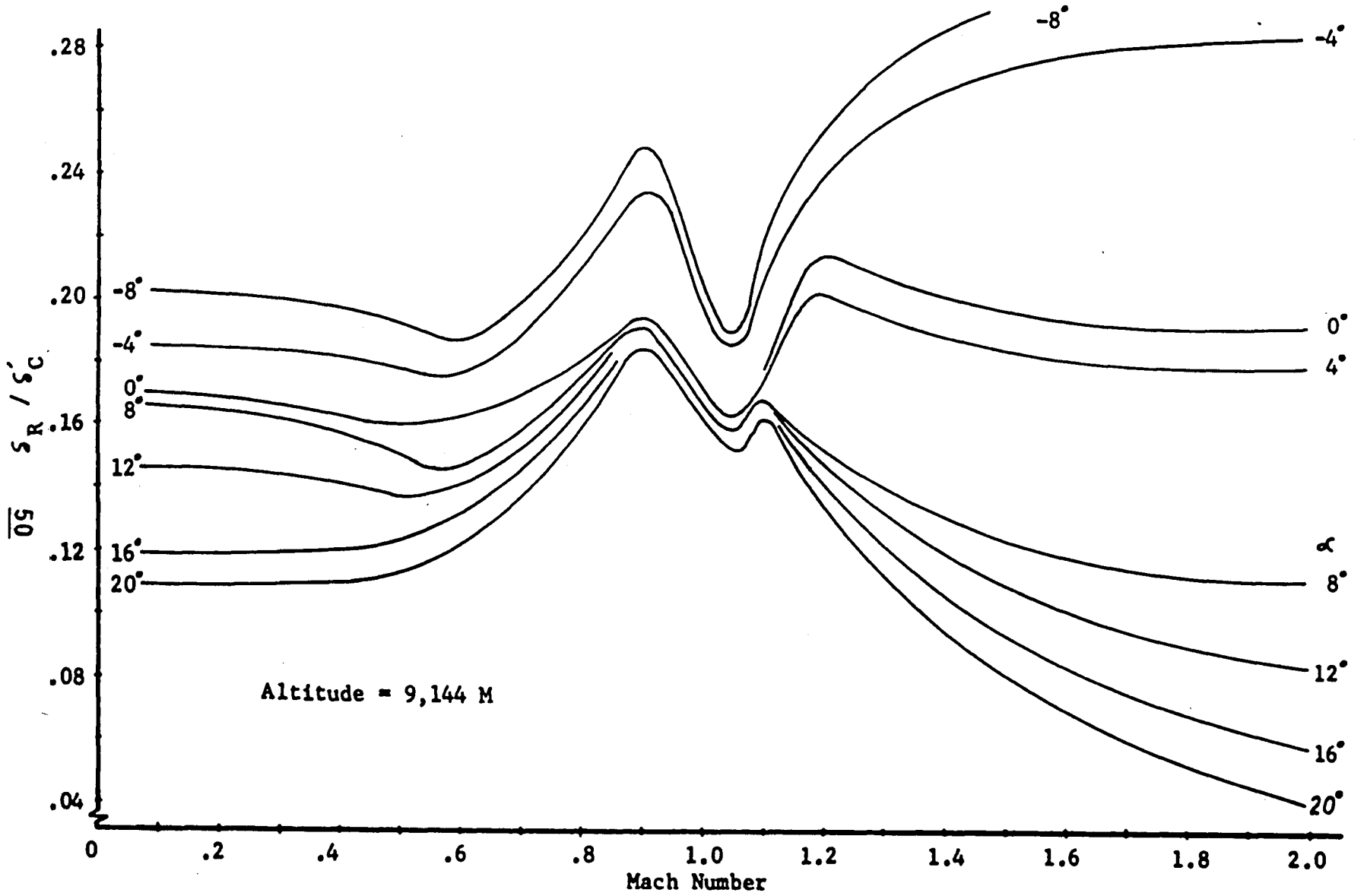

Figure 23. FP Mode: Rudder to Canard Ratio

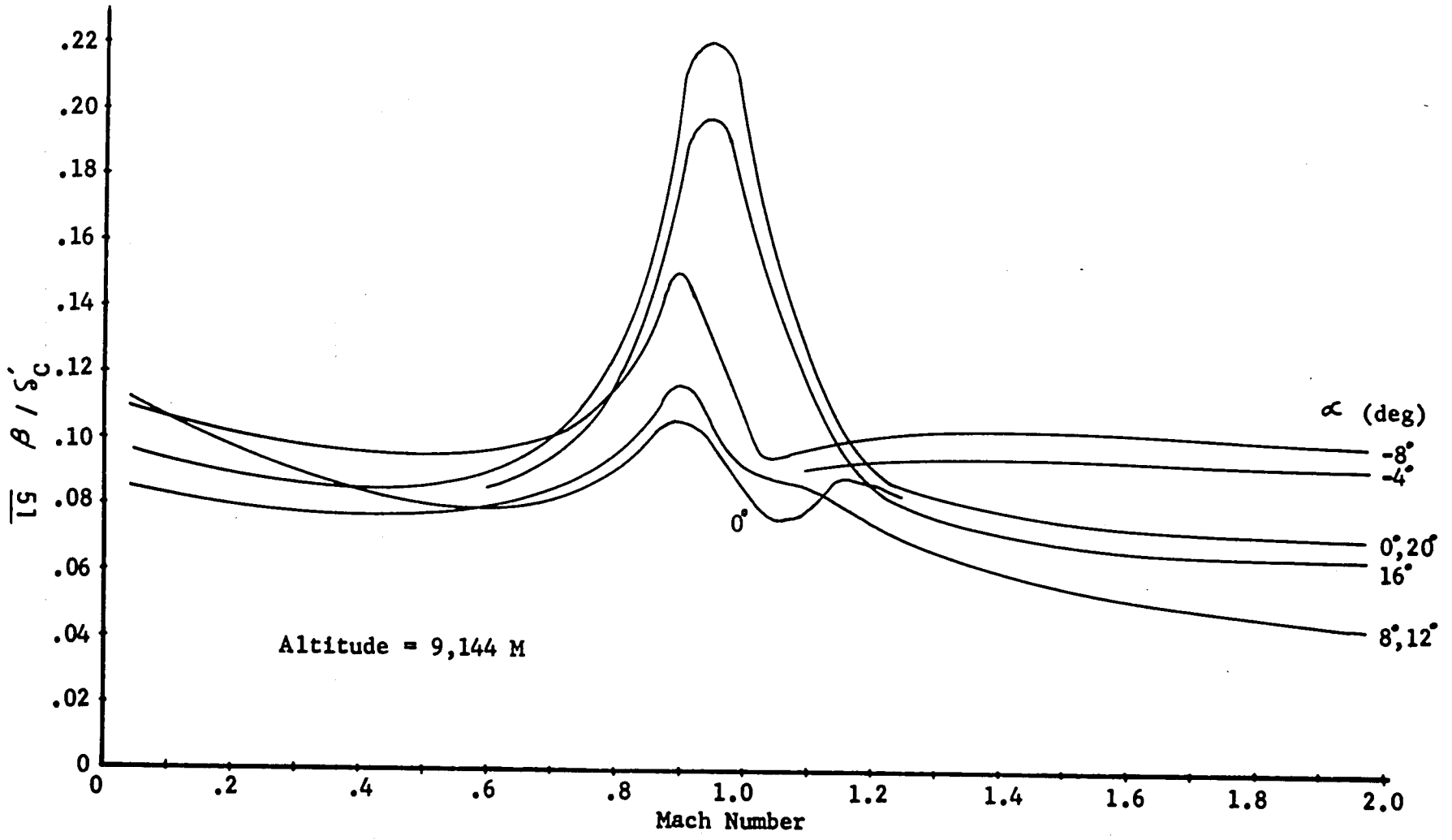

Figure 24. FP Mode: Sideslip Angle to Canard Ratio

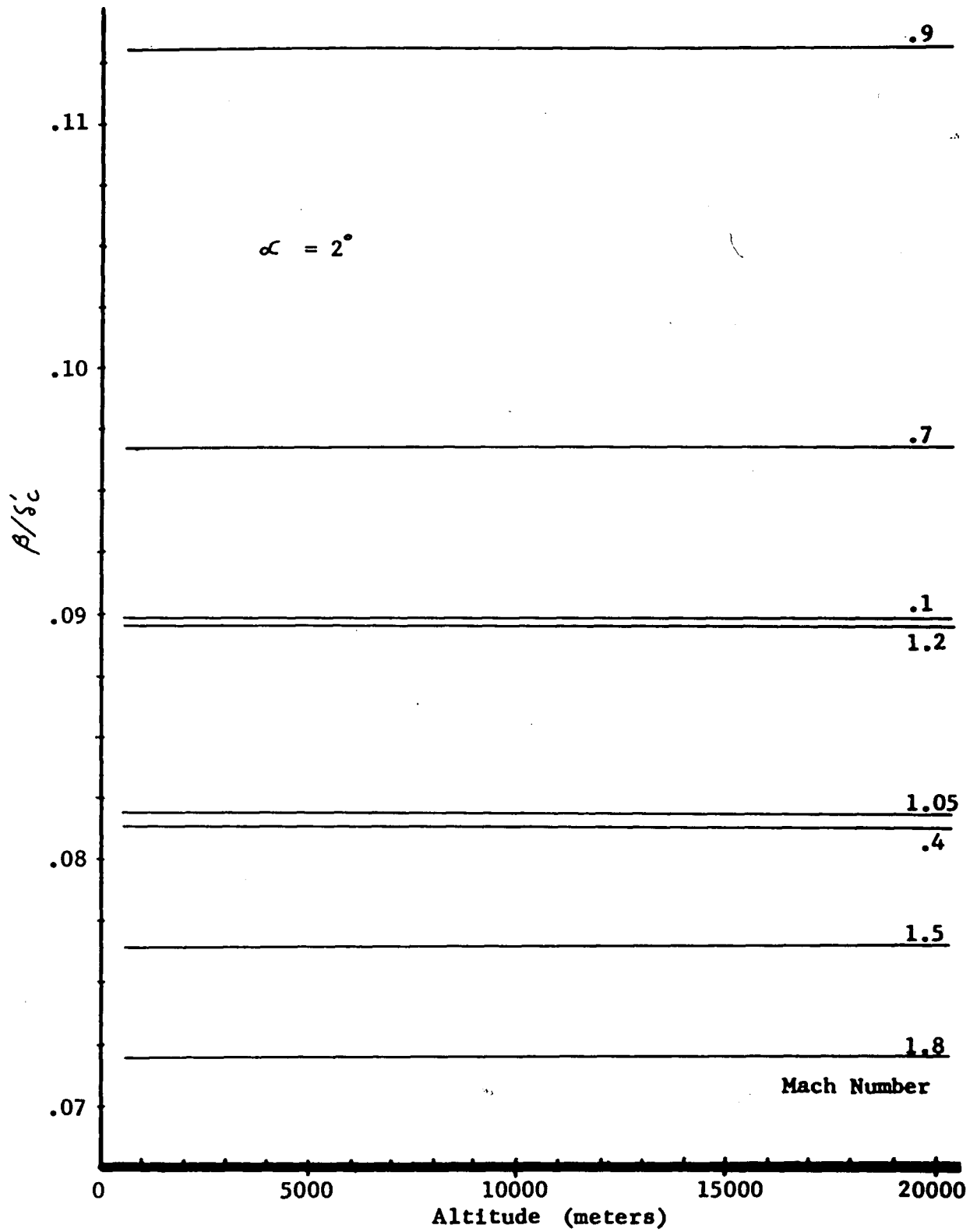

Figure 25. FP Mode: Sideslip to Canard Ratio vs. Altitude

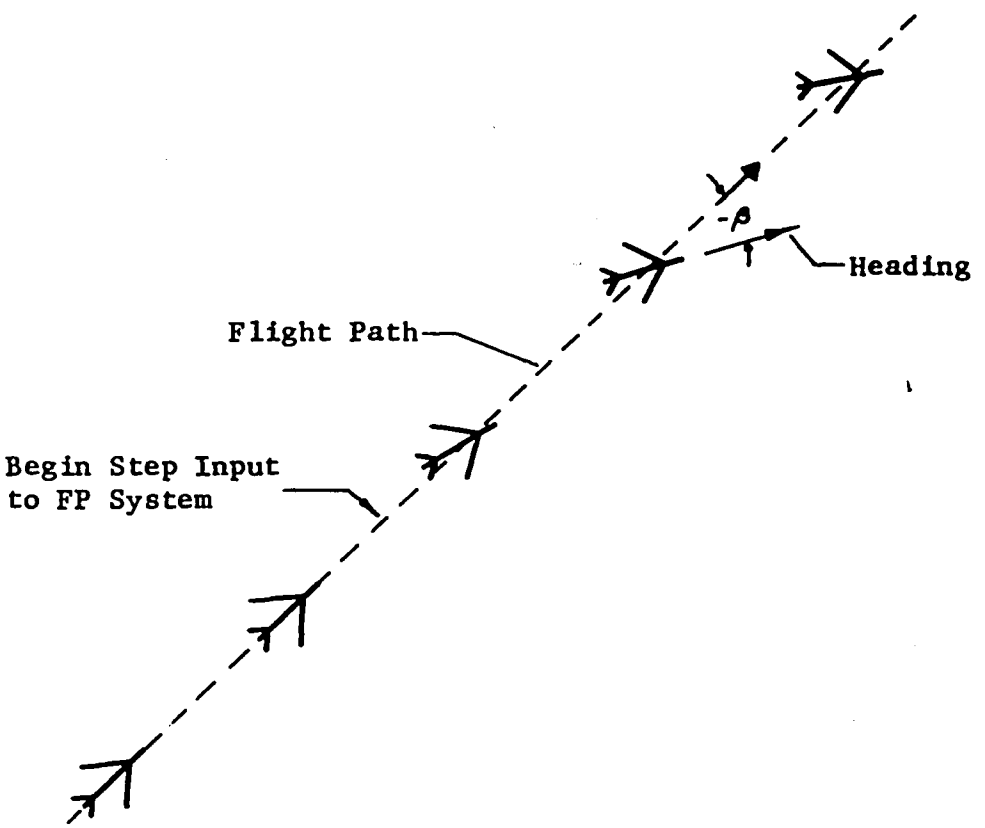

Figure 26. Simplified Sketch of Fuselage Pointing Mode Response

Mathematically, we have

$$S_h^{T(k)} \equiv \frac{\partial\ \ell n T(k)}{\partial\ \ell n(k)} = \frac{T(h)/T(k)}{h/k} = \frac{T(k)}{k}\,\frac{k}{T(h)}\ .$$

The approximate value of the sensitivity function may be evaluated for a given percent change in k by finding the corresponding percent change to T(k) and taking the ratio (i.e. $S_{approx}\ \frac{\%\Delta T(k)}{\%\Delta k}$). In many cases this is adequate and may, in fact, be beneficial for highly nonlinear functions with parameters subject to larger error. The approximation also has the advantage of being easier to calculate, avoiding the necessity of evaluating the derivatives of the function.

The study of the sensitivity of the above interconnect gains to errors in the aerodynamic parameters used in their calculation is an important matter since unacceptably uncoordinated flight maneuvers may result from parameters that have been approximated or not precisely calculated. The approximate sensitivity functions based on a 10% change in the aerodynamic derivatives were calculated for both the WLT and FP modes. The tabulated results are shown in Figures 27-30. Note that $S(T(k);k) = S_k^{T(h)}$.

The figures show that for the WLT mode the δ_V'/δ_C' interconnect ratio is moderately sensitive to changes $C_{\ell_{\delta_V'}}$, $C_{\ell_{\delta_C'}}$, $C_{\ell_{\delta_R}}$, $C_{N_{\delta_C'}}$, and $C_{N_{\delta_R}}$ with absolute sensitivity values being

Sensitivity Function	Mach No. / α	.4 / -2°	.4 / 2°	.4 / 6°	.8 / -2°	.8 / 2°	.8 / 6°	1.2 / -2°	1.2 / 2°	1.2 / 6°	Comments
$S(\frac{\delta_V'}{\delta_C'} ; C_{\ell_{\delta_V'}})$		- .88	- .90	- .91	- .91	-.91	-.91	-.90	-.95	-.96	---
$S(\frac{\delta_V'}{\delta_C'} ; C_{\ell_{\delta_C'}})$		- .37	- .47	-1.14	1.12	.31	.53	.12	.17	.36	---
$S(\frac{\delta_V'}{\delta_C'} ; C_{\ell_{\delta_R}})$		1.33	1.45	2.13	- .12	.68	.47	.87	.88	.70	High at Low Mach Nos.
$S(\frac{\delta_V'}{\delta_C'} ; C_{N_{\delta_C'}})$		1.33	1.42	2.04	- .12	.66	.44	.86	.81	.61	High at Low Mach Nos.
$S(\frac{\delta_V'}{\delta_C'} ; C_{N_{\delta_R}})$		-1.29	-1.41	-2.07	.11	-.66	-.45	-.85	-.84	-.67	High at Low Mach Nos.
$S(\frac{\delta_V'}{\delta_C'} ; C_{y_{\delta_C'}})$		--	--	.1	--	--	--	--	--	--	Negligible
$S(\frac{\delta_V'}{\delta_C'} ; C_{y_{\delta_R}})$		--	.1	.16	--	--	--	--	--	--	Negligible

Note: Absolute Values of Sensitivity Less Than .1 Not Recorded

FIGURE 27. WLT Mode: Sensitivity Values of Elevon/Canard Ratios to Aerodynamic Coefficients for An Altitude of 9,144 Meters.

Sensitivity Function	Mach No. / α	.4 / -2°	.4 / 2°	.4 / 6°	.8 / -2°	.8 / 2°	.8 / 6°	1.2 / -2°	1.2 / 2°	1.2 / 6°	Comments
$S(\frac{\delta_R}{\delta_C} ; C_{N_{\delta_C}})$		.97	.97	.95	.97	.96	.95	.97	.96	.93	----
$S(\frac{\delta_R}{\delta_C} ; C_{N_{\delta_R}})$		-.94	-.97	-.97	-.96	-.96	-.97	-.96	-1.0	-1.0	----

Note: Absolute Values of Sensitivity Less Than .1 Not Recorded.

FIGURE 28. WLT Mode: Sensitivity Values of Rudder/Canard Ratios to Aerodynamic Coefficients for an Altitude of 9,144 Meters.

Sensitivity Function	Mach No. / α	.4 / -2°	.4 / 2°	.4 / 6°	.8 / -2°	.8 / 2°	.8 / 6°	1.2 / -2°	1.2 / 2°	1.2 / 6°	Comments
$S(\frac{\delta\dot{v}}{\delta\dot{c}} ; C_{\ell_\beta})$		6.40	2.10	.94	1.09	2.43	1.03	- .19	- .22	2.80	Unpredictable
$S(\frac{\delta\dot{v}}{\delta\dot{c}} ; C_{\ell_{\delta\dot{v}}})$		- .88	- .88	- .83	- .87	- .86	- .81	- .91	- .95	- .90	----
$S(\frac{\delta\dot{v}}{\delta\dot{c}} ; C_{\ell_{\delta\dot{c}}})$		1.61	.40	--	- .16	- .42	--	.11	.16	- .61	----
$S(\frac{\delta\dot{v}}{\delta\dot{c}} ; C_{\ell_{\delta\dot{R}}})$		-7.10	-1.50	--	--	-1.08	--	1.10	1.11	-1.20	High at Low Mach Nos. with Negative α.
$S(\frac{\delta\dot{v}}{\delta\dot{c}} ; C_{N_\beta})$		- .56	--	.28	.19	.15	.18	.37	.36	.19	----
$S(\frac{\delta\dot{v}}{\delta\dot{c}} ; C_{N_{\delta\dot{c}}})$		-1.91	--	.54	.77	.55	.58	.85	.80	.55	----
$S(\frac{\delta\dot{v}}{\delta\dot{c}} ; C_{N_{\delta_R}})$		2.20	--	- .71	- .88	- .63	- .67	-1.10	-1.10	- .64	----
$S(\frac{\delta\dot{v}}{\delta\dot{c}} ; C_{y_\beta})$		-5.24	-1.85	-1.10	-1.20	-2.33	-1.10	- .15	- .11	-2.70	Unpredictable
$S(\frac{\delta\dot{v}}{\delta\dot{c}} ; C_{y_{\delta\dot{v}}})$		--	--	--	--	--	- .12	--	--	--	Negligible
$S(\frac{\delta\dot{v}}{\delta\dot{c}} ; C_{y_{\delta\dot{c}}})$		1.30	.56	.43	.40	.87	.51	--	--	1.10	----
$S(\frac{\delta\dot{v}}{\delta\dot{c}} ; C_{y_{\delta_c}})$		4.70	1.57	.91	.98	1.81	.84	.13	--	1.96	----

Note: Absolute Values of Sensitivity Less Than .1 Not Recorded.

FIGURE 29. FP Mode: Sensitivity Values of Elevon/Canard Ratios to Aerodynamic Coefficients for an Altitude of 9,144 Meters.

Sensitivity Function	Mach. No. / α	.4 / -2°	.4 / 2°	.4 / 6°	.8 / -2°	.8 / 2°	.8 / 6°	1.2 / -2°	1.2 / 2°	1.2 / 6°	Comments
$S(\frac{\delta R}{\delta C} ; C_{\ell_\beta})$		--	--	--	--	--	--	--	--	- .14	Negligible
$S(\frac{\delta R}{\delta C} ; C_{N_\beta})$		.27	.29	.44	.23	.26	.28	.40	.40	.32	----
$S(\frac{\delta R}{\delta C} ; C_{N_{\delta C}})$		.93	.92	.86	.93	.92	.90	.92	.90	.90	----
$S(\frac{\delta R}{\delta C} ; C_{N_{\delta R}})$		-1.10	-1.10	-1.14	-1.10	-1.10	-1.00	-1.10	-1.20	-1.00	----
$S(\frac{\delta R}{\delta C} ; C_{y_\beta})$		- .26	- .27	- .36	- .22	- .23	- .22	- .34	- .34	- .16	----
$S(\frac{\delta R}{\delta C} ; C_{y_{\delta C}})$		--	--	.14	--	--	--	--	--	--	Negligible
$S(\frac{\delta R}{\delta C} ; C_{y_{\delta R}})$		.24	.23	.30	.19	.17	.17	.29	.28	.11	----

Note: Absolute Values of Sensitivity Less Than .1 Not Recorded

FIGURE 30. FP Mode: Sensitivity Values of Rudder/Canard Ratios to Aerodynamic Coefficients for an Altitude of 9,144 Meters.

around 1.5. The most active values appear to be $S(\delta_V'/\delta_C'; C_{\ell_{\delta_R}})$, $S(\delta_V'/\delta_C'; C_{N_{\delta_C'}})$, and $S(\delta_V'/\delta_C'; C_{N_{\delta_R}})$ which take on relatively high absolute values ($\geq 2.$) at low Mach numbers and high angles of attack.

The δ_R/δ_C' interconnect ratio for WLT is moderately sensitive to only $C_{N_{\delta_C'}}$ and $C_{N_{\delta_R}}$, with absolute values remaining fairly constant (≈ 1.0) with flight condition.

The interconnect ratios for the FP mode are more sensitive to changes in the aero parameters than for the WLT mode. The δ_R/δ_C' ratio is again mostly dependent upon $C_{N_{\delta_C'}}$ and $C_{N\delta_R}$, with absolute values of sensitivity around 1.0. The δ_V'/δ_C' ratio is seen to be highly sensitive, especially to changes in C_{ℓ_β}, $C_{\ell_{\delta_C'}}$, $C_{\ell_{\delta_R}}$, $C_{N_{\delta_C'}}$, $C_{N_{\delta_R}}$, C_{y_β}, $C_{y_{\delta_C'}}$, and $C_{y_{\delta R}}$, with absolute values reaching 6 or 7. Worthy of note are the values due to C_{ℓ_β}, C_{N_β}, and C_{y_β} which take on large values at low Mach numbers and negative angles of attack.

5.1.3 *Control System*

The primary lateral-directional control system for HiMAT, as developed by Rockwell International, is shown in Figure 12. The parts of the system pertinent to DSF have been isolated and are shown in Figure 31. In order to maintain the original dynamics, the signals for the new modes will enter the system,

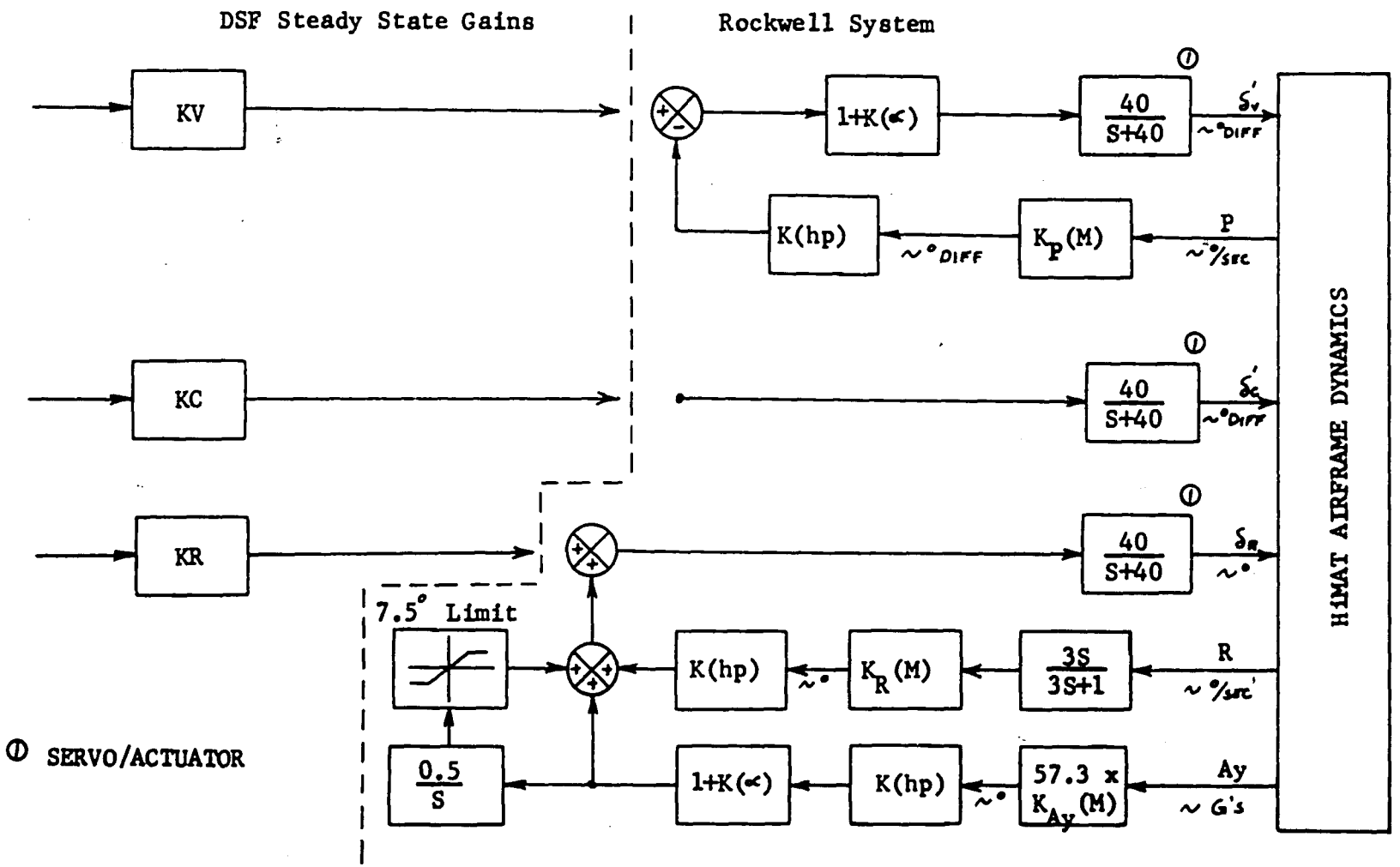

Figure 31. Rockwell System Applicable to DSF

in the case of the elevons and rudders, just ahead of the three feedback paths. The third and most important signal will be through a direct open loop path to the differential canard surfaces.* The possibility of using feedback to the canards was studied, but it was not found advantageous, and the overall general handling qualities would have been altered by its inclusion.

The forward loop gains for the DSF system (KV, KC, and KR) are based on the computed interconnect ratios and on any non-zero feedback which may be present. These differ depending upon the mode desired.

5.1.3.1 WLT Mode

Since the canard signal is dominant for any DSF mode, and since there is no feedback path, the value of KC_{WLT} is constant and may be chosen arbitrarily, to be adjusted later by a cockpit controller gain so that a maximum command input yields the maximum allowable differential canard surface deflection. The value of KC_{WLT} is chosen as unity.

During the steady state, roll rate should be zero, so there is no contribution to the elevon signal from feedback. Thus,

* The servo/actuators for the canard surfaces have been modelled similar to those for the elevons and rudders.

the value of KV_{WLT} is just the interconnect ratio, δ_V'/δ_C', calculated for WLT, based on a unity canard signal.

The calculation of KR_{WLT} is more complex, since there are steady state feedback signals to the rudder which are not zero. The yaw rate signal may be ignored, even though there is a finite yaw rate, since a wash-out has been included in the loop. The rest of the directional control system must be considered and is redrawn in a simplified fashion in Figure 32.

The feedback loop integrator has been replaced by a constant input, since at steady state the limiter will be in effect and will be producing a constant value. Solving for the input to the rudder servo/actuator yields

$$x = (KR_{WLT})r + L + H_{Ay} ,$$

where r is the input, Ay is the resulting lateral acceleration, H is the feedback gain, and L is the limiter-produced constant. Since KR_{WLT} is being solved to satisfy the previously calculated interconnect ratios; for an input, r, we want $x - r\ \delta_R/\delta_C'$ and $Ay = r\ A_y/\delta_C'$. Thus,

$$(KR_{WLT})r = r\frac{\delta_R}{\delta_C'} - L - rH\frac{A_y}{\delta_C'}$$

$$KR_{WLT} = \frac{\delta_R}{\delta_C'} - \frac{L}{r} - H\frac{A_y}{\delta_C'} \quad .$$

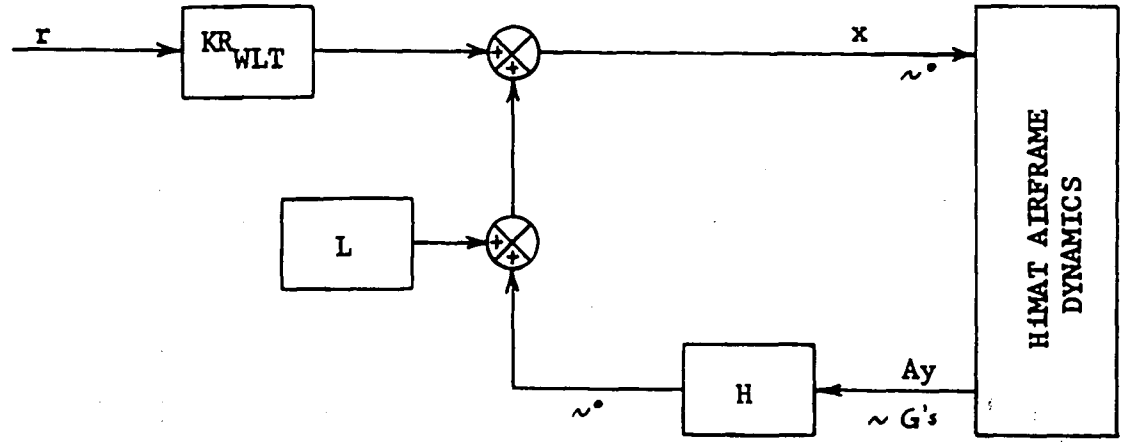

Figure 32. Simplified Steady State Directional Control System

The value of KR_{WLT} is seen to be not only a function of the system gains and the interconnect ratios, but also of the input, due to the constant L generated by limiting the feedback integrator. After many computer simulations during the design stages of the WLT mode, it was found that the feedback loop integrator was not critical to system performance, and that its ommission would not be detrimental. Therefore, in order to keep the scheduling of KR_{WLT} simple, the integrator is disabled while in the WLT mode. Thus, we obtain

$$KR_{WLT} = \frac{\delta_R}{\delta_C} - H \frac{A_y}{\delta_C} ,$$

which is now only a function of the interconnect ratios and the primary system gains. The value of 'H' is

$$H = (K_{A_y}(K(hp))(K(\alpha) + 1) ,$$

which is taken from the Rockwell System.

Calculations for KR_{WLT} were carried out for many flight conditions on a hand calculator and are shown plotted in Figure 33.

5.1.3.2 *FP Mode*

By definition, the ideal steady state during the FP mode is characterized by zero roll rate, zero yaw rate, and zero lateral acceleration. These feedback paths, therefore, do not influence the value of the forward gains KV_{FP} and KR_{FP}. If, as

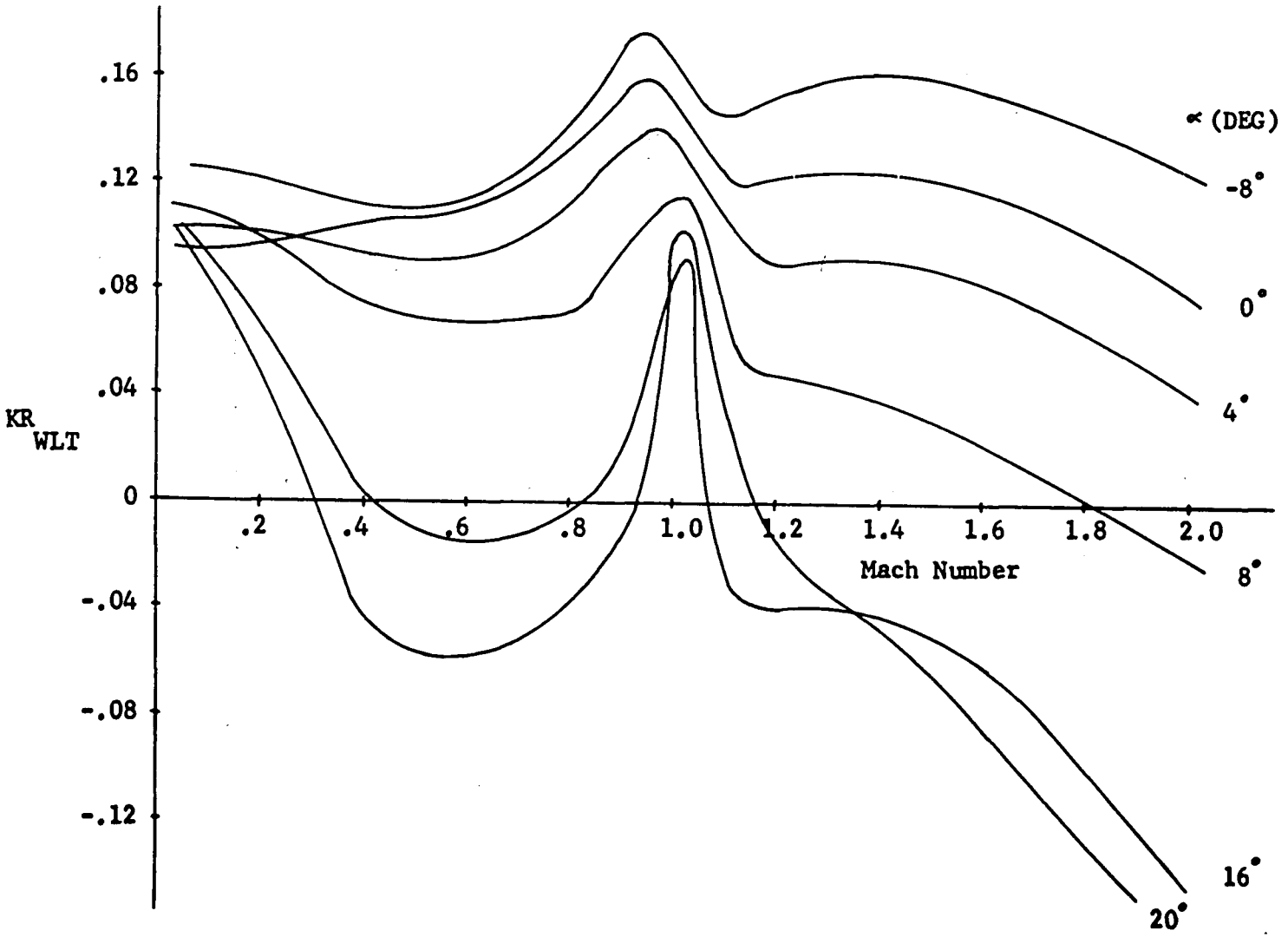

Figure 33. WLT Mode- Steady State Rudder Gain Schedule

with the WLT mode, the value of KC_{FP} is chosen as unity, then KV_{FP} and KR_{FP} are simply the interconnect ratios scheduled on Mach number and angle of attack. Since the canard surfaces attain greater steady state deflections than do either the elevons or rudders, a command input gain will later be set so that maximum control input results in maximum canard movement.

5.2 Transient Response*

The block diagram of Figure 34 shows the three inputs of Figure 31 connected into one, and includes the filters necessary to tailor final response.

These filter blocks (G_{DSF}, GV_{DSF}, GC_{DSF}, GR_{DSF}) remain to be determined. For clarity, G_{DSF} will be referred to as the input filter, whereas GV_{DSF}, GC_{DSF}, and GR_{DSF} are the branch filters.

The main design criteria for the transient response, as stated earlier, is taken from a report by the McDonnell Aircraft Company, and is in the form of a normalized frequency response [12]. The curve is shown in Figure 35 and applies to the lateral acceleration response for the WLT mode, and to the

---

* The transient response analysis was done using s-plane techniques with much use of the "CONTROL" computer program developed at the NASA, Dryden Flight Research Center [6].

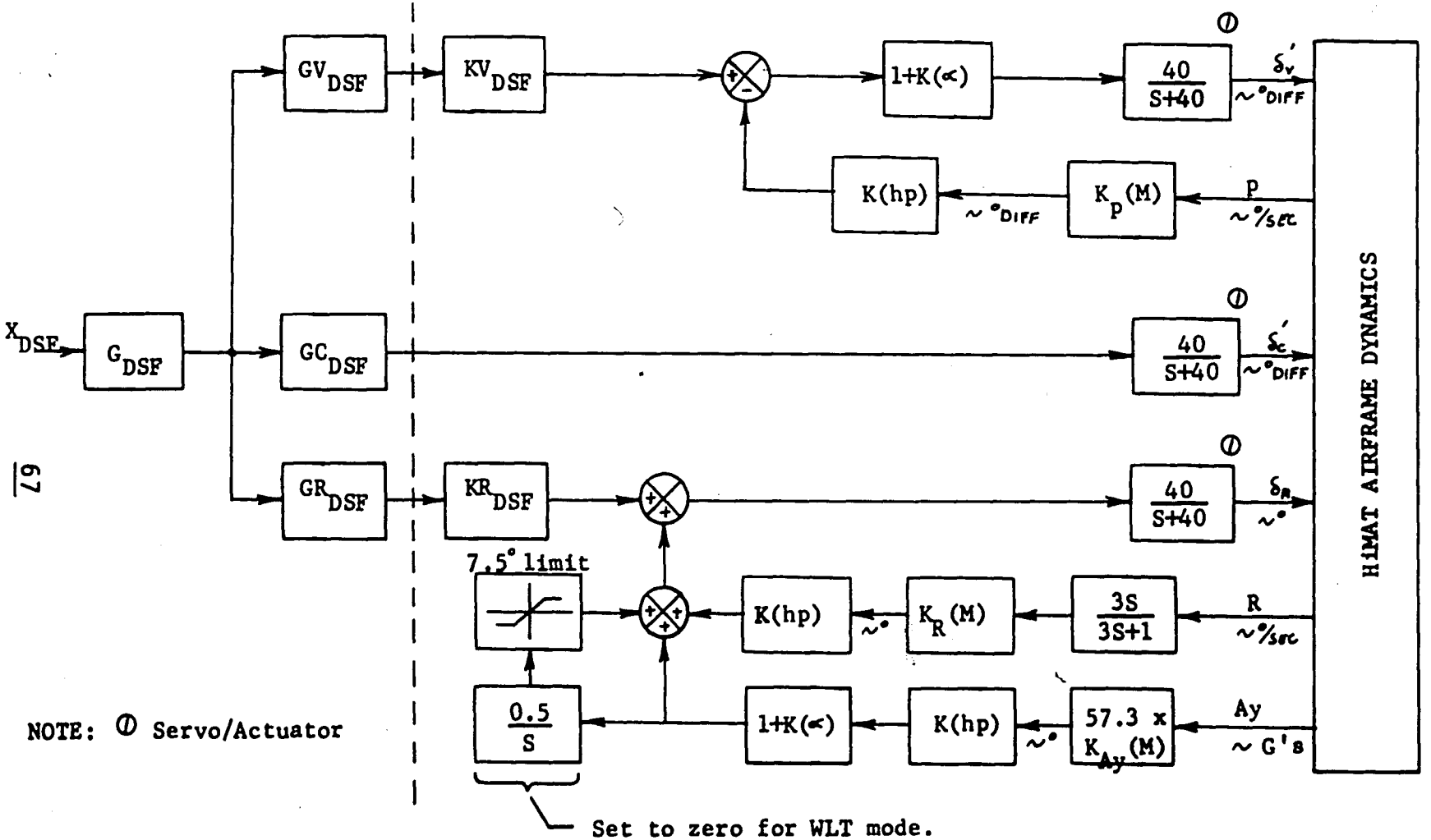

Figure 34. General DSF Control System Design

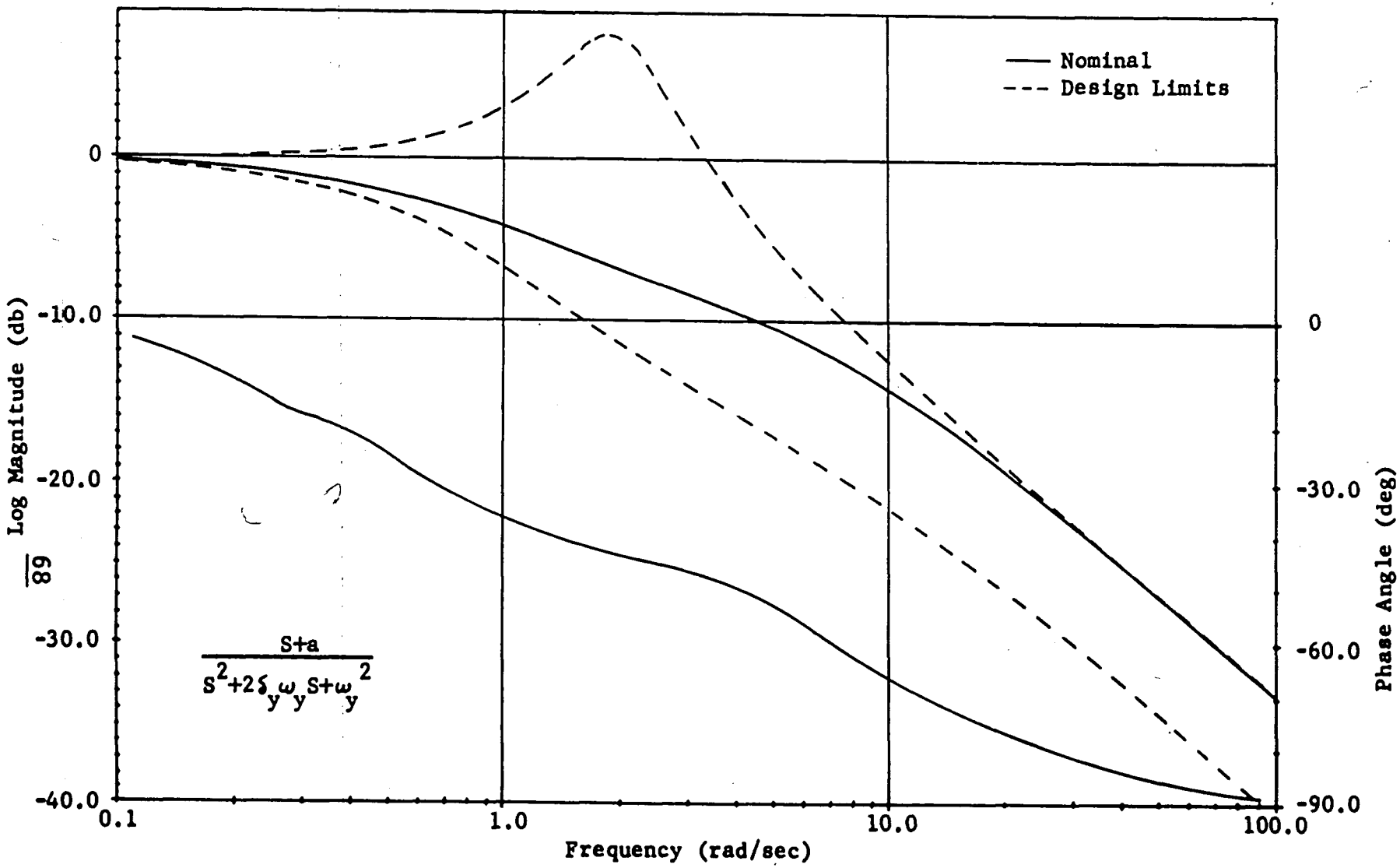

Figure 35. Frequency Response Model

sideslip angle response for both the FP and LT modes. The other criteria decided upon include the military specifications on Dutch roll [14] and the ideal time responses qualitatively defining a "best" system.

The system will be designed so that the branch filters are primary in minimizing those vehicle responses which ideally should remain unchanged throughout a given commanded DSF maneuver. The input filter will then be used to tailor the sideslip or lateral acceleration response, whichever is applicable, to match the ideal as closely as possible.

5.2.1 Branch Filtering

Initial computer simulations of the systems of Figure 34 with GV = GC = GR = G = 1 give an overall feel for how much and what type of filtering might be necessary. This has been done for both the WLT and FP modes for various representative flight conditions.

5.2.1.1 WLT Mode

Figure 36 shows the log magnitude curves for the WLT mode at a flight condition of Mach = .8, altitude = 9144 m, and angle of attack = 2°. These curves appear to be a fairly good representation for the entire flight envelope based on a series of system simulations for varying flight conditions.

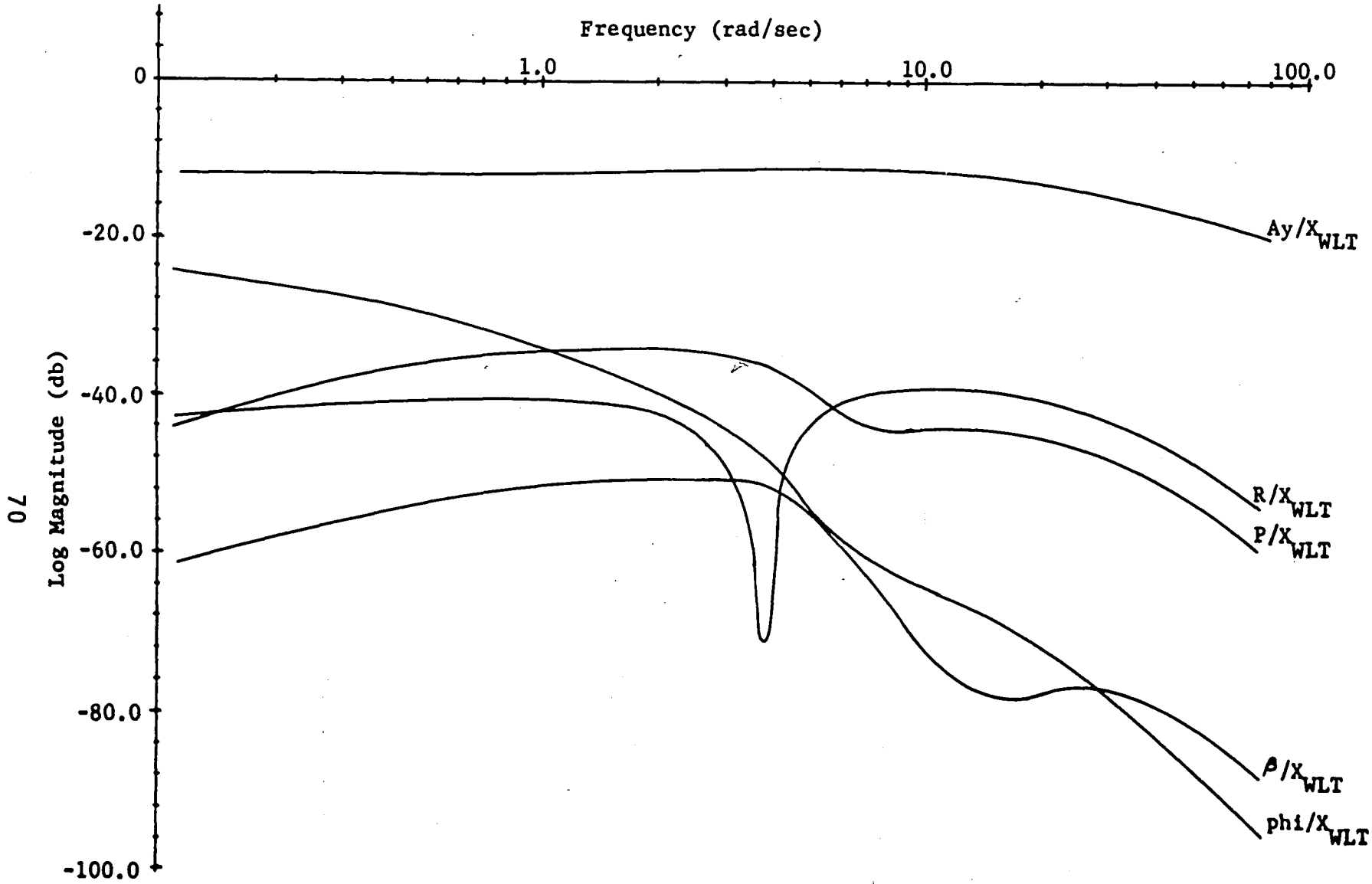

Figure 36. WLT Mode - Frequency Response for System of Figure 34 (Mn=.8, hp=9144m, =2)

The units for the plotted output responses are:

Ay: g's

p: rad/sec

r: rad/sec

β: rad ,

and it can be seen from the graph that the roll rate, yaw rate, and sideslip angle responses are quite small relative to the lateral acceleration response. Thus, it seems that no branch filtering is necessary for the WLT mode yielding GV = GC = GR = 1 in Figure 34. This conclusion is further supported later in this report by time response simulations.

5.2.1.2 FP Mode

The frequency response log magnitude curves for the fuselage pointing mode at a flight condition of Mach = .8, altitude = 9,144 m, and angle of attack = 2° are shown in Figure 37. Based on a series of computer simulations over a broad range of flight conditions, these curves appear to be a good overall representation of the entire flight envelope.

The graph shows similarity of curve shapes throughout the given frequency range with the exception of a fairly "flat" β/X_{FP} response below 3 rad/sec. This suggests using an input filter rather than branch filtering to minimize the responses

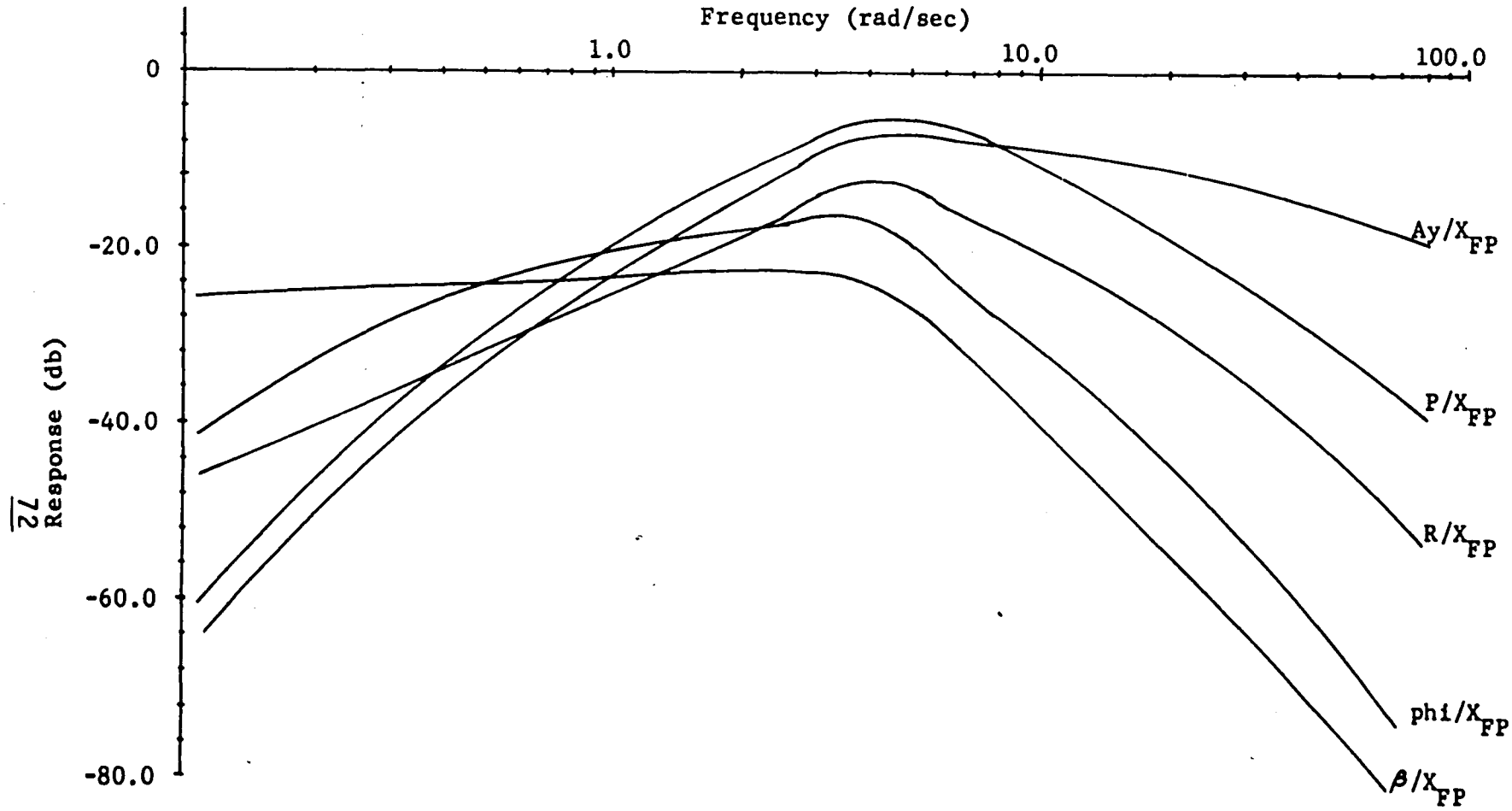

Figure 37. FP Mode - Frequency Response for System of Figure 34. (Mn=.8, hp=9144m, α =2°)

of roll rate, yaw rate, and lateral acceleration. A glance at Figure 35 shows that tailoring the sideslip response to this model should markedly reduce the peak values of the other outputs to acceptable levels.

5.2.2 Input Filtering

As defined earlier, the input filter is shown as "G_{DSP}" in Figure 34 and will be used primarily to tailor the commanded output response to the nominal frequency response model of Figure 35. The other outputs will be altered similarly, but this should not be a detrimental effect. In fact, the FP mode should benefit from this with decreased roll rate and lateral acceleration, as mentioned above.

5.2.2.1 WLT Mode

The magnitude plot of the lateral acceleration frequency response without filtering is shown in Figures 38-40 for three different flight conditions. The model envelope from Figure 35 has been included to show the tailoring necessary to bring the curve within the design limitations. All three unfiltered responses remain relatively "flat" through 20 rad/sec where they dip downward to a slope of 20 db/decade with a corner frequency around 30 rad/sec. This suggests that a constant function can be utilized and the scheduling based on flight condition is not needed.

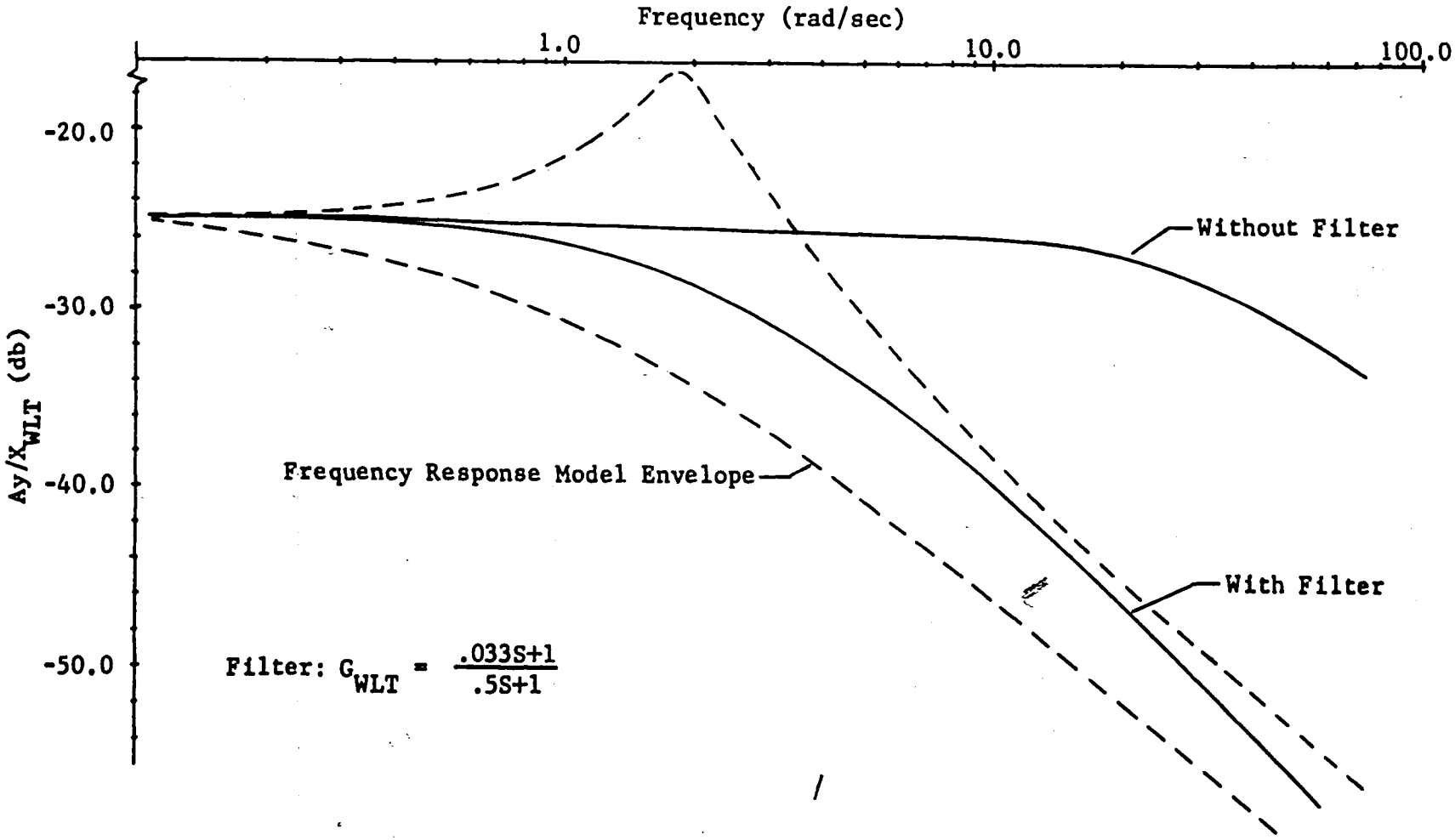

Figure 38. WLT Mode: Lateral Acceleration Response at Mn=.4, hp=9144m, α =2°; with and without Input Filter.

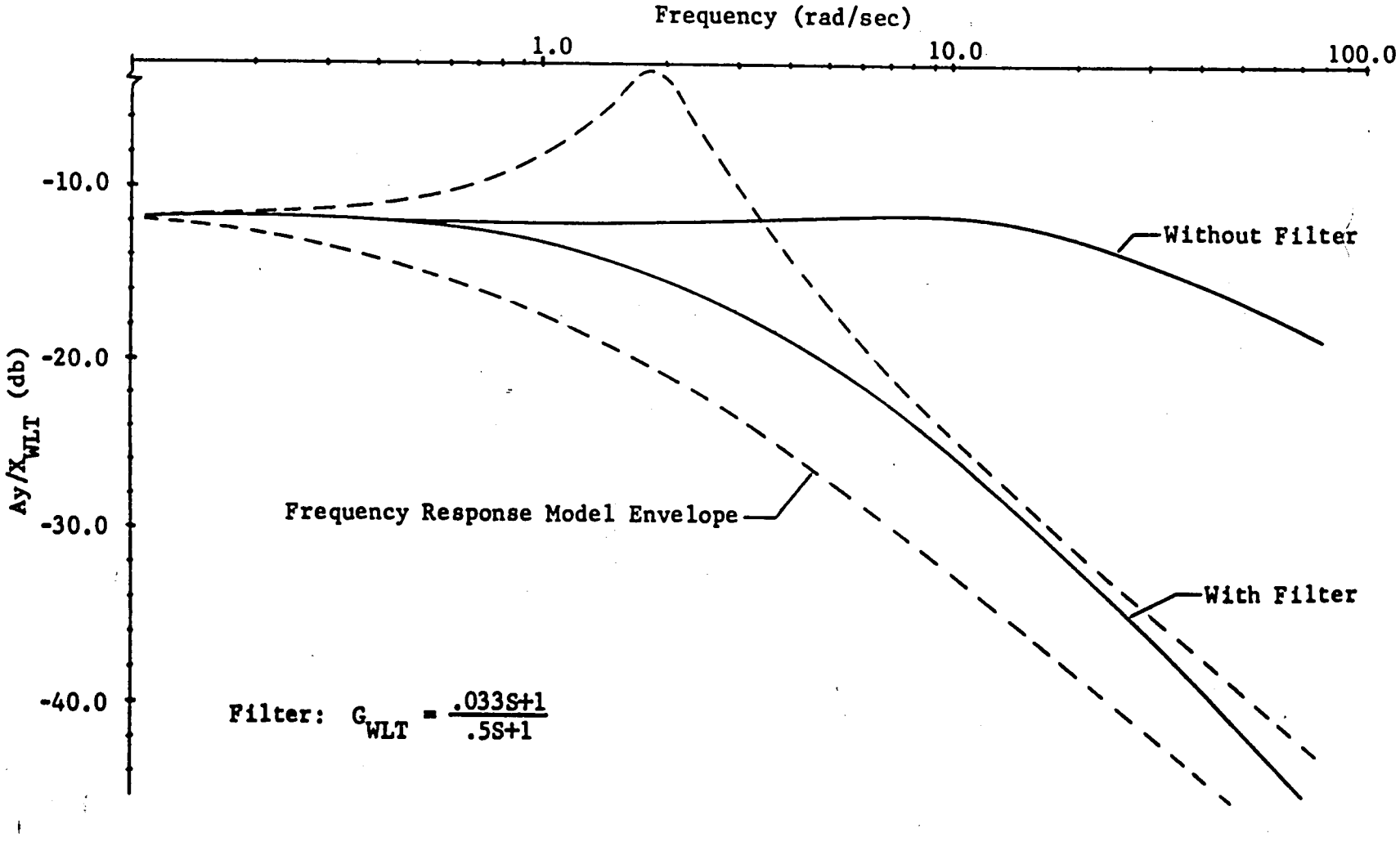

Figure 39. WLT Mode: Lateral Acceleration Response at Mn=.8, hp=9144m, α =2°; with and without Input Filter.

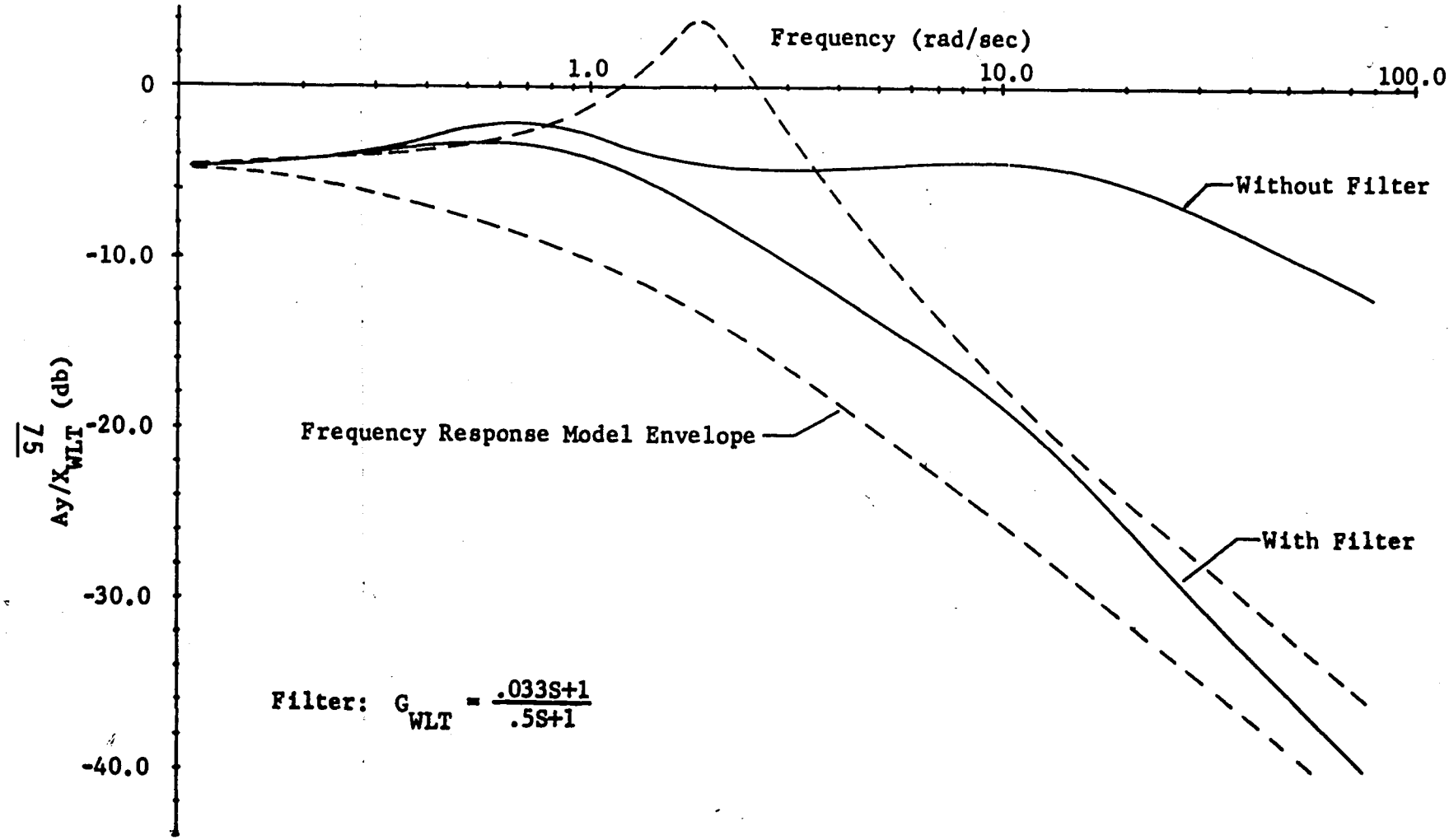

Figure 40. WLT Mode: Lateral Acceleration Response at Mn=1.2, hp=9144m, α=2°; with and without Input Filter.

Simple lag-lead compensation appears to be the only filtering necessary, and a few trial calculations with the corresponding frequency plots show that the corner frequencies should be at 2 rad/sec and 30 rad/sec. The lag function $2/(s + 2)$ matches the corner of the response model and produces the desired shape through the middle frequency range. The lead portion with a zero at 30 rad/sec controls the tail-off in the higher frequencies so that the curve is fully contained in the envelope. The input filter for the WLT mode becomes

$$G_{WLT} = \frac{.033\ s+1}{.5\ s+1}$$

and is applicable throughout the HiMAT flight envelope. The filtered lateral acceleration responses are included in Figures 38-40 along with the unfiltered curves.

5.2.2.2 *FP Mode*

The magnitude frequency response curve for the sideslip response without input filtering is shown for three flight conditions in Figures 41-43. The envelope for the frequency response model has been superimposed on them.

Unlike the unfiltered curves for the WLT mode lateral acceleration response, the FP mode beta curves through the flight envelope do not share the same relative shape or corner frequencies. Instead, the curves tend to drop at 40 db per decade

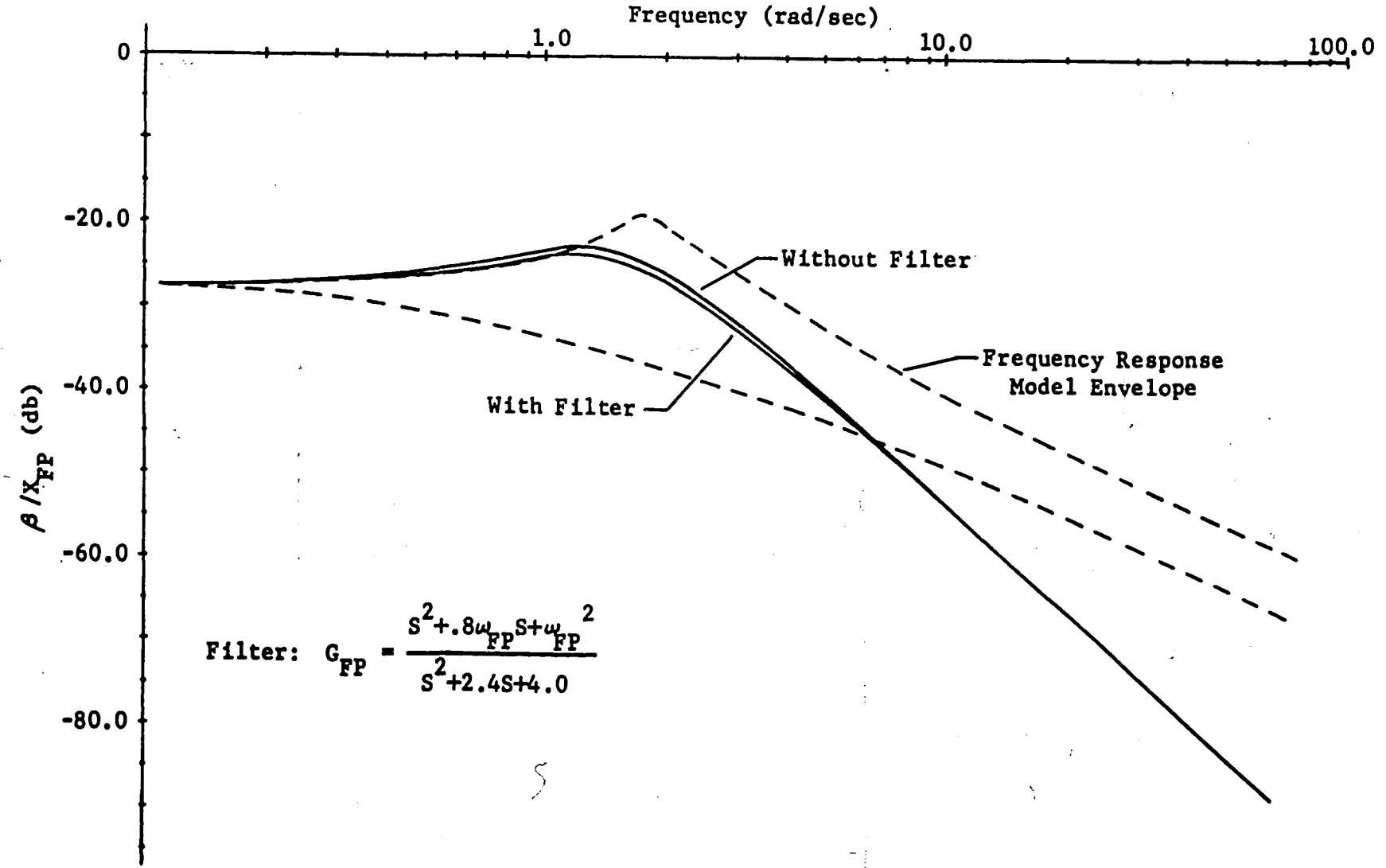

77

Figure 41. FP Mode: Sideslip Response at Mn=.4, hp=9144m, α=2°; with and without Input Filter.

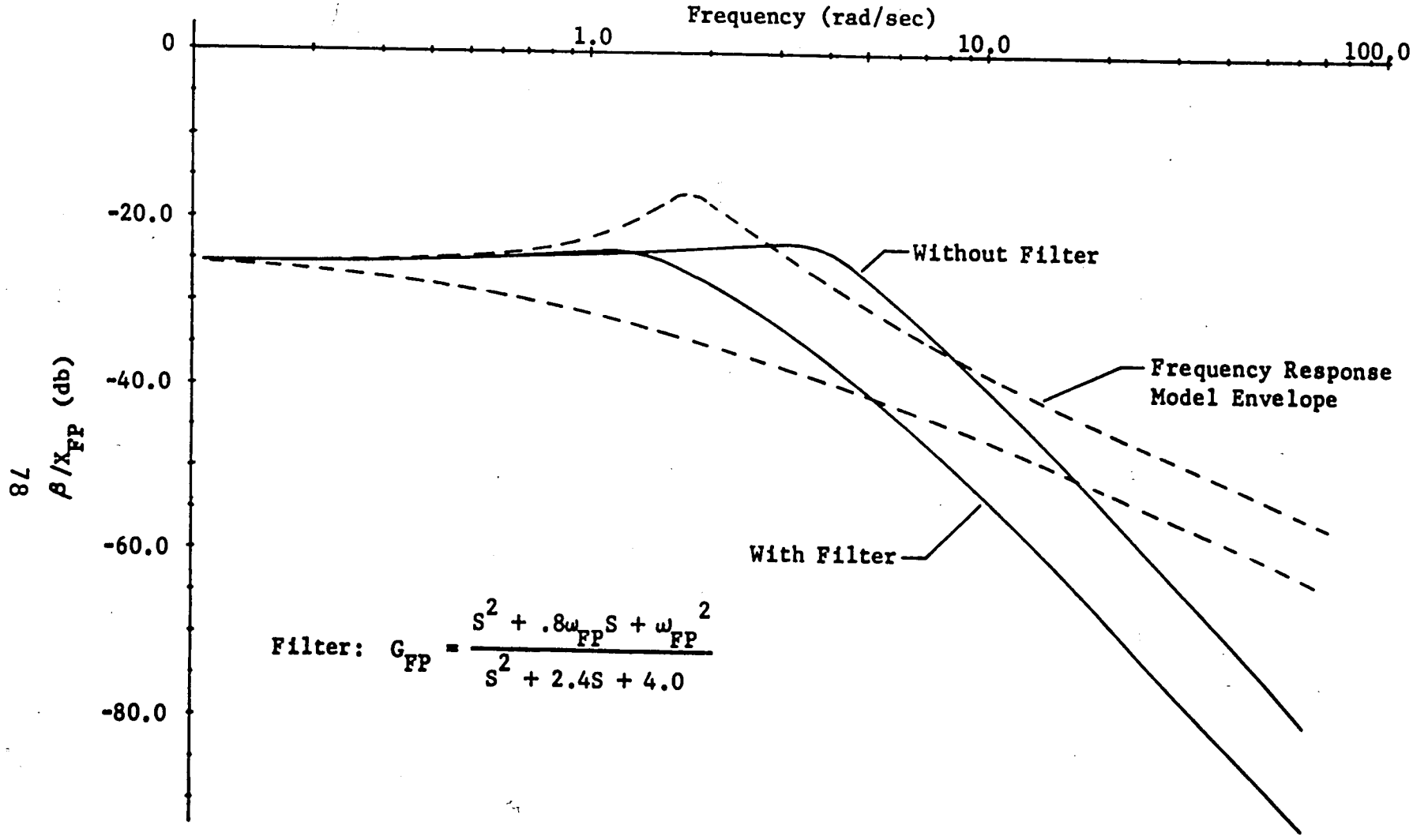

Figure 42. FP Mode: Sideslip Response at Mn=.8, hp=9144m, α=2°; with and without Input Filter.

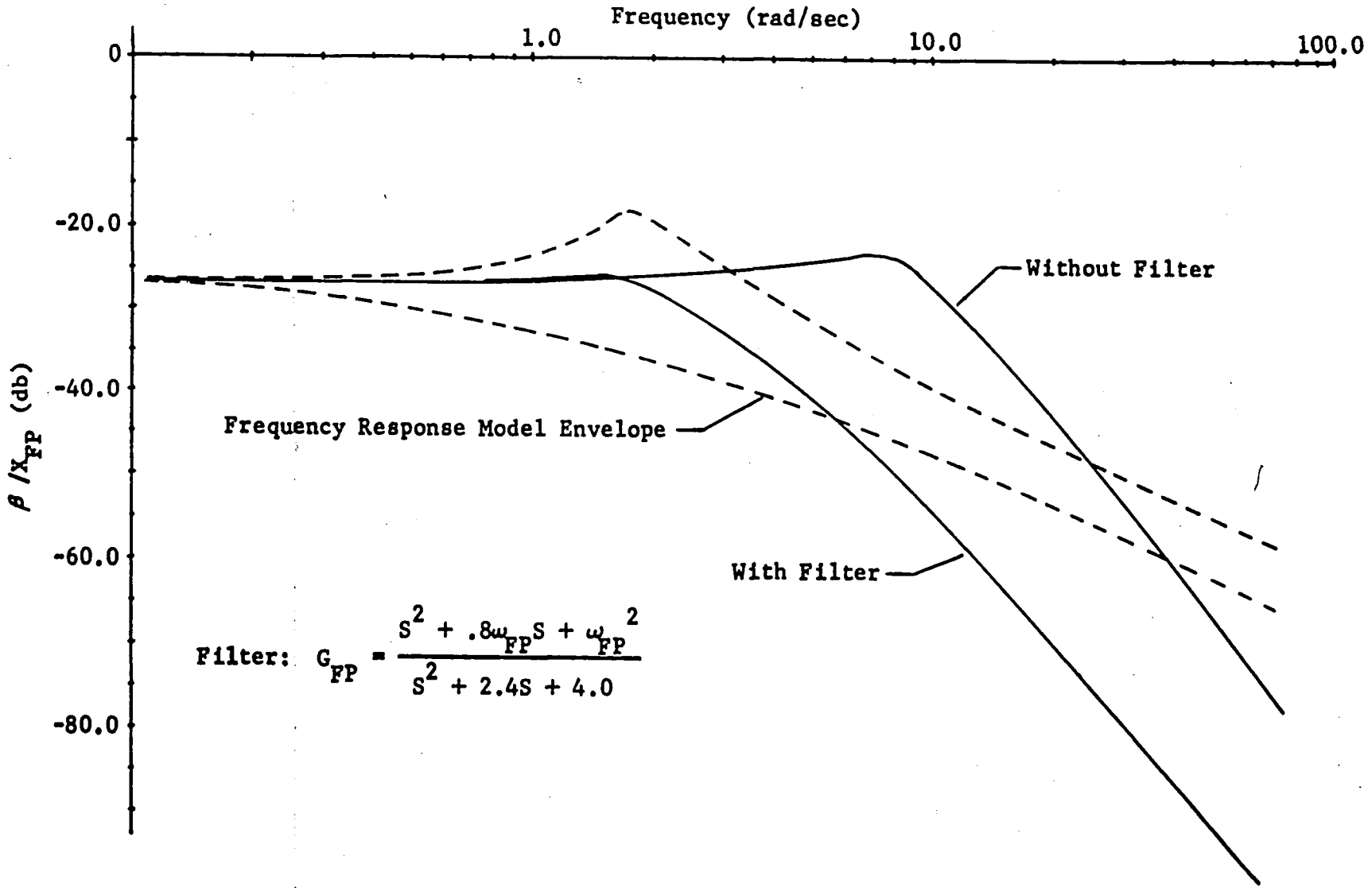

Figure 43. FP Mode: Sideslip Response at Mn=1.2, hp=9144m, α=2°; with and without Input Filter.

at corner frequencies which vary nearly exponentially with Mach number. This suggests a second-order lag-lead compensating filter with the numerator scheduled on Mach number. Some simple response comparison and superposition yields the following filter:

$$G_{FP} = \frac{s^2 + .8\omega_{FP}\, s + \omega_{FP}^2}{s^2 + 2.4\, s + 4.}$$

The value of "ω_{FP}" is obtained by plotting the values of the unfiltered sideslip response corner frequencies throughout the vehicle's Mach range and is shown in Figure 44. The second-order denominator is used to obtain a "model" corner frequency at 2 rad/sec with a damping ratio of 0.6. The filter's second-order numerator is used to eliminate the corner of the original response utilizing a 0.4 damping ratio.

The filtered sideslip responses are shown with the unfiltered responses and the model envelope in Figures 41-43. The overall shape is now independent of Mach number, but it must be noted that the slope of the high end response is -40 decibels per decade rather than the ideal -20 db/decade, and the curves depart below the model near 6 rad/sec. This can be rectified by using a first-order lead-lag of the form (.5 s+1)/(.025 s+1), but this may not be advantageous. Figures 45-47 show the roll

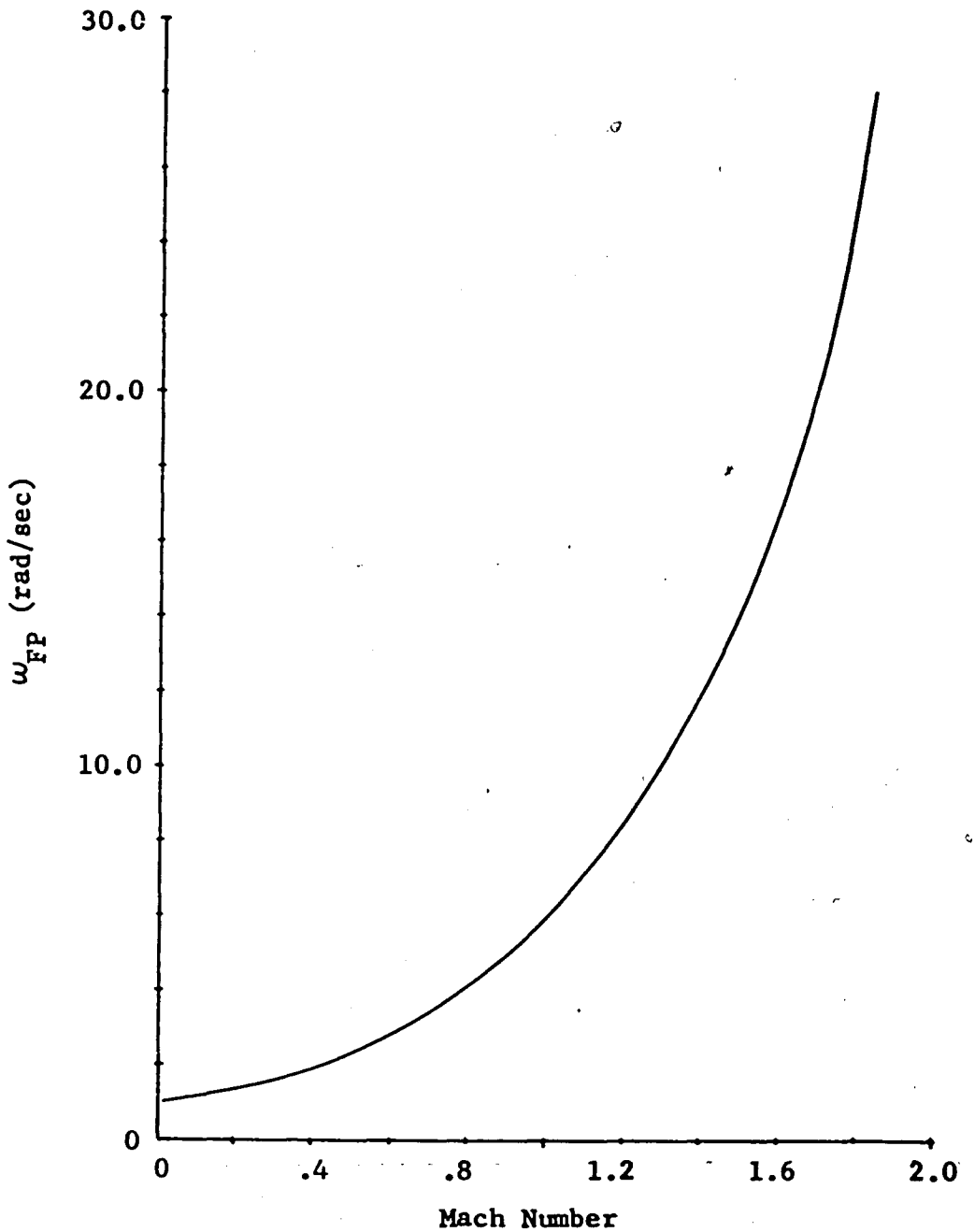

Figure 44. FP Mode: Input Filter Schedule - ω_{FP} vs. Mach Number.

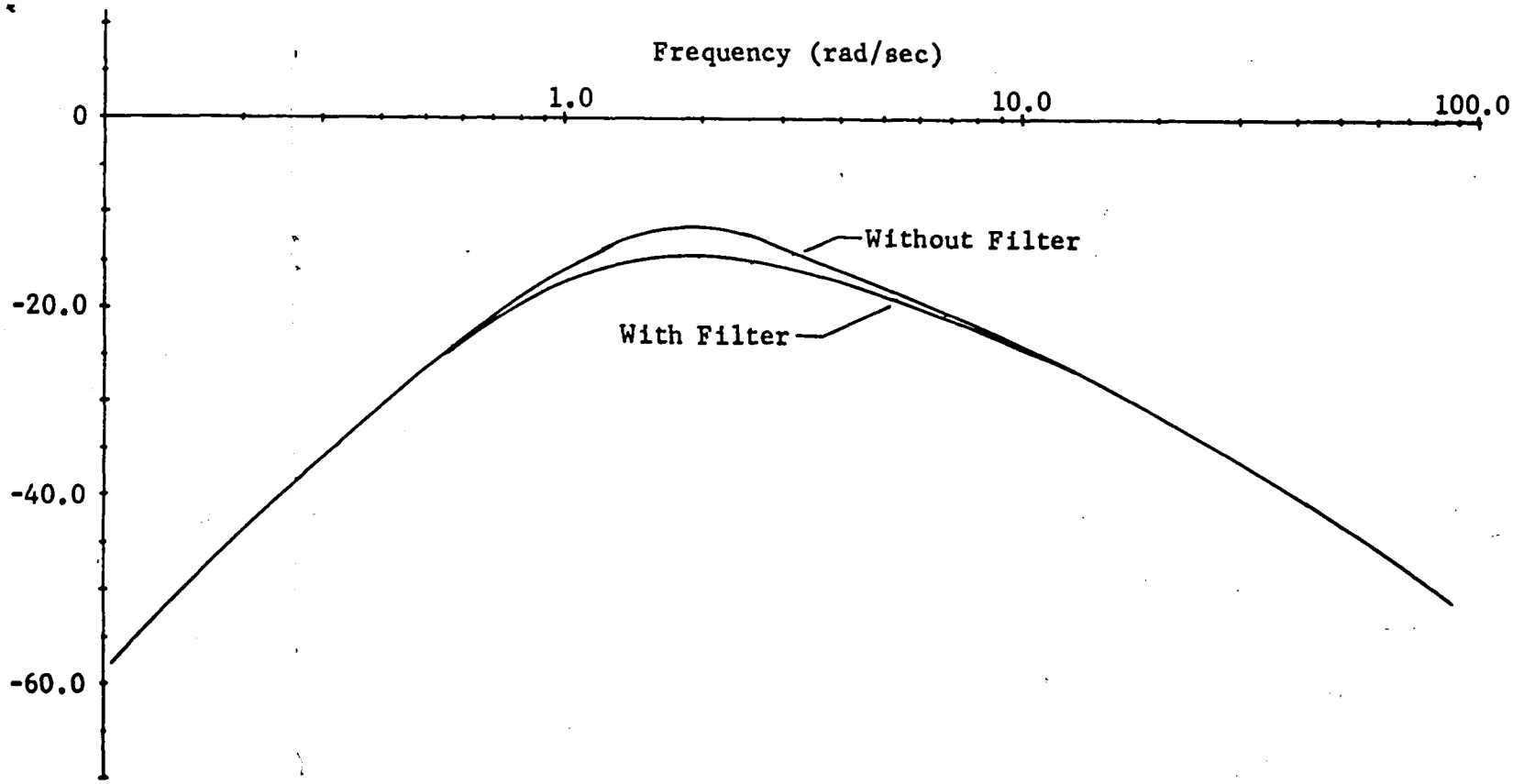

Figure 45. FP Mode: Roll Rate Response at Mn=.4, hp=9144m, α=2°; with and without Input Filter.

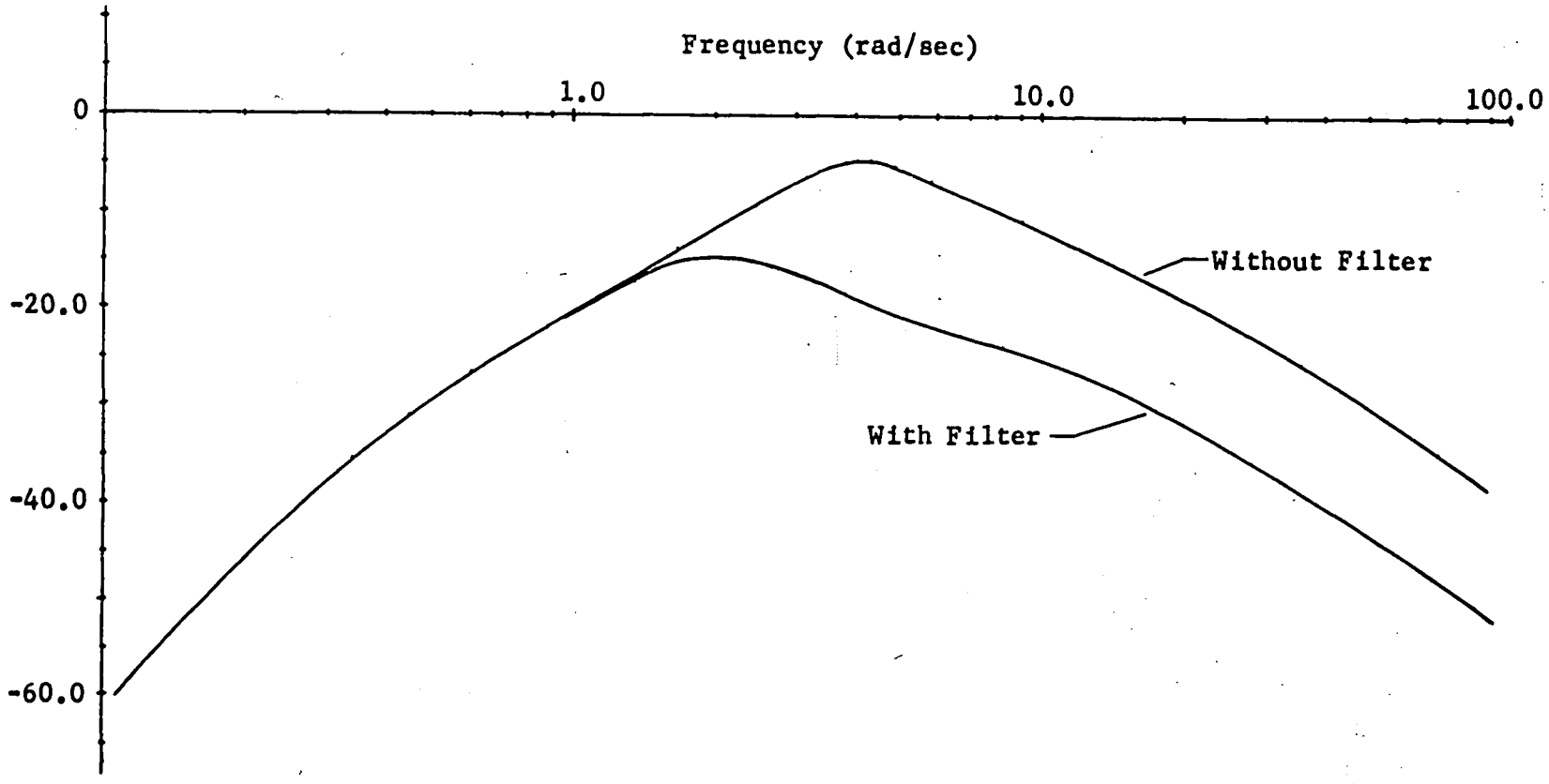

Figure 46. FP Mode: Roll Rate Response at Mn=.8, hp=9144m, α=2°; with and without Input Filter.

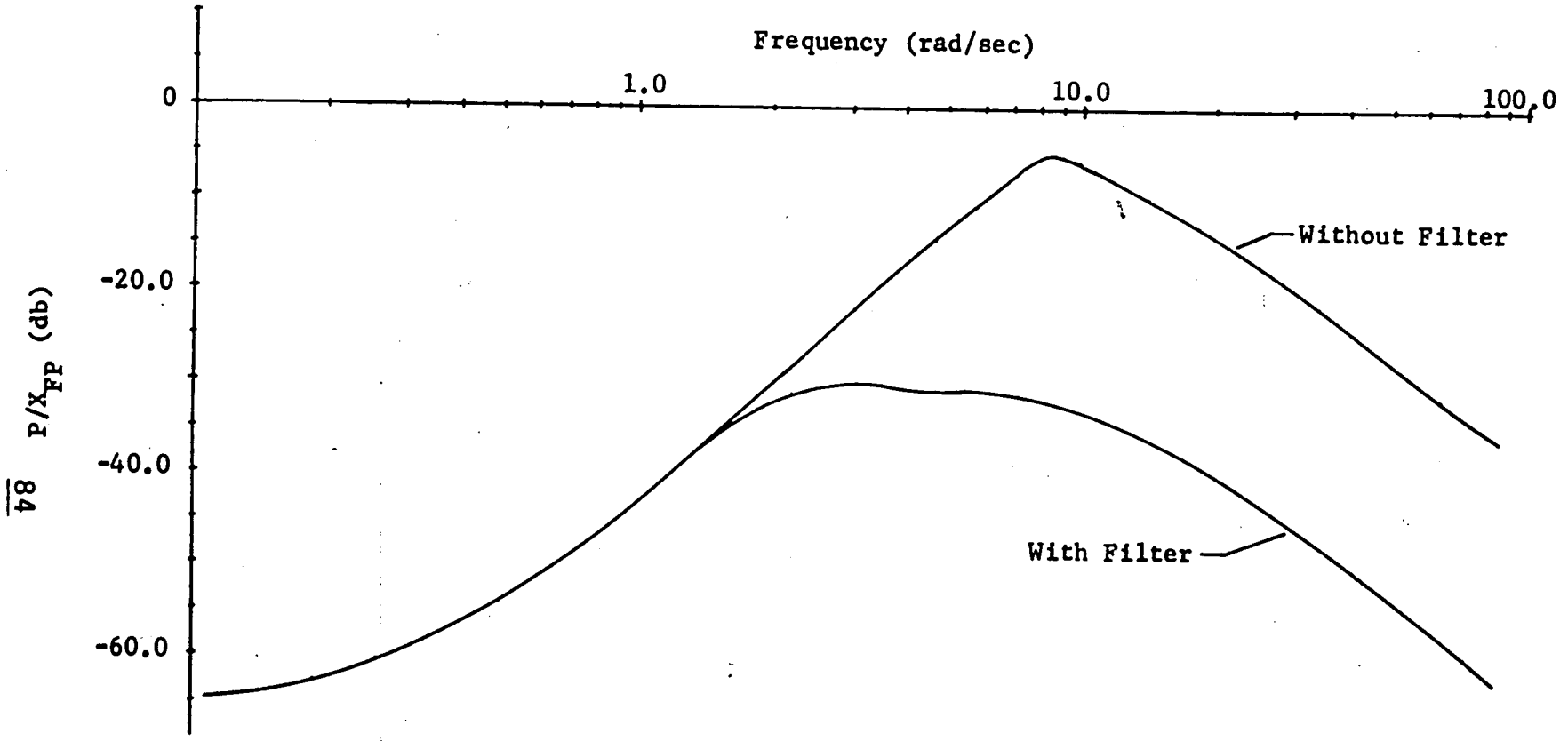

Figure 47. FP Mode: Roll Rate Response at Mn=1.2, hp=9144m, α=2°; with and without Input Filter.

rate responses with and without the second-order filter. Above Mach = .4 the filtered responses show a marked decrease in the maximum value over the unfiltered version. This is a desired result, as was mentioned in Section 5.2.1.2. If the additional first-order lead-lag filter is used, the sideslip response will conform to the model, but the roll rate and other responses which should be minimized will have greatly increased maximum values in the higher frequencies. For this reason, it would be justified to allow departure from the frequency model at the bottom of the envelope. This change will cause a decreased sideslip response above the area around 6 rad/sec, and is not likely to noticeably degrade the handling qualities. This decision also allows use of the simpler design.

5.3 Final Details

The block diagram of Figure 48 depicts the completed direct side force control system. Only the primary control gain, K_{DSF}, remains to be determined. The 30° limiter block included is used to prevent the DSF system from saturating any of the control surfaces, leaving some motion left for primary flight control.

Note that the rudder trim system from the original Rockwell flight control system is retained in the direct side force mode. This allows for any system 'balancing' that may be necessary without the need for constant rudder pedal pressure.

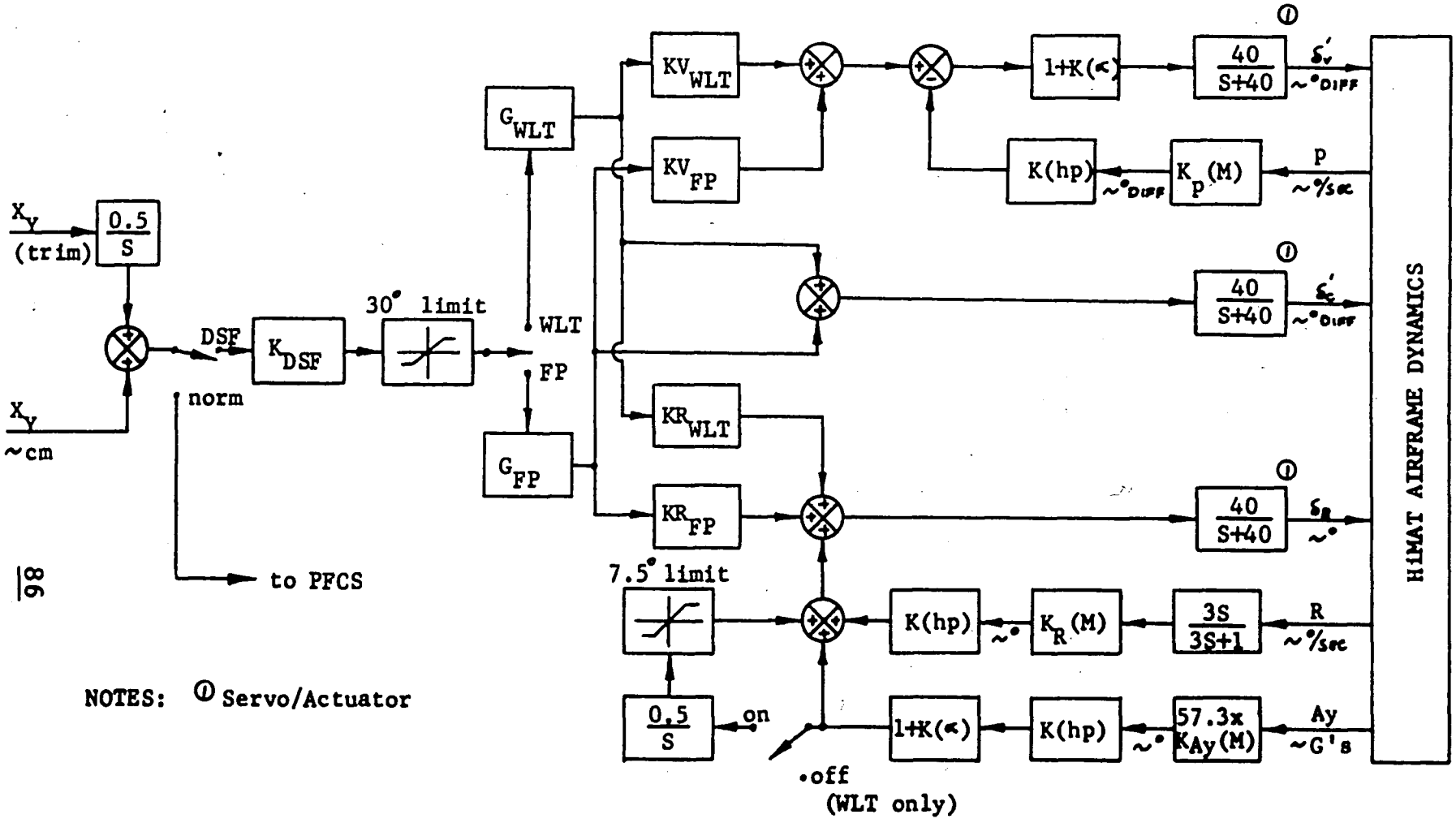

Figure 48. HiMAT Direct Side Force Control System

5.3.1 Control System Gain

With the limiter, the maximum possible input to the DSF system creates a 30° differential of the canard surfaces. From the Rockwell PFCS, the maximum rudder pedal movement is 8.89 cm and it is recommended in Section 4.3 that only half the available pedal be utilized for full DSF input. Thus, the values of K_{DSF} should be 6.75°/cm. This will be valid for all DSF modes.

5.3.2 Verification and Criteria Check

The response computer simulations were run for both DSF modes for many representative flight conditions. The results from two of these are plotted in Figures 49 and 50 for mach = .8, ALT = 9,144 m and α = 2°. The input to the system was a step, simulating maximum pedal movement. The wings level turn response curves appear very close to ideal with the exception of the bank angle plot which has a slope of approximately .5 degrees per second. This is not as degrading as suggested, however, since pilot reflex would unknowingly counteract this effect. It must be noted that the lateral acceleration response is an extremely clean exponential with no overshoot with an acceptable rise time.

The fuselage pointing responses are shown in Figure 50. Except for sideslip, they are not as close to ideal as are the

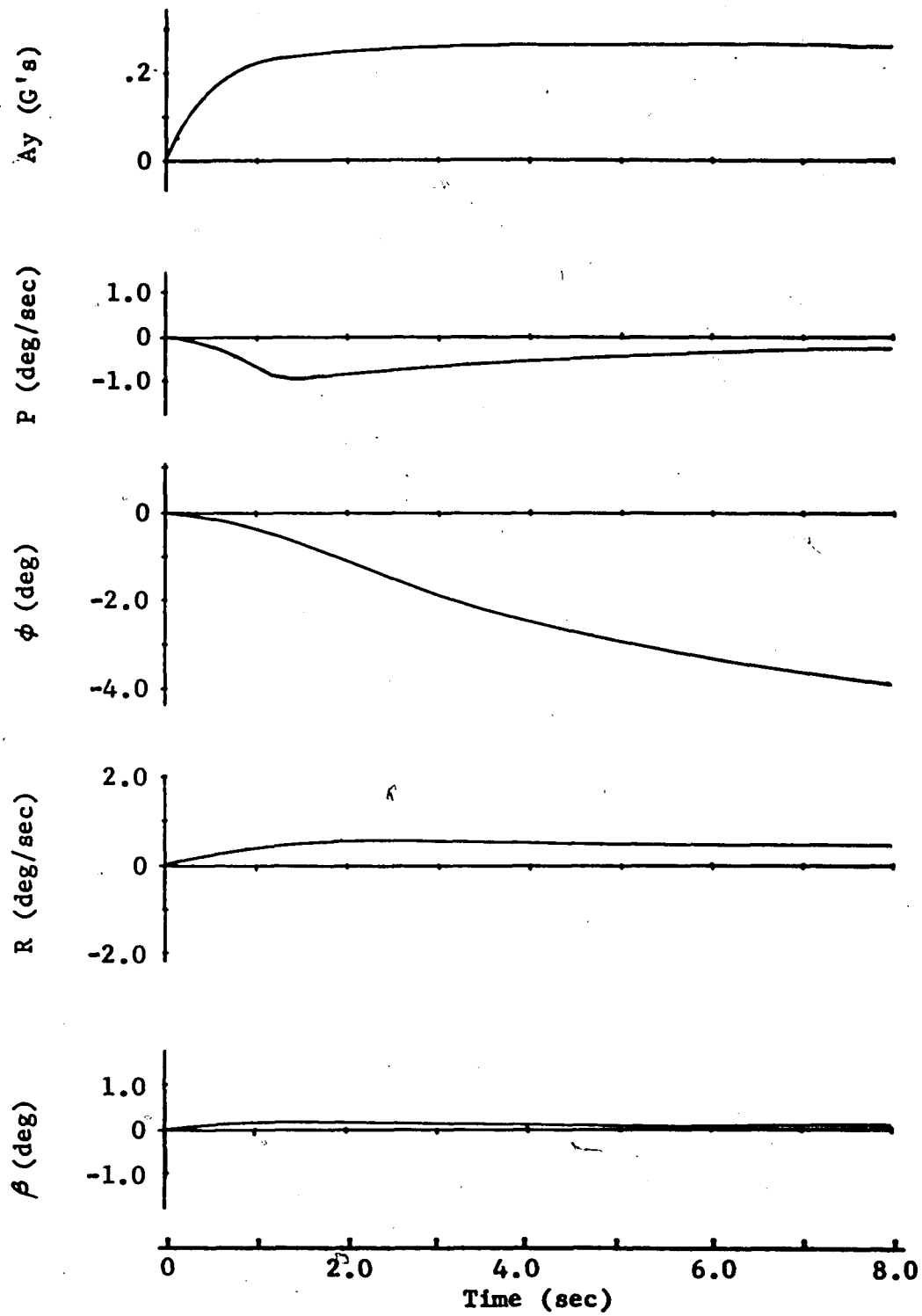

Figure 49. WLT Mode: System Time Response to a Step Input; Mn=.8, hp=9144m, α=2°.

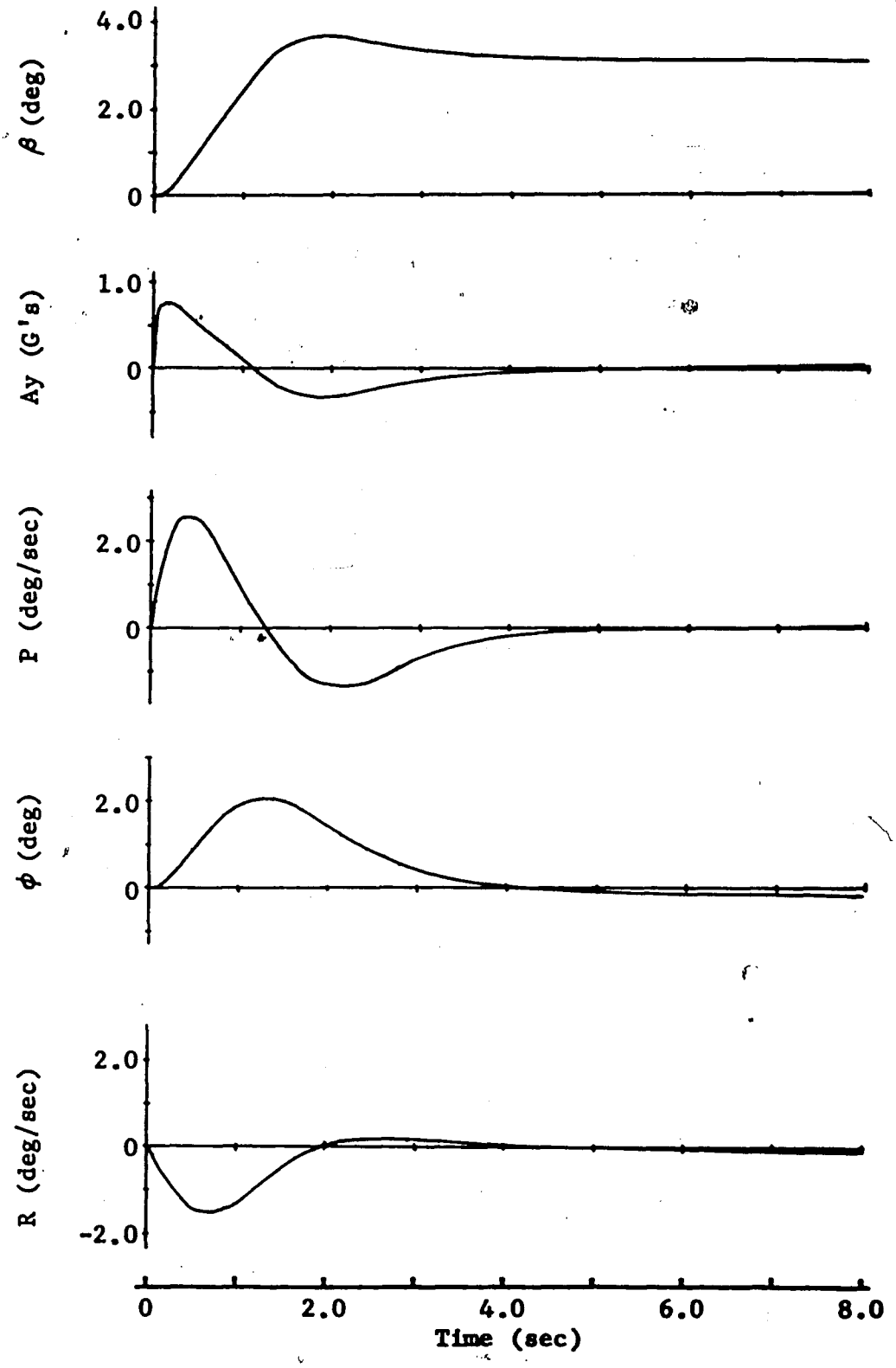

Figure 50. FP Mode: System Time Response to a Step Input; Mn=.8, hp=9144m, $\alpha = 2^{\circ}$.

WLT responses, but they are still acceptable. It must be kept in mind that these are maximized responses simulating a full rudder pedal step input, thus Figure 50 represents a "worse case." The sideslip response, most important for the FP mode, shows an excellent exponential rise with minimized overshoot and good rise time.

5.3.2.1 *Dutch Roll Requirement and Coupling Limits*

Figure 51 depicts the basic Class IV, Category A, Level I Military Dutch Roll Requirements in graphical form. Also plotted are values for the HiMAT direct side force system at three representative flight conditions. Referencing the time histories, it can be seen that all the points are well within the required areas. It should be noted here that the $|\phi/\beta|$ parameter loses some of its meaning in the FP mode since sideslip is the controlled response.

Section 4.2.2 of this paper contains recommended coupling limits for the DSF system. Those parameters that contain a normal acceleration term, A_z, cannot be applied here since the longitudinal system is considered distinct and is not covered at all in this HiMAT DSF system design. The other applicable coupling limits are easily satisfied due to acceptable handling qualities of the HiMAT Primary Flight Control System.

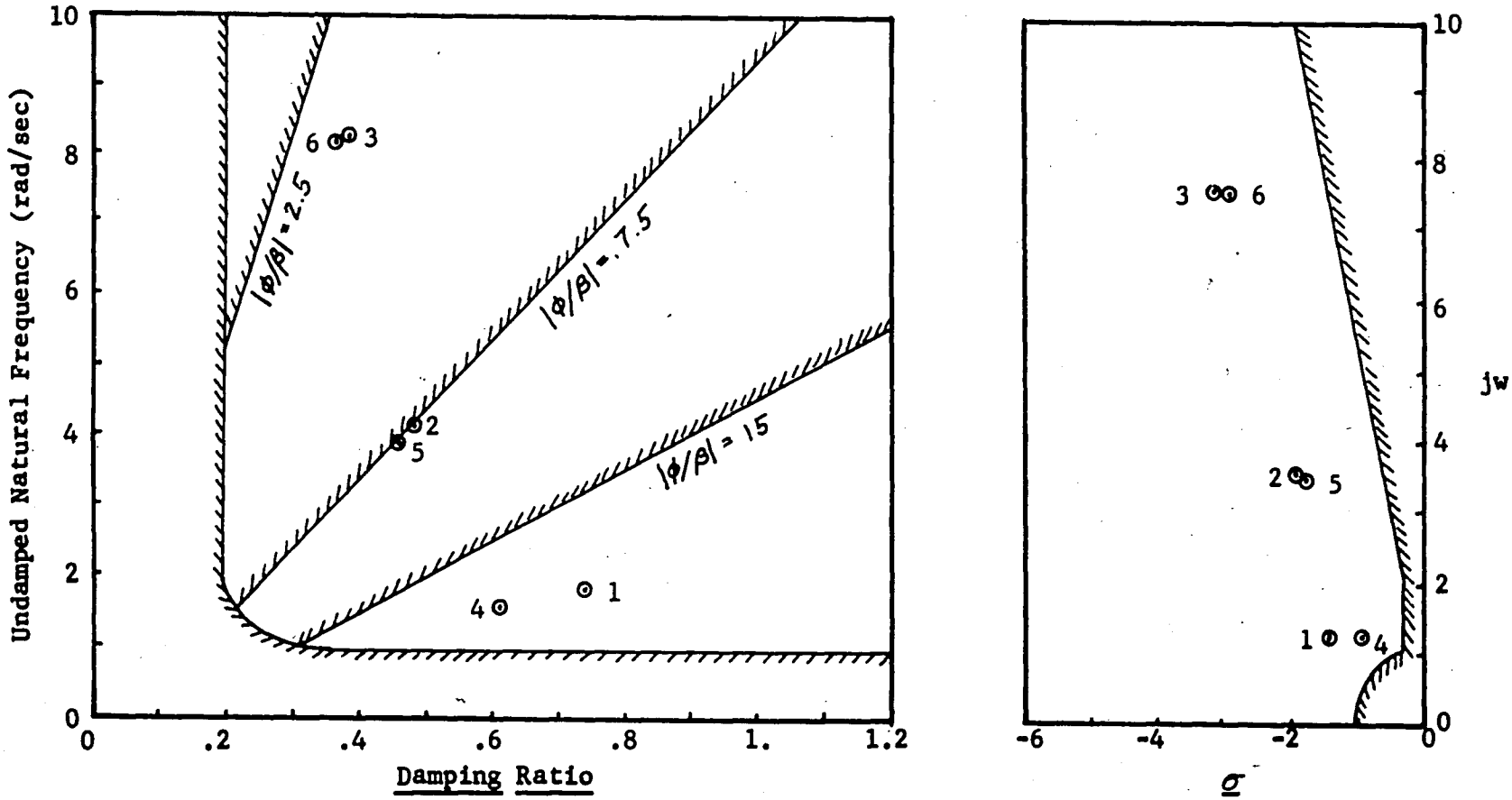

WLT Mode: 1) Mach = .4
2) Mach = .8
3) Mach = 1.2

FP Mode: 4) Mach = .4
5) Mach = .8
6) Mach = 1.2

Note: Angle of Attack = 2

Figure 51. HiMAT Direct Side Force System Dutch Roll Values for an Altitude of 9,144 meters.

SUMMARY AND CONCLUSIONS

A literature survey of direct side force control systems is performed and a system design presented for the NASA/Rockwell HiMAT research vehicle.

The search is done to determine what design criteria have been established for direct side force control systems which are applicable to class IV airplanes. Major contributions from the McDonnell Aircraft Company, General Dynamics, Boeing, and the Cornell Aeronautical Laboratory have been summarized. The findings are discussed, compared, and used in selecting DSF design criteria suitable for the HiMAT RPV program.

Three modes of DSF control are designated: wings level turn (WLT), fuselage pointing (FP), and lateral translation (LT). They are defined as:

- o WLT - Direct proportional control of lateral acceleration with minimum change in both sideslip and roll angles.
- o FP - Direct proportional control of yaw attitude and sideslip angle with minimum change in lateral flight path and roll angles.
- o LT - Direct proportional control of flight path and sideslip angle with minimum change in yaw attitude and roll angle.

Further definition is done through a set of ideal normalized time responses for each mode. The WLT and FP modes appear to have the most practical applications.

A major design criterion recommended for HiMAT is a low order frequency response model for the pertinent higher order system responses. For the WLT mode, the model applies to the lateral acceleration response, and for the FP and LT modes, it applies to the sideslip angle response. The form for both response models is the same and has the form

$$K \frac{s+a}{s^2+2\delta_y w_y s+w_y^2}$$

where

$$a = 1.8$$

$$\delta_y = 1.6$$

$$w_y = 2.0 \ .$$

Design limits are set at $a < 4.$ and $\delta_y > .3$.

A decoupled DSF system is recommended, while the following level I flying quality limits are set for variations from this ideal:

- WLT sideslip coupling limits

  $\beta/A_y \geq -2$ deg/G

  No positive limit set

- longitudinal coupling limits

  $\Delta A_z/A_y = 0.3$ steady state for WLT

  $\Delta A_z/A_y = 0.2$ transient for WLT

  $\Delta A_z/\beta = .025$ G's/deg, transient and steady state for LT

- roll coupling limits

  $0 \leq p/r \leq 8.$

The rudder pedals are suggested as the best form of cockpit controller since much of the piloting of class IV airplanes is done 'feet-on-the-floor', and test pilots have found this mechanization the most natural and easy to coordinate. The recommended sensitivity and authority of the system is stated and level I flying quality limits are set. A design goal of 1.0 G's lateral acceleration authority is included, but may be increased to the limits of the vehicle since pilot comfort is not a design factor with HiMAT.

All of the above criteria are then used in designing a DSF system for HiMAT in the WLT and FP modes. The Rockwell designed lateral-directional control system is the foundation with input filters and interconnects to the elevons, canards, and rudders to achieve the desired motion.

Initial calculations are done for a wide range of flight conditions. These show that the vehicle's flight envelope may

be well represented by considering mach numbers .4, .8, and 1.2, all at an altitude of 9,144 meters (30,000 feet) at an angle of attack of 2 degrees. The final design calculations are done around these three flight conditions. The small-perturbation linear equations of motion are used with no coupling considered between the lateral-directional and longitudinal axes.

A direct side force system is obtained with satisfactory handling qualities. Only minor deviations from the recommended design criteria are present which arise from a determination to keep the system as straight-forward and as simple as possible.

The maximum side force system capabilities for HiMAT are approximately 2 g's lateral acceleration for the WLT mode and approximately 6.6 degrees sideslip angle for the FP mode. For WLT, this maximum occurs around Mach 1.8 at sea level and decreases as speed decreases and altitude increases. For FP, the maximum occurs in a narrow band around mach 1.0 at high angles of attack with no dependence of altitude. Away from mach 1.0, the sideslip angle has a maximum of approximately 3 degrees.

REFERENCES

1. Boeing Company, "An Investigation of the Potential Benefits of Direct Side Force Control From a Mission Viewpoint," Report No. D180-17508-1, Boeing Company - Research and Engineering Division, Seattle, Washington, July 1973.

2. Brulle, R. V. and Anderson, D. C., "Design Methods for Specifying Handling Qualities for Control Configured Vehicles," AFFDL Technical Report AFFDL-TR-73-142, Volume I, November 1973.

3. Chalk, C. R., et al.,: Background Information and User Guide for MIL-F-8785 (ASF), "Military Specification--Flying Qualities of Piloted Airplanes," AFFDL Technical Report AFFDL-TR-69-72, August 1972.

4. Cornell Aeronautical Laboratory, "A Flight Test Investigation of Direct Side Force Control," Cornell Aeronautical Laboratory, Inc., Buffalo, New York, AFFDL Technical Report AFFDL-TR-71-1906, September 1971.

5. Dommasch, Sherby, Connolly, Airplane Aerodynamics, Pitman, New York, 1957.

6. Edwards, John W., "A Fortral Program for the Analysis of Linear Continuous and Sampled-data Systems," NASA TM X-56038, NASA Dryden Flight Research Center, Edwards, Calif., January 1976.

7. Elsanker, W. K., "HiMAT Flight Control System Control Law Design Requirements, Functional and Performance Characteristics," Report No. DAR 12100-01, Rockwell International, 28 April 1976.

8. Etkin, B., Dynamics of Flight: Stability and Control, Wiley, New York, 1959.

9. General Dynamics, "Fighter CCV Phase I Report - Configuration Selection and Control System Design," General Dynamics - Fort Worth Division, AFFDL Technical Report AFFDL-TR-75-106, September 1975.

10. General Dynamics, "Fighter CCV Phase II Report - Detail Design," General Dynamics - Fort Worth Division, AFFDL Technical Report AFFDL-TR-76-119, January 1977.

11. Kubbat, W. J., "Investigations of Direct Force Control for CCV Aircraft During Approach and Landing," Messerschmitt-Boelkow-Blohm G.M.B.H., Munich, West Germany, January 1975.

12. McDonnell Aircraft Company, "Direct Side Force Control Criteria for Dive Bombing, Volumes I and II," McDonnell Aircraft Company, AFFDL Technical Report AFFDL-TR-76-78, September, 1976.

13. McRuer, D., Ashkenas, I., and Graham, D., Aircraft Dynamics and Automatic Control, Princeton University Press, 1973.

14. Military, "Military Specification--Flying Qualities of Piloted Airplanes," Report No. MIL-F-8785B (ASG), Military, 7 August 1969.

15. Papacostas, D. T., "The Use of Sensitivity Functions to Match Transfer Functions to Time-Domain Performance Criteria," unpublished Master's Thesis, Lehigh University, 1976.

16. Rockwell International, "HiMAT Critical Design Review Oral Briefing, Book 1," Report No. DAR 32000-0, Rockwell International, February 1977.

17. Rockwell International, "Summary Data Package for HiMAT Control System," Report No. 77LA-4018-429B, Rockwell International, February 1977.

18. Roskam, Jan, Flight Dynamics of Rigid and Elastic Airplanes, Vol. I & II, Roskam Aviation & Engng. Corp., Lawrence, KS, 1972.

19. Stapleford, R. L., et al.,: "Outsmarting MIL-F-8785B (ASG), The Military Flying Qualities Specification," Report No. STI TR-190-1, August 1971.

20. Thelander, J. A., "Aircraft Motion Analysis," AFFDL Technical Documentary Report FDL-TDR-64-70, March 1965.

APPENDIX I

FLIGHT PHASE CATEGORIES [3]

Category A

a. Air-to-ground combat (CO)

b. Ground attack (GA)

c. Weapon delivery/launch (WD)

d. Aerial recovery (AR)

e. Reconnaissance (RC)

f. In-flight refueling (receiver) (RR)

g. Terrain following (TF)

h. Antisubmarine search (AS)

i. Close formation flying (FF)

Category B

a. Climb (CL)

b. Cruise (CR)

c. Loiter (LO)

d. In-flight refueling (tanker) (RT)

e. Descent (D)

f. Emergency descent (ED)

g. Emergency deceleration (DE)

h. Aerial delivery (AD)

Category C

a. Takeoff (TO)

b. Catapult takeoff (CT)

c. Approach (PA)

d. Wave-off/go-around (WO)

e. Landing (L)

APPENDIX II

CLASSIFICATION OF AIRPLANES [3]

Class I Small, light airplanes such as

- Light utility
- Primary trainer
- Light observation

Class II Medium weight, low-to-medium maneuverability airplanes such as

- Heavy utility/search and rescue
- Light or medium transport/cargo/tanker
- Early warning/electronic countermeasures/airborne command control, or communications relay
- Antisubmarine
- Assault transport
- Reconnaissance
- Tactical bomber
- Heavy attack
- Trainer for Class II

Class III Large, heavy, low-to-medium maneuverability airplanes such as

- Heavy transport/cargo/tanker
- Heavy bomber
- Patrol/early warning/electronic countermeasures/airborne command, control, or communications relay

Trainer for Class III

Class IV — High-maneuverability airplanes such as

- Fighter/interceptor
- Attack
- Tactical reconnaissance
- Observation
- Trainer for Class IV

APPENDIX III

FLIGHT LEVELS [3]

Level 1	Flying qualities clearly adequate for the mission Flight Phase
Level 2	Flying qualities adequate to accomplish the mission Flight Phase, but some increase in pilot workload or degradation in mission effectiveness, or both, exists.
Level 3	Flying qualities such that the airplane can be controlled safely, but pilot workload is excessive or mission effectiveness is inadequate, or both. Category A Flight Phases can be terminated safely, and Category B and C Flight Phases can be completed.

VITA

Russell Lund Schuetz was the second son of Mr. and Mrs. Kenneth N. Schuetz, born on 3 December 1952, in Newark, New Jersey. He attended elementary school in Roseland, New Jersey, and in 1971 graduated with honors from West Essex Regional High School, North Caldwell, New Jersey.

Mr. Schuetz entered Lehigh University in Bethlehem, Pennsylvania, in September 1971, and graduated Cum Laude in 1975 receiving the degree of Bachelor of Science in Mechanical Engineering. He was admitted to the Graduate School of Lehigh in September of that year in the same department.

Russ became a member of the Pi Tau Sigma honorary Mechanical Engineering fraternity in 1973 and was elected President the following year. He has since worked at the National Aeronautics and Space Administration, Dryden Flight Research Center in Edwards, California, and is currently employed by Martin Marietta Aerospace in Denver, Colorado.